INAUGURAL – Dissertation

zur

Erlangung der Doktorwürde

der

Naturwissenschaftlich-Mathematischen

Gesamtfakultät

der

Ruprecht-Karls-Universität Heidelberg

vorgelegt von

Volker Martin (M.Sc.)

aus

Überlingen am Bodensee

Tag der mündlichen Prüfung: 24.07.2017

Preparation of Dual Functionalized Surfaces for Covalent Immobilization of BMP-6 and Adhesive Ligands for Biological Applications

Gutachter:

Prof. Dr. Joachim P. Spatz
Physikalisch-Chemisches Institut
Ruprecht-Karls-Universität Heidelberg
Max-Planck-Institut für Medizinische Forschung, Heidelberg

apl. Prof. Dr. Reiner Dahint
Physikalisch-Chemisches Institut
Ruprecht-Karls-Universität Heidelberg

Parts of this thesis are submitted to the journal *Scientific Reports*:

Martin V, Zambarda C, Posa F, Mori G, Seckinger A, Grgurevic L, Vukicevic S, Cavalcanti-Adam EA. Surface immobilization of BMP-6 and RGD ligands at the nanoscale promotes myoblast adhesion and SMAD signaling. (**2017**).

Table of Content

1 Abstract

The median age of our population causes osteoporosis, bone fractures and disorders, which are also caused by multiple myeloma. In the past 25 years, regenerative medicine had gained in importance, especially for regeneration and renewal of bone tissue, which consists of different cell types composed in a very complex architecture. The growth factor bone morphogenetic protein 6 (BMP-6) belongs to the transforming growth factor β (TGF- β) superfamily and it induces the differentiation of mesenchymal stem cells into mature osteoblasts in bone leading to new bone formation. Besides induction of osteogenic differentiation, BMP-6 is also known to induce cell death in multiple myeloma cells in high concentrations. However, a systemic application is not practicable, since uncontrolled diffusion causes a wide range of side-effects. Immobilization of growth factors allows local treatment of bone fractures and defects, while it prevents uncontrolled release of growth factors. Furthermore, the required amount of growth factors can be reduced tremendously.

The objective of this work was the covalent immobilization of BMP-6 co-presented with clicked integrin ligands on a structured gold nanoparticle (AuNP) platform, using block-copolymer micellar nanolithography (BCMN) developed by Prof. Spatz and co-workers, to study integrin signaling in connection with growth factor responses. BMP-6 was selectively bound to gold nanoparticles organized in a hexagonal structure on the surface allowing to control the amount and density on the surface. I showed that surface co-presentation of BMP-6 and RGD or $\alpha_5\beta_1$ integrin selective ligand promotes SMAD1/5 phosphorylation and osteogenic differentiation of the standard model system C2C12, even at amounts as low as 1 ng, whereas soluble BMP-6 application is significantly less effective. Additionally, BMP-6 was immobilized on gold nanostructured polyethylene glycol diacrylamide (PEG-DA) hydrogels containing different concentrations of cRGD in order to study the influence of the stiffness on the cell signaling. Furthermore, this approach was used to investigate the effect of immobilized BMP-6 in low doses on the multiple myeloma cell line OPM-2 to induce cell death.

This approach provides for the first time the successful presentation of BMP-6 in small and defined amounts on surfaces in combination with adhesive ligands. Furthermore, covalent immobilization hinders protein release while maintaining the biological activity of the growth factor.

2 Zusammenfassung

Das durchschnittliche Alter unsere Bevölkerung verursacht Osteoporose, Knochenfrakturen und -fehlbildungen, welche auch durch das Multiple Myelom verursacht werden. In den vergangenen 25 Jahren hat die regenerative Medizin an Bedeutung gewonnen, insbesondere für die Regeneration und die Erneuerung von Knochengewebe, welches sich aus verschiedenen Zelltypen in einer sehr komplexen Struktur zusammensetzt. Der Wachstumsfaktor *Bone Morphogenetic Protein 6* (BMP-6, knochenmorphogenetisches Protein 6) gehört zu der transformierenden Wachstumsfaktoren β (Transforming Growth Factor β, TGF-β) Superfamilie, und es initiiert die Differenzierung von mesenchymalen Stammzellen in reife Osteoblasten, was zur Knochenneubildung führt. Neben der Initiierung der osteogenen Differenzierung ist BMP-6 auch bekannt dafür, dass es in hohen Konzentrationen den Zelltod in multiplen Myelomzellen herbeiführt. Eine systemische Behandlung ist jedoch nicht praktikabel, da eine unkontrollierte Diffusion eine Reihe von Nebenwirkungen verursacht. Die Immobilisierung von Wachstumsfaktoren erlaubt die lokale Behandlung von Knochenfrakturen und –defekten, während sie auch die unkontrollierte Freisetzung von Wachstumsfaktoren verhindert. Des Weiteren kann die benötigte Menge an Wachstumsfaktoren drastisch verringert werden.

Das Ziel dieser Arbeit war die kovalente Immobilisierung von BMP-6 auf einer goldnanostrukturierten Plattform, unter Verwendung von *block-copolymer micellar nanolithography* (BCMN) entwickelt von Prof. Spatz und Mitarbeitern, zusammen mit integrinselektiven Liganden, was die Erforschung von Integrinsignalisierung in Verbindung mit Reaktionen auf Wachstumsfaktoren ermöglicht. BMP-6 wurde selektiv an Goldnanopartikel gebunden, welche auf der Oberfläche hexagonal organisiert sind. Dies ermöglicht es, die Menge und die Dichte auf der Oberfläche zu kontrollieren. Ich konnte zeigen, dass die Oberflächencopräsentation von BMP-6 und cRGD bzw. dem α5β1 Integrin selektiven Liganden in Mengen von weniger als 1 ng die SMAD 1/5 Phosphorylierung und die osteogenen Differenzierung in dem Standardmodellsystem C2C12 fördert, während das gelöste BMP-6 signifikant weniger effektiv war. Um den Einfluss der Steifigkeit auf die Zellsignalisierung zu untersuchen, wurde BMP-6 auf Polyethylenglykoldiacrylamid (PEG-DA) Hydrogele mit einer goldnanostrukturierten Oberfläche und cRGD in verschiedenen Konzentrationen immobilisiert. Darüber hinaus wurde dieses Konzept für die Untersuchung

des Effekts von gering dosierten, immobilisierten BMP-6 auf die multiple Myelom Zelllinie OPM-2 eingesetzt mit der Absicht den Zelltod zu initiieren.

Dieses System ermöglicht zum ersten Mal die erfolgreiche Präsentation von BMP-6 auf Oberflächen in kleinen und definierten Mengen in Kombination mit adhäsiven Liganden. Des Weiteren verhindert die kovalente Immobilisierung eine Proteinfreisetzung, während die biologische Aktivität des Wachstumsfaktors erhalten bleibt.

3 Introduction

3.1 Bone and Growth factors

Growth factors (GFs) are a large family of polypeptidic molecules, which stimulate and modulate cell responses such as proliferation, differentiation, migration, cell adhesion, cell survival and chemotaxis (see **Figure 3.1**). GFs can be found in all tissues[1-3]. Naturally secreted from cells, many GFs directly interact with the surrounding extra cellular matrix (ECM). Furthermore, they can also be sequestered by the ECM in order to interact with cell surface receptors in a specific binding[4-5].

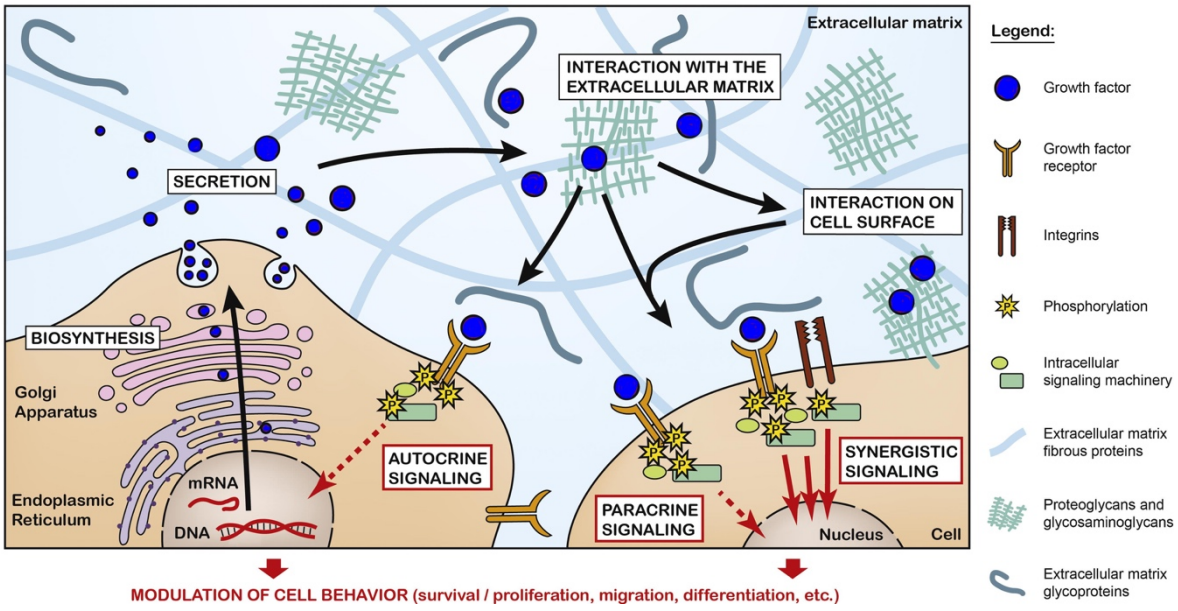

Figure 3.1 The path of growth factors in cell signaling from the biosynthesis to the different interactions with the ECM. Growth factors are synthesized in the cell and released into the ECM, where they interact with different components followed by binding and activating cell receptors. Growth factors form complexes with their cognate receptors. Adapted and modified from Mitchell *et al.*[6]

The native protein form of growth factors used in regenerative medicine causes limitations and properties such as low stability, short circulating half-time and rapid rate of cellular internalization. Moreover, their activity is locally restricted in tissue as a function control by spatial and temporal effects[6-7]. The fibroblast growth factor (FGF-1), for example, displays its low stability in an effective half-life of only 1 h in serum at 37 °C[8]. General problems in

handling and medical usage of growth factors in research are reflected by the poor recombinant expression yield, difficulty of purification, high production costs, high required concentration and lack of appropriate delivery methods[9]. By developing delivery systems many of the above-mentioned challenges can be circumvented.

A plethora of cellular signaling events like organism development, angiogenesis, wound healing and regeneration as well as generation of new tissue are mediated by GFs[3, 10-11].

3.1.1 Bone morphogenetic proteins

It's well-known that different growth factors are involved in the process of bone formation by stimulating pre-osteoblasts' proliferation[12]. Bone morphogenetic proteins (BMPs) comprise a family of growth factors, which possess chemotactic, mitogenic, osteogenic and differentiating properties thus playing an important role in bone formation[13]. In 1965, Marshal R. Urist showed that formation of new bone could be induced by implanting demineralized, lyophilized segments of bone into ectopic sites[14]. In 1971, Urist and Strates proposed the name "Bone Morphogenetic Protein"[15]. One year later, it could be shown that also demineralized bone matrix was able to induce bone formation in ectopic sites[16]. In the beginning, BMPs were isolated from bone, which was a cumbersome procedure and the yield was very low[17]. BMPs are glycosylated and extracellular matrix-associated molecules, that are members of the Transforming Growth Factor Beta (TGF-β) superfamily[18-19]. In general, this type of growth factors is a hetero- or homodimer consisting of about 120 amino acids per subunit. Seven of the 120 amino acids are conserved cysteine residues, six of these forming intramolecular disulfide bonds creating a knot motif. The other stabilizes the dimer through an intermolecular disulfide bridge[20-21]. By today, about 20 different human BMPs including the growth differentiation factors (GDF) have been found, which can be divided into subfamilies based on their sequence similarity and functions, whereby not all members are osteogenic[13]. Besides BMP-3 and BMP-13, which act either as a BMP negative regulator or as an inhibitor of bone formation, all BMPs are mainly involved in bone and cartilage formation[22]. In **Table 3.1** the most investigated and known BMPs are listed.

Table 3.1 Overview of BMP family members[23]. BMP types are listed with their alternative names and their functions in human body.

BMP type	Alternative name	Function
BMP-1	-	Metalloprotease acting on procollagen I, II and III, involved in cartilage development.
BMP-2	BMP-2a	Bone and cartilage formation, key role in osteoblast differentiation.
BMP-4	BMP-2b	Regulation of teeth, limbs and bone formation.
BMP-5	-	Cartilage development.
BMP-6	Vgr-1; Dvr-6	Key role in joint integrity, bone morphogenesis, estrogen mediation.
BMP-7	OP-1	key role in osteoblast differentiation and in renal development and repair.
BMP-8	OP-2	Involved in bone and cartilage development.
BMP-9	GDF-2	Promoting chondrogenic differentiation of human multipotent mesenchymal stem cells.
BMP-10	-	Role in the trabeculation of the embryonic heart.

Interestingly, BMP-1 belongs neither to the BMP family nor to the TGF-β superfamily, although it is called a bone morphogenetic protein. It is a metalloprotease, which is able to induce cartilage formation *in vivo* and cleave the C-terminus of procollagen I, II and III[24]. In 2005, Hari Reddi suggested to change BMPs' name to body morphogenetic proteins, because of their effective range, which is not limited to the bone, but plays also an important role in the whole body[25].

3.1.2 Bone/body morphogenetic protein 6 (BMP-6)

In 1989, BMP-6 was isolated from murine embryonic cDNA library. Because of its homology to *Xenopus* Vg-1, it received the name Vgr-1[26]. Celeste *et al.*[27] isolated Vgr-1 from human and bovine bone and named it BMP-6. The successful expression of the BMP-6 mRNA in mammals could be shown in different cell types. BMP-6 is produced by bone

marrow-mesenchymal (BMSC) and hematopoietic stem cells[28]. Furthermore, BMP-6 is a homodimer with the 2 monomers connected through a disulfide bond. In **Figure 3.2**, the three-dimensional structure of the BMP-6 homodimer is presented. The fact, that the protein consists of two monomers can be used to develop heterodimers by co-expression of two different recombinant BMP subunits. Valera *et al*.[29] engineered a heterodimer consisting of BMP-2 and BMP-6 and showed that it was more effective than BMP-2 or BMP-6 homodimers as an inductor of differentiation in human embryonic stem cells (ES).

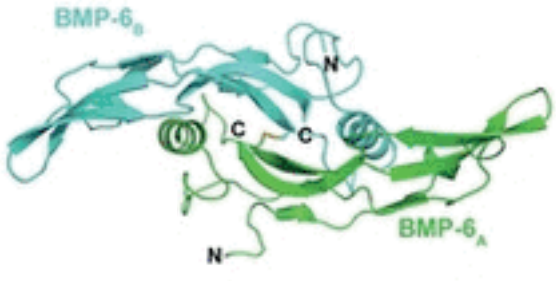

Figure 3.2 The three-dimensional structure of BMP-6 homodimer. BMP-6 consists of two monomers A (green) and B (blue). The C- and N-terminus of each BMP-6 monomer are indicated with C and N, respectively. Adapted and modified from Saremba *et al*.[30]

SMAD proteins are a group of intracellular proteins, which are involved in cell signaling processes induced by extracellular growth factors of the TGF-β superfamily. The name SMAD originates from the homological gene of the fruit fly *Drosophila melanogaster* MAD (mother against decapentaplegic) and from the protein gene Sma (small body size) of the nematode *Caenorhabditis elegans*[31].

Ebisawa *et al*.[32] showed that BMP-6 strongly binds to activin receptor-like kinase (ALK)-2, which is also known as ActR-I, as well as to type II receptors, i.e. BMP type II receptor (BMPR-II) and activin type II receptor (ActR-II) C2C12 cells. Additionally, a similarity between BMP-6 and BMP-2 is the weak bond to BMPR-IA (ALK-3). Moreover, they detected the binding of BMP-6 to BMPR-IB (ALK-6) in ROB-C26 cells, mesenchymal progenitor cell line. BMP-6 binds extracellularly, but SMAD proteins are phosphorylated intracellularly.

It is known that BMP-6 induces the phosphorylation of the receptor-regulated SMADs (R-SMAD, SMAD1, SMAD5 and SMAD8)[32] by binding to ActR-II and ActR-I (**Figure 3.3**).

After phosphorylation, R-SMADs are released from the BMP receptor and form a complex with the common mediator SMAD (Co-SMAD, SMAD4). Nucleocytoplasmic shuttling of the SMAD complex activates transcription of target [28]. Sieber *et al.*[33] showed that BMPs are also capable to induce gene transcription independent of SMAD molecules. However, there are only rudimental investigations about BMP-6 induced signaling pathways beside the SMAD dependent pathways. Furthermore, BMP signaling is rather complex with cross-talks between different signaling pathways and negative feedback mechanisms[34-36].

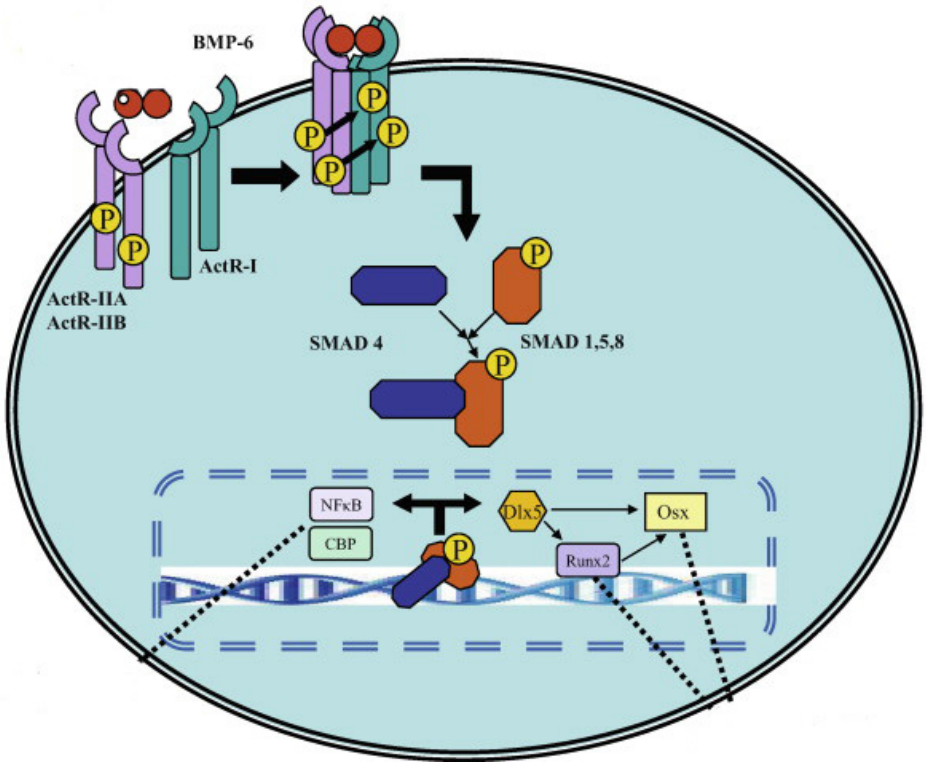

Figure 3.3 Induction SMAD 1,5,8 phosphorylation by BMP-6. BMP-6 shows a high affinity to ActR-I and ActR-II receptors, which activates SMAD phosphorylation. SMAD complex acts as transcription factor. Adapted and modified from Vukicevic *et al.*[28]

Induction of osteogenic differentiation

Osteogenic differentiation is the process of bone development, which is known to be induced by BMPs[37-39]. C2C12 is an immortalized mouse myoblastoma cell line and a standard model system used to study the differentiation of myoblasts, osteoblasts, and myogenesis.

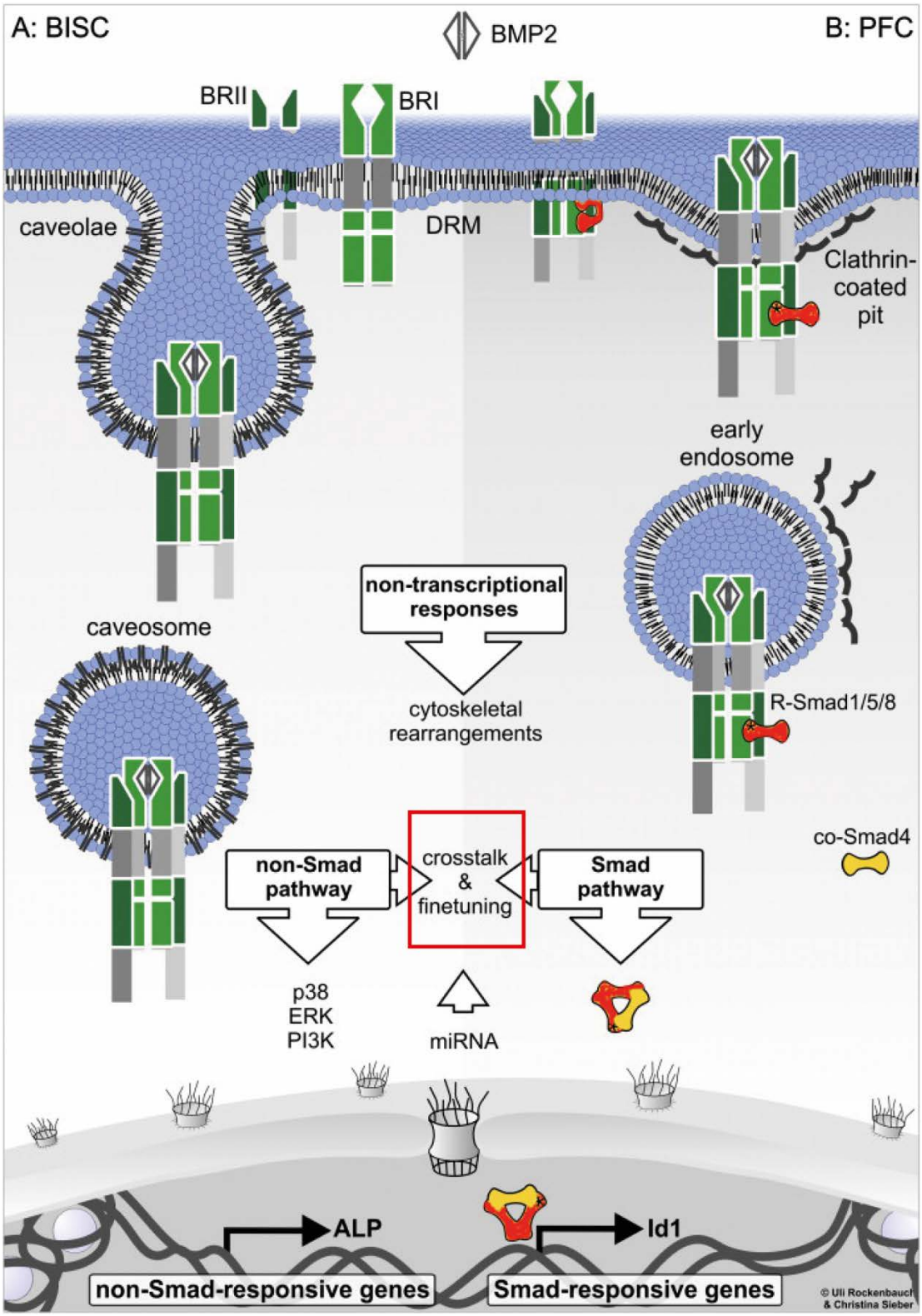

Figure 3.4 BMP-2 SMAD and non-SMAD signaling pathway. A) Signaling via BMP-induced signaling complex (BISC). The non-SMAD pathway is activated by BPM-2 binding to its high affinity type I receptor (BRI). Then Type II receptor (BRII) is recruiting into the complex of BMP-2 and BRI. B) Signaling via preformed complex (PFC). The SMAD pathway is activated by binding of BMP-2 to a PFC of type I and type II receptor. Adapted and modified from Sieber *et al*.[33]

C2C12 cells are undifferentiated mesenchymal cells which differentiate into osteoblasts upon stimulation by BMPs. Ebisawa *et al.*[32] published that recombinant human BMP-6 induces alkaline phosphatase (ALP) activity in C2C12 cells, which is a typical osteoblastic marker. ALPs are enzymes which are able to hydrolyze phosphate ester of different molecules, such as proteins, nucleotides and alkaloids. BMP-2 is also known to induce ALP activity via the non-SMAD pathway by BMP-induced signaling complex (BISC) (see **Figure 3.4**)[33]. It is assumed that BMP-6 induces the ALP activity in a similar way, although it has not been investigated so far. Moreover, the ALP activity induced by BMP-6 was 10-fold higher than of BMP-7. Similar to BMP-2[39] and BMP-7[40], BMP-6 inhibits the myoblastic differentiation of C2C12 cells and induces osteoblastic differentiation. BMP-2, BMP-6 and BMP-9 are known to be the most potent inducers of osteoblastic differentiation in mesenchymal stem cells (MSCs)[41-43]. However, Mizrahi *et al.*[44] showed that BMP-6 seems to induce bone formation in genetically modified MSCs more efficiently than BMP-2. Furthermore, they proposed the preferred use of BMP-6 instead of BMP-2, since BMP-2 had been shown to cause adverse side-effects.

BMP-6 effect on multiple myeloma

The multiple myeloma is a malignant disease of the hematopoietic system which causes the ongoing monoclonal production of antibody-producing cells, namely plasma cells[45]. B-lymphocytes normally differentiate into plasma cells after antigen contact, but the degenerated plasma cells produce non-functional antibodies and part of antibodies, respectively, which are called paraproteins. The multiple myeloma is the most common malignant disease of the bone and the bone marrow, respectively. Every year, 4-5 of 100000 people at an age of 60 to 70 are affected [46]. The survival rate was significantly improved by introduction of new medicines like Bortezomib, Lenalidomid and Thalidomid within the last ten years[47-49]. However, there is still no treatment available, which can cure the patients completely. Moreover, the multiple myeloma influences the bone remodeling compartments (BRCs) and corrupts them. In succession, the bone resorption is increased, while the bone regeneration is reduced[50-51] (see **Figure 3.5**). This causes osteolytic defects in the bone, thereby creating a survival space ("niche"), in which the multiple myeloma cells can withdraw during chemotherapy treatment[52].

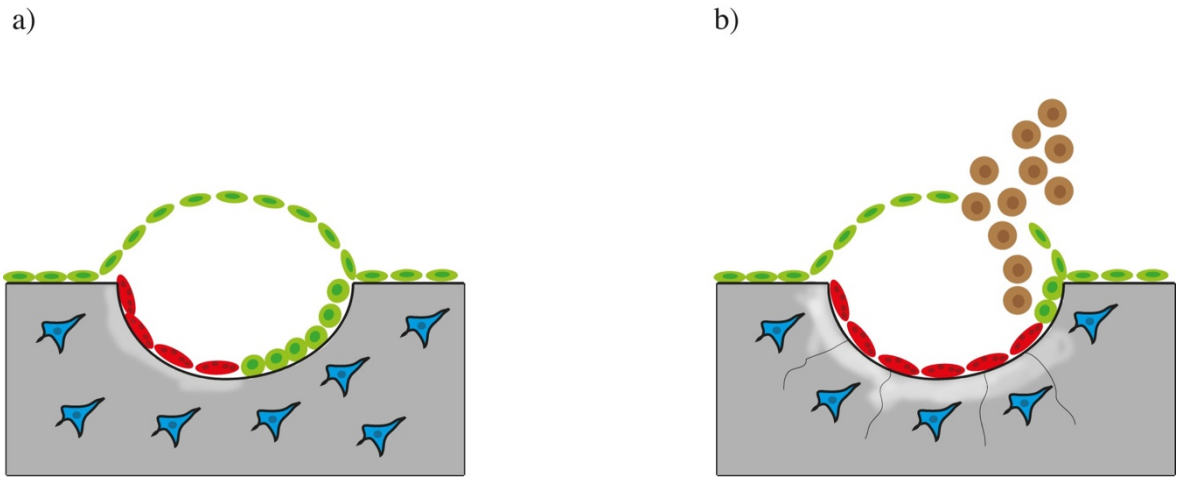

Figure 3.5 Osteolytic defects caused by multiple myeloma. a) Osteoblastic bone formation (green) and osteoclastic bone resorption (red) are balanced in a normal system. b) By interaction with multiple myeloma (brown) cells, the balance is disturbed and the bone resorption is enhanced, while bone formation is decreased. Adapted from Seckinger *et al*.[52]

Recently, Seckinger *et al*.[53] published the cell death inducing effect of BMP-6 on multiple myeloma cells. They showed that BMP-6 reduced the cell viability significantly in concentrations higher than 0.160 μg/ml. The highest efficiency could be detected in concentration of 4 μg/ml. Furthermore, they could show that BMP-6 could be qualified to heal the osteolytic defects due to its high capacity in induction of osteogenic differentiation. However, the high amount of BMP-6 which is required to obtain effects in multiple myeloma viability makes it unattractive since the systemic treatment in such high concentration would likely cause uncontrolled side-reactions in the body. Moreover, the costs for such a therapy would be too expensive for patients' treatment. A delivery system is required, to reduce or avoid side-reactions with the locally applied treatment. Additionally, it can help to reduce the required amount of BMP-6 in the body.

3.2 Growth factor immobilization

Growth factors are potent and promising proteins for therapeutically applications in regenerative medicine. Especially in replacing or repairing damaged cells, tissues and organs transplantations can be avoided or postponed[54]. To accomplish these aims, different approaches to immobilize growth factors had been developed stimulating tissue regeneration. Challenges which arise in growth factor immobilization are the requirement to

maintain the growth factor's biological activity and the generation of cell-friendly biomaterials.

3.2.1 Immobilization strategies

There are two main strategies for immobilization: non-covalent and covalent. The non-covalent method can be further divided into physisorbed or electrostatic interactions, such as growth factor's natural affinity for biomaterial matrices and the affinity for endogenous extracellular matrix (ECM). An overview of the different strategies is shown in **Figure 3.6**.

Non-covalent immobilization by engineered biomatrices

To face the challenges mentioned above, the focus has been on the use of natural ECM-derived materials like hyaluronan or chitosan, which offer a physiologically relevant environment for cells[55] (see **Figure 3.6** a). The fibroblast growth factor 2 (FGF-2) and the vascular endothelial growth factor A (VEGF-A), for example, bind to fibrin[56-57]. By using fibrin sealants as binding platform, the effect on endothelial cell proliferation and blood reperfusion is enhanced[58]. Another strategy is the direct modification of the biomaterial in order to increase the affinity to the growth factors. By tuning gelatin-based hydrogels to be more acidic or more basic, the sustained delivery of FGF-2 from negatively charged and of BMP-2 from positively charged gels could be shown[59-60]. Some growth factors bear a heparin-binding site, which can be used to immobilize them by using the natural affinity for glycosaminoglycans (GAGs) and heparin-like molecules. In this way, strong heparin growth factors, such as FGF-2, can be coupled with a heparin-binding domain crosslinked into fibrin gels[61]. Migliorini *et al.*[62] recently published surfaces presenting BMP-2 through heparan sulfate (HS), which is a ubiquitous component of the ECM. In this method, the reducing end of the HS is used to immobilize BMP-2. Furthermore, the natural arrangement of HS proteoglycans in the ECM is mimicked.

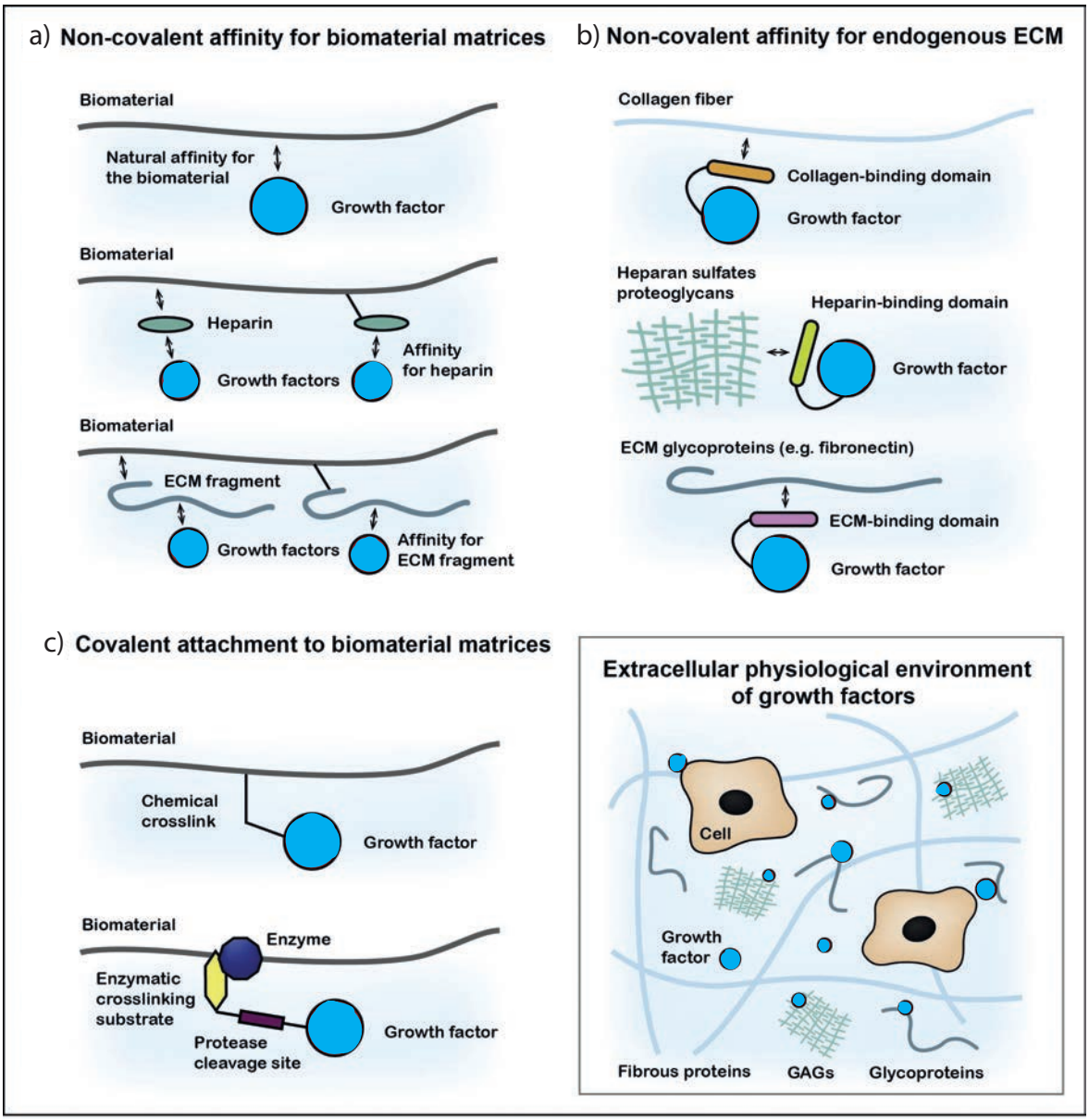

Figure 3.6 Overview about different strategies for growth factor immobilization. a) By using the natural affinity of growth factors to exogenous biomatrices, growth factors can be non-covalently immobilized. b) The extracellular matrix can be used as delivery matrix through binding of growth factors via ECM binding domains. c) Growth factors can be covalently immobilized to biomatrices by applying chemical or enzymatic techniques. Adapted and modified from Mitchell *et al*.[6]

Non-covalent immobilization for GF delivery via endogenous ECM components

ECM proteins and fibers, such as collagen or fibronectin, had become a good and promising target for the endogenous binding and presentation of growth factors. By fusion between collagen-binding domains (CBD) and growth factors, it could be shown that the delivery of

the nerve growth factor β (NGFβ) and brain-derived neurotrophic factor (BDNF), respectively, by collagen scaffolds improve peripheral nerve and spinal cord regeneration, respectively[63-64]. Similarly, Hauff *et al.*[65] showed the immobilization of biotinylated BMP-2 to biotinylated cellular fibronectin (cFN) crosslinked by NeutrAvidin. The modification of growth factors allows the mimicking of physiological growth factor delivery in order to optimize the therapeutic effects on morphogenetic processes.

Covalent immobilization strategies

Besides the above-mentioned methods, growth factors can be coupled enzymatically to biomatrices containing enzymatic sequences. This allows a site-specific control of growth factor immobilization, which can reduce the interference with bioactive sites of the growth factor to a minimum. Ehrbar *et al.*[66-67] fused a transglutaminase substrate sequence at the growth factor terminus to arrange a new connection to fibrin and PEG matrices.

Due to avoid any uncontrolled diffusion of growth factors, the covalent, chemical immobilization onto biomaterials is the method of choice. This method of immobilization prevents internalization of the growth factors by cells, which prolongs their lifetime compared to the duration of soluble growth factors. These facts might influence the effect of the growth factors on cells. In literature, there are many strategies for the covalent immobilization of growth factors published[68], e.g. using His-Tag coupling. A common method is to address primary amines or carboxylate groups of the growth factors as reactive moieties by using carbodiimides. Chiu *et al.*[69] crosslinked VEGF-A/angiopoietin-1 to collagen scaffolds thus creating a bioactive material, which supports vascularization. Another way of covalent immobilization was published by Pohl *et al.*[70-71], who used an alkanethiol linker containing an NHS (*N*-hydroxysuccinimide) ester group to immobilize BMP-2 on a homogeneous gold surface by addressing the primary amine groups of the protein (see **Figure 3.7**). To have a better control about the amount of immobilized BMP-2 on the surface, this method was further developed by Schwab *et al.*[72]. Instead of a homogeneous gold surface they employed gold nanostructured glass surfaces. To prevent unspecific binding of the BMP-2, the space between the gold particles was passivated with protein repellent polyethylene glycol (PEG). This approach allowed the determination of the amount of the immobilized BMP-2 by knowing the interparticle distance.

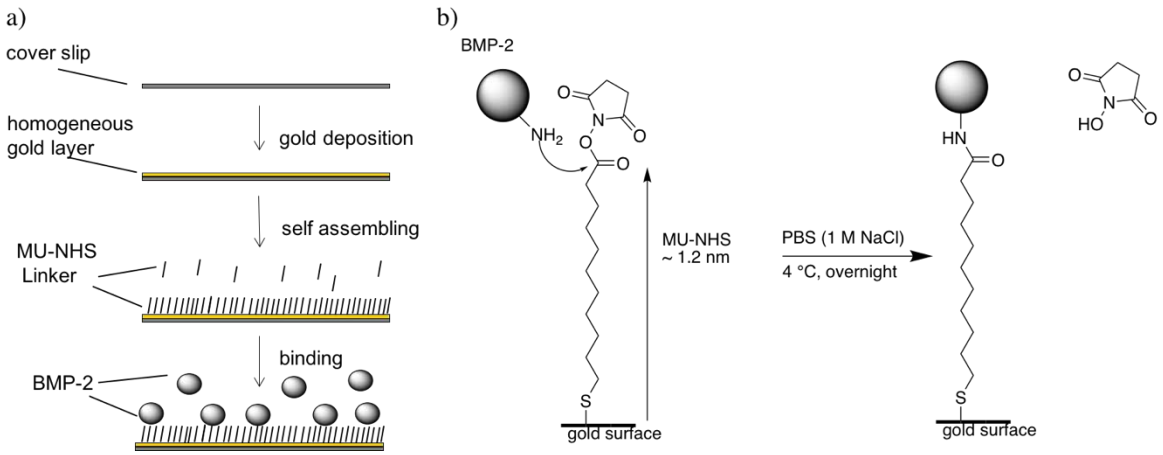

Figure 3.7 Preparation scheme of immobilized BMP-2 on homogeneous gold surfaces. a) Glass surfaces are coated with a gold layer and decorated with a SAM of the MU-NHS linker. Then BMP-2 is covalently immobilized with the NHS ester. b) Reaction scheme of the coupling process. Adapted from Pohl *et al.*[70]

Since the passivating PEG does not allow cell adhesion on the surfaces, this approach cannot be used for studies longer than a few hours. With this approach cells need to be stimulated from the top. The space between the surface and the cells harbors only a few μl of culture medium. Under these conditions, cells cannot survive for a long time. Therefore, the PEG background needs to be modified, which at the same time facilitates cell adhesion.

3.2.2 Adhesive ligands

Cell migration and adhesion are very essential processes for cells. The heterodimeric integrins belong to the most important family of cell adhesion receptors, which serve as bidirectional signaling units transducing interaction between the cell and extracellular matrix proteins[73]. These interactions lead to activation of intracellular pathways of integrin signaling promoting cell adhesion and migration. Intensive studies since the late 1980s have provided structural data revealing ligand recognition sites and biological functions[74]. At least 24 subtypes create the integrin family, which can consist of a different assemble of non-covalent association of 18 α and 8 β subunits[75]. Integrins control the cell polarity, survival and adhesion, in which force transmission from focal adhesions to ECM proteins are mediated, known as mechanotransduction[76]. In 1985, Ruoslahti and co-workers identified the integrin dimers $\alpha_v\beta_3$ and $\alpha_5\beta_1$, which recognize the RGD sequence, a tripeptide

consisting of arginine, glycine and aspartic acid[77]. In 1984, the RGD motif was described as the minimal adhesive binding motif[78], which means that it is the most simple molecule providing cell adhesion. Kessler and co-workers developed cyclic RGD (cRGD) peptides by cyclization, introduction of D-amino acids and structural studies in the early 1990s [79-81]. This peptide can be used to coat surfaces in order to promote cell adhesion. Furthermore, Rechenmacher *et al*.[82] described more peptides mentioning integrin $\alpha_v\beta_3$ and $\alpha_5\beta_1$ selective ligands which can be used to generate adhesive layers on surfaces. These ligands specifically address β_3 and β_1 integrin subunits, respectively. They allow the generation of an adhesive background in order to promote cell adhesion. Schenk *et al*.[83] described the modification of polyethylene glycol containing trimethoxy silane group and alkyne as reactive moieties. By applying copper(I)-catalyzed azide alkyne cycloaddition (CuAAC), also known as click reaction, ligands such as cRGD and $\alpha_5\beta_1$ selective ligand containing an azide group can be coupled to the PEG which are immobilized via the trimethoxy silane to the surfaces (see **Figure 3.8**).

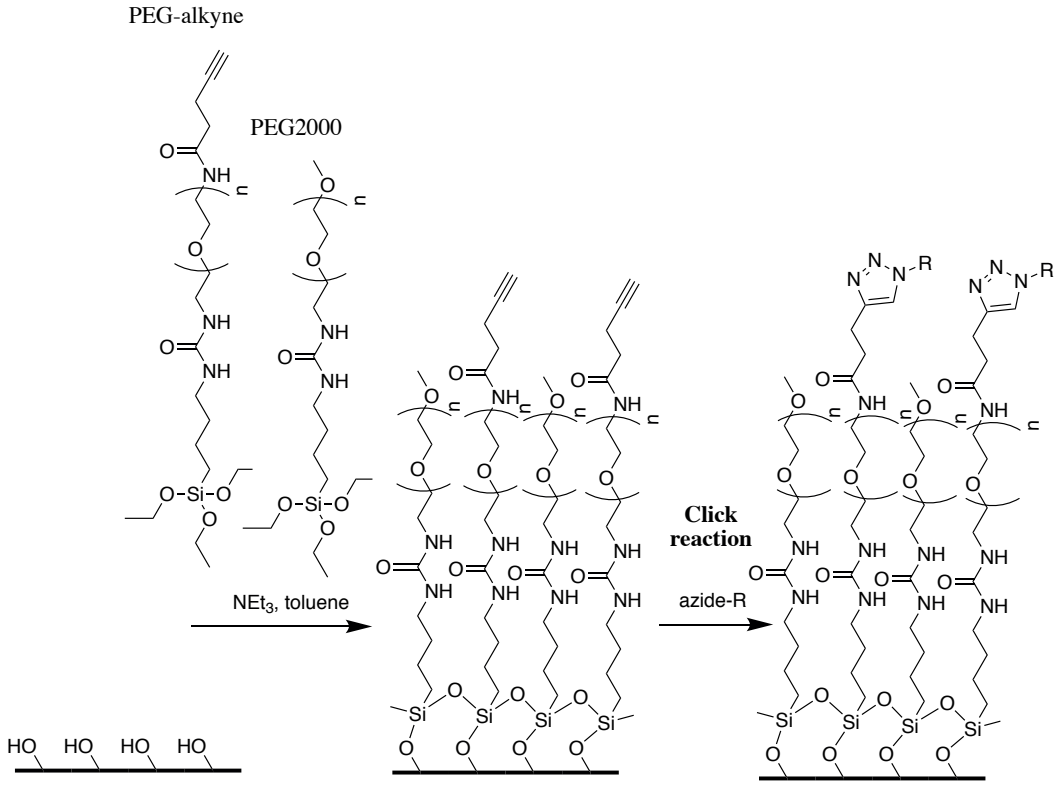

Figure 3.8 Schematic illustration of glass surfaces functionalization with PEG containing alkyne. By using copper(I)-catalyzed azide alkyne cycloaddition (CuAAC), the PEG layer is functionalized with molecules containing azide moieties. Adapted from Schenk *et al*.[83]

3.2.3 Immobilization of single molecules on gold nanostructured surfaces

Nanotechnology is one of the most promising techniques in the 21st century. It allows for usage systems, which are more than three orders of magnitude smaller than the recent components of the microelectronics. As mentioned before, the focus of interest has been on the immobilization of active proteins like growth factors[84], whereas physisorption release techniques do not allow to continuously stimulate and control the amount of immobilized protein, whereas block copolymer micellar nanolithography (BCMN) enables the control of the immobilized protein's density. The BCMN was established by Prof. Spatz and co-workers and offers an ideal platform for the investigations of interactions between cells and specific ligands or proteins in defined orders and spacings. This technique allows the production of nanostructured surfaces in a quasi-hexagonal array. The particle size can be varied between 1 - 15 nm and the inter particle spacing adjusted between 30 – 250 nm[85-86]. It is also possible to prepare a gradient spacing. Block copolymers, which consist of a hydrophobic polystyrene (PS) and a hydrophobic poly(2-vinylpyridine) (P2VP) unit (see **Figure 3.9**), are used for self-assembling micelles in an apolar solvent. At a concentration above the critical micelle concentration (CMC) micelle is reversed formed with the hydrophilic P2VP forming the core of the micelle. These micelles are loaded with a metal salt such as $HAuCl_4$.

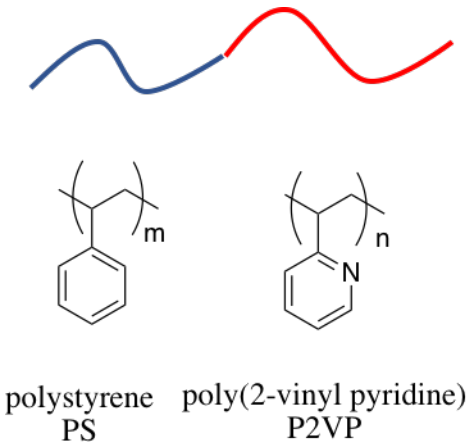

Figure 3.9 Structure of diblock copolymer. It consists of a non-polar polystyrene block (PS) and a polar poly(2-vinyl pyridine) block (P2VP).

To coat the micelles on the surfaces, either dip coating or spin coating (see section 5.1.2.3) techniques can be applied. Dip coating allows a uniform coverage of various kinds of solid substrates over large areas with high accuracy[87]. Cleaned glass substrates are immersed into the micelle solution as described in the scheme (**Figure 3.10**) and retracted with constant velocity. During this step called dip-coating, polymer chains bind to the surface forming a micellar monolayer on the surface (see **Figure 3.10** a) Another method to form a micellar monolayer on the surface is spin-coating. It is described in section 5.1.2.3. Subsequently, the substrates are treated with plasma in order to remove all polymers and reduce the gold salt to elementary gold forming a quasi-hexagonal array of gold nanoparticle (see **Figure 3.10** b). The resulting nanostructured surfaces can be visualized by using scanning electron microscopy (SEM, **Figure 3.10** c).

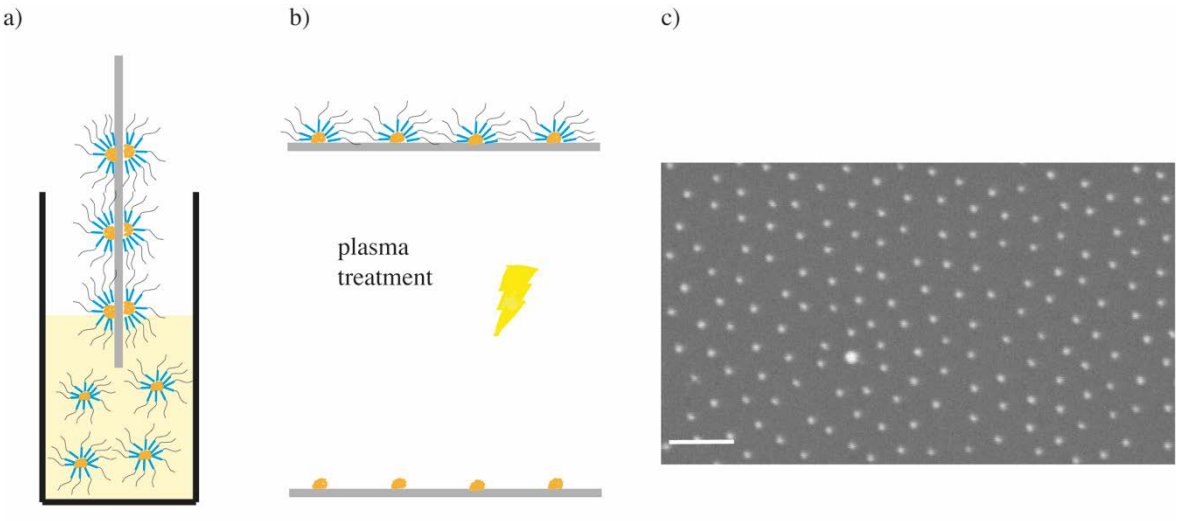

Figure 3.10 Preparation of nanostructured surfaces by BCMN. a) By immersing glass substrates into micellar solution, the block copolymers adsorb on the hydrophilic glass surface. Subsequently, the substrates are retracted at constant speed and the solvent evaporates leading to a quasi-hexagonal arrangement of the gold nanoparticles on the surface. b) By plasma treatment, the polymer matrix is removed and the gold ions are reduced to elementary gold. c) Gold nanostructured surface analyzed by SEM. The average interparticle distance is 100 nm (scale bar = 200 nm). Adapted from Baha-Schwab[88].

Several parameters influence the spacing of the gold particles. First, the spacing depends on the molecular weight of the diblock copolymers corresponding to their length, especially the size of the hydrophobic PS unit[85, 89-90]. Other parameters, which influence the spacing, are the concentration of the polymer solution as well as the dipping speed[86-87, 91-92]. Besides the spacing, the size of the gold nanoparticles can be varied from 1 – 15 nm by adjusting the

loading of the micellar core with metal salt[93]. This makes the BCMN favorable to prepare precisely tunable gold nanopatterns on surfaces. By controlling the distance between the nanoparticles, also the concentration of biomolecules or peptides, which can be immobilized using the particles as anchor points, can be varied[94-95].

In this work, BCMN was applied to generate controlled and covalent immobilization of growth factors to study their effect on intracellular signal transduction. 80 % of the gold nanoparticles carry exactly one protein, while 20 % carry none or two proteins. Based on that, the required amount was calculated and reduced to a minimum. Furthermore, it enables the long-term investigation of cell stimulation by growth factors. By covalent coating the area between the nanoparticles with protein-repellent PEG, unspecific protein adsorption is prevented, which facilitates the immobilization of molecules to the gold nanoparticles and avoids removing of the nanoparticles. Furthermore, the PEG background can be modified to serve as an additional anchor point for other molecules. This enables the co-immobilization of cell adhesive ligands between the gold nanoparticles carrying growth factors. This approach allows to mimic the natural cell micromillieu under controlled conditions.

4 Motivation

In the last decades, growth factors have been promising candidates for therapeutical treatment in regenerative medicine. However, a systemic application is not practicable, since uncontrolled diffusion causes a wide range of side-effects. Therefore, the goal of this study is to engineer dual functionalized surfaces presenting both, covalently immobilized BMP-6 and adhesive ligands using thiol-gold interaction and click chemistry for coupling to the PEG passivation layer, respectively. This approach was used to investigate the short- and long-term effect of the anchored growth factor and the adhesive ligands on C2C12 differentiation. So far, the chemical covalent immobilization of BMP-6 has not been published. However, in line with the approach presented by Pohl *et al.*[70] and Schwab *et al.*[72] who studied BMP-2 immobilization the amount and the surface density of the immobilized protein was controlled. BMP-6 seems to induce bone formation in genetically modified MSCs more efficiently than BMP-2. Furthermore, BMP-2 has been shown to cause adverse side-effects. This makes BMP-6 to the preferred choice above BMP-2.

To prove the covalent immobilization of BMP-6, gold surfaces coated with a bifunctional thiol-NHS linker and subsequently coupled with BMP-6 by addressing their primary amine groups to the surface were used. Block copolymer micellar nanolithography (BCMN) allows to fabricate gold nanostructured surfaces hexagonally arranged. These gold particles can be utilized to serve as anchor-points for the MU-NHS linker, which allows to determine the density and amount of immobilized growth factor by measuring the interparticle distance. Furthermore, the passivation of the interparticle space with protein-repellent PEG prevents the unspecific binding of BMP-6 to the glass surface. By modification of the PEG layer with alkyne moieties, it can be functionalized with cell adhesive ligands bearing an azide group, such as RGD and $\alpha_5\beta_1$ integrin selective ligands. This allows the long-term stimulation by immobilized BMP-6, since cells are able to adhere to the substrate's surface. Otherwise cells would die.

In this work, the approach explained above is developed to investigate and characterize the ability of immobilized BMP-6 to trigger short-term signaling and to induce osteogenic differentiation of C2C12 by long-term stimulation. Moreover, the minimal ligand density of iBMP-6 necessary to trigger cell signaling is determined. Finally, the developed set-up shall be tested in multiple myeloma cell lines by stimulating with immobilized BMP-6.

5 Material and Methods

5.1 Surface preparation

5.1.1 Preparation of homogenously coated gold surfaces

Glass coverslips (H 875 (24 x 24) mm^2, H 873 (20 x 20) mm^2, Carl Roth & Co GmbH, Karlsruhe) were precleaned with precision wipes (Kimberly-Clark Professionals, Koblenz-Rheinhafen), placed in custom-made Teflon racks and sonicated (Sonorex Super RK 102H, BANDELIN electronic GmbH & Co. KG, Berlin) for 15 min in a 1:1 mixture of ethylacetate (p.a., Carl Roth) and methanol (p.a. Carl Roth). After rinsing with methanol and drying in a nitrogen flow, the clean surfaces were successively coated with a 15 nm chromium layer (120 mA, 1.3 x 10^{-2} mbar, 40 s) and a 50 nm gold layer (60 mA, 5.0 x 10^{-2} mbar, 60 s) by using a MED 020 sputter coating system (BAL-TEC AG, Witten).

5.1.2 Preparation of gold nanostructured surfaces

5.1.2.1 Activation and cleaning of glass substrates

Piranha solution, a 3:1 mixture of concentrated sulfuric acid (95 %, Sigma-Aldrich, St. Loius, USA) and hydrogen peroxide (30 %, p.a., AppliChem), was used to clean the coverslips. The peroxymonosulfuric acid (H_2SO_5, Caro's acid) removes organic contaminations and activates the glass surface for the passivation with PEG2000 (see section 5.1.4.2). The substrates were washed with MilliQ water (18.2 MΩ x cm) and dried under nitrogen flow. Surfaces were further processed immediately.

5.1.2.2 Preparation of micellar gold solution

The poly(styrene-*b*-2-vinylpyridine) diblock copolymer (PS-*b*-P2VP, Polymer Source Inc., Montreal, Canada) (**Table 5.1**) was dissolved in the appropriate volume of toluene (p.a., Merck, Darmstadt) in a glass flask, which was cleaned according to section 5.1.1. The solution was stirred at RT for 24 h. Depending on the desired loading rate (L) < 1, which describes the molar ratio of P2VP-units and the metal salt $HAuCl_4$, a stoichiometric amount

of $HAuCl_4$ trihydrate (Sigma-Aldrich, St. Louis, USA) was added to the prepared solution. The amount of $HAuCl_4$ required is calculated by equation 5.1:

$$m(HAuCl_4) = \frac{m(Polymer) \cdot M(HAuCl_4 \cdot 3\,H_2O) \cdot P2VP_{units} \cdot L}{M(\mathrm{PS} + \mathrm{P2VP})} \qquad 5.1$$

Table 5.1 Overview of the characteristics of the polymers used in this work, specified by their chain length. PS: polystyrene; P2VP: poly-2-vinylpyridine

Polymer	$M_{PS\text{-}block}$ [g/mol^{-1}]	$M_{P2VP\text{-}block}$ [g/mol]	PS_{units}	$P2VP_{units}$
PS(30000)-*b*-P2VP(12500)	30000	12500	288	119
PS(110000)-*b*-P2VP(52000)	110000	52000	1056	495
PS(190000)-*b*-P2VP(55000)	190000	55000	1824	523

The molecular weight of $HAuCl_4$ depends on the amount of crystal water. In this work $HAuCl_4$ trihydrate (M($HAuCl_4$) = 393.83 g/mol) was utilized. The molecular weight M(Polymer) and the amount of $P2VP_{units}$ of the used polymers are listed in **Table 5.1**. The mixture was stirred for 24 h until all $HAuCl_4$ was dissolved. The micellar solution was purified through a polytetrafluoroethylene (PTFE) filter with a pore size of 0.22 μm (Millipore, Eschborn) to remove polymer aggregates and undissolved metal salt residues. The gold solution was stored under nitrogen atmosphere and light protected. A list of the used micellar polymer/gold solution is given in **Table 5.2**.

Table 5.2 Polymers used for the production of nanopatterns. M: molecular weight of the diblock copolymer, c: concentration of the polymer, L: loading or molar ratio between $HAuCl_4$ and PS-*b*-*P2VP*

Polymer	M [g/mol]	c [mg/l]	L
PS(30000)-*b*-P2VP(12500)	42500	5	0.5
PS(110000)-*b*-P2VP(52000)	162000	5	0.5
PS(190000)-*b*-P2VP(55000)	245000	3	0.5

5.1.2.3 Spin coating

The cleaned glass substrates were placed in a ws-650 mz-23 npp spin coater system (Laurell, North Wales, USA). Then a specific volume (substrate-size depended: (20 x 20) mm^2: 20 μl; (24 x 24) mm^2: 25 μl) of the gold polymer solution was applied in the center of the spinning substrate (9000 rpm). The fluid was spread by the centrifugal force. After evaporation of the solvent, substrates were exposed for 45 min to an isotropic microwave-induced hydrogen plasma (PVA TePla AG, Wettenberg) to reduce the gold ions to metallic gold and burn off the polymer. For this purpose, either a TePla PS 210 (p_{H2} = 0.3 mbar, 600 W) or a TePla100-E (p_{H2} = 0.4 mbar, 150 W) was used. In the last step, the gold nanoparticle substrates were tempered at 300 °C for 72 h by using a drying oven (Binder GmbH, Tuttlingen). Two samples of each batch (n = 20) were analyzed by scanning electron microscope (SEM) at different positions on the samples. The obtained images were further analyzed by using a plug-in for ImageJ (Research Services Branch, Image Analysis Software, NIH, USA) written by Dr. Philippe Girard (Institute Jacques Monod, Paris), based on an algorithm developed by Kansal *et al*. In order to ensure a good quality, the order parameter ϕ and the average distance between neighboring gold nanoparticles were determined.

5.1.2.4 Dip coating

Dip coating offers another possibility to decorate glass substrates with a hexagonally ordered micellar monolayer. Glass coverslips were retracted from gold polymer solutions (see **Table 5.2**) with constant velocity by using a custom-made dip-coating device in order to form a micellar monolayer. After evaporation of toluene, substrates were plasma treated as described in section 5.1.2.3. Substrates prepared with this method consist of a dipping edge.

5.1.3 Functionalization of homogeneous gold surfaces

5.1.3.1 Immobilization of heterobifunctional linkers

In order to immobilize BMP-6 to homogeneous gold surfaces, the heterobifunctional linker 11-mercaptoundecanoyl-*N*-hydroxysuccinimide ester (MU-NHS, ProChimia Surfaces, Poland) was bound to the gold surface through its thiol group. The MU-NHS was dissolved

in DMSO (p.a., Carl Roth) to obtain a final concentration of 1 mM. Substrates with homogeneous gold surface were incubated in the solution at RT for 4 h. After removing unreacted linker from the surfaces by sonicating in DMSO for 2 min, the substrates were rinsed with DMSO and methanol (p.a., Carl Roth) and finally dried in nitrogen stream.

5.1.3.2 Surface immobilization of BMP-6

The *N*-hydroxysuccinimide ester group of the linker reacts with free primary amines (Lysine residues and N-terminus) of the BMP-6 protein under physiological to slightly alkaline conditions (pH 7.5 – 8.5) to obtain a stable amide bond. Lyophilized, glycosylated and carrier-free recombinant human BMP-6 expressed in mammalian cells (Genera Research d.o.o., Crotia) was dissolved in sterile 4 mM HCl to obtain a stock solution with a concentration of 100 μg/ml. Aliquots were stored at -20 °C. The stock solution was diluted in PBS (Gibco, Life Technologies GmbH, Darmstadt) containing 1 M NaCl (Sigma-Aldrich, St. Lois, USA) in order to obtain a solution with a final concentration of 1 μg/ml (approx. 33 nM). The BMP-6 solution was adjusted to pH 8.5 immediately prior to use by adjusting with 10 mM KOH (Carl Roth).

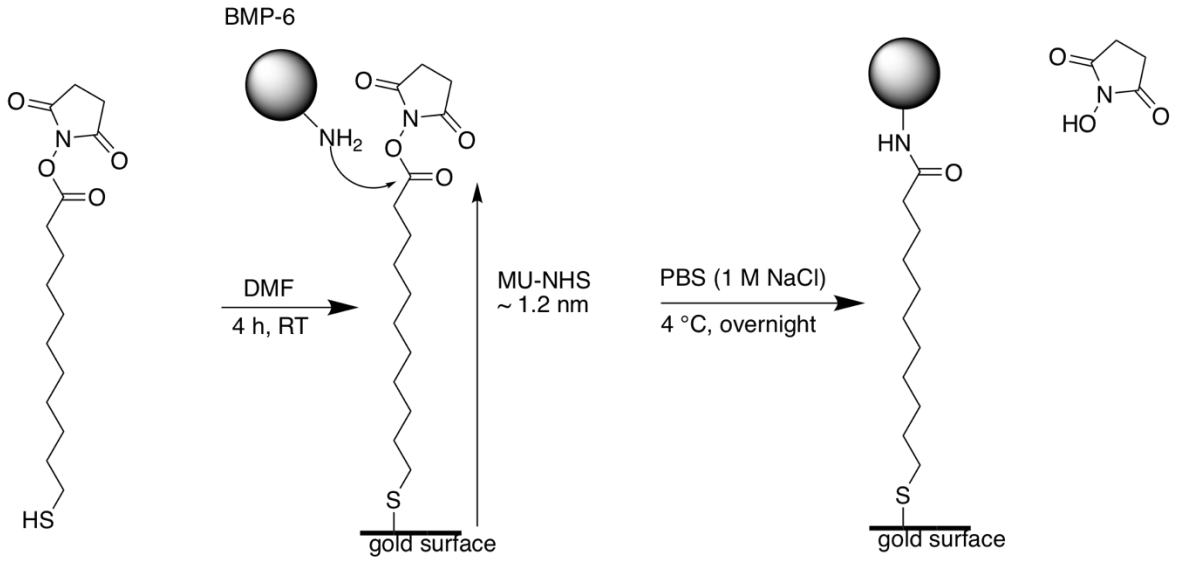

Figure 5.1 Immobilization of BMP-6 to homogenous gold surfaces. The heterobifunctional MU-NHS linker binds through its thiol group to gold surfaces. Afterwards BMP-6 is covalently coupled to the NHS ester by free primary amines.

In custom-made poly(dimethyl siloxane) (PDMS, Sylgard 184, silicone elastomer kit, Dow Corning, Midland, USA) chambers MU-NHS-functionalized surfaces were incubated with the BMP-6 working solution overnight at 4°C. After sonication in PBS containing 1 M NaCl for 1 min, the substrates were washed three times in PBS / 1 M NaCl to remove unbound protein.

The surface concentration of the immobilized BMP-6 (Γ= amount of BMP-6 on the surface / surface area) was calculated by the equation 5.2:

$$\Gamma(BMP-6) = \frac{M\ (BMP6)}{area\ (BMP6) \times N_A} = \frac{30000\,\frac{g}{mol}}{(8\ nm)^2 \times \frac{\sqrt{3}}{4} \times 6.022 \times 10^{23}\ mol^{-1}} \approx 80\ ng/cm \qquad 5.2$$

The following parameters were assumed:

I) The diameter of a BMP-6 dimer is approximately 8 nm.

II) The molecular weight of a dimer is 30000 g/mol.

III) The binding of BMP-6 by the MU-NHS linker to the surface follows a hexagonal distribution[70].

5.1.4 Functionalization of gold nanostructured glass surfaces

5.1.4.1 Synthesis of PEG2000 and PEG3000-alkyne

α-Methoxy-ω-amino poly(ethylene glycol) (Iris Biotech GmbH, Germany) (1 g, 0.5 mmol, MW 2160 g/mol) and α-amino-ω-propargylacetamido poly(ethylene glycol) (1.66 g, 0.5 mmol, MW 3317 g/mol), respectively, were dissolved in dry DMF (4 ml, p. a., Carl Roth) under argon atmosphere and stirred for 10 min. 1.1 equivalents of 3-(triethoxysilyl) propylisocyanate (95 %, Sigma Aldrich) were added and the mixture was stirred at RT for 16 h. The reaction was cooled down to 0 °C for 10 min and a 10-fold excess of ice-cold diethyl ether (Sigma-Aldrich) was added. After 1 h the suspension was filtrated and the precipitate was washed with cold ether. The purified product was dried under reduced pressure for 24 h to yield a white powder. Synthesis was performed in cooperation with F. Schenk (Physical Chemical Institute, Heidelberg University) and the characterization of the product is described in Schenk *et al.*[83] in detail (**Figure 5.2**).

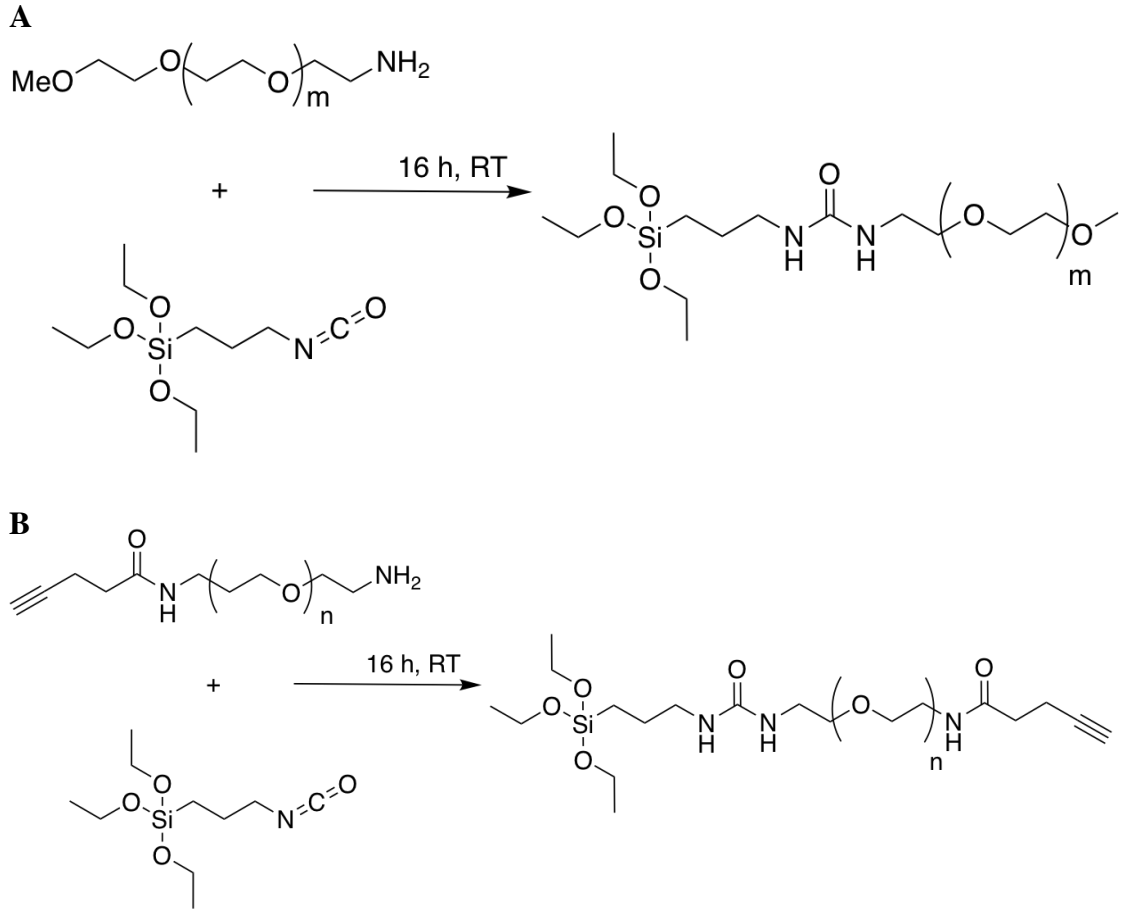

Figure 5.2 Synthesis of PEG2000 (A) and PEG3000-alkyne (B). Condensation of α-methoxy-ω-amino poly(ethylene glycol) (m = 47) and 3-(triethoxysilyl) propylisocyanate (A). Condensation of α-amino-ω-propargylacetamido poly(ethylene glycol) (n = 72) and 3-(triethoxysilyl) propylisocyanate (B).

5.1.4.2 Covalent immobilization of PEG2000

The space between gold nanoparticles was passivated with a protein repellent PEG2000 monolayer in order to avoid non-specific protein and cell interactions with glass. The triethoxysilane groups of PEG2000 react with the silicon dioxide covalently coupled to the surface (**Figure 5.3**).

Nanopatterned substrates were activated in reactive oxyden plasma (p_{O2} = 0.4 mbar, 150 W) for 10 min. Afterwards the surfaces were immersed in a solution of 250 μM PEG2000 in dry toluene (p.a., Merck) and 0.01 equivalents of triethylamine (≥99.5 %, Sigma Aldrich) at 80 °C for 14 h under argon atmosphere. The samples were sonicated in ethylacetate (p. a.) and methanol (p. a.) for 5 min each. The substrates were rinsed with methanol and dried in

a stream of nitrogen to be immediately processed. The covalent coupling of BMP-6 was performed as described in section 5.1.3.

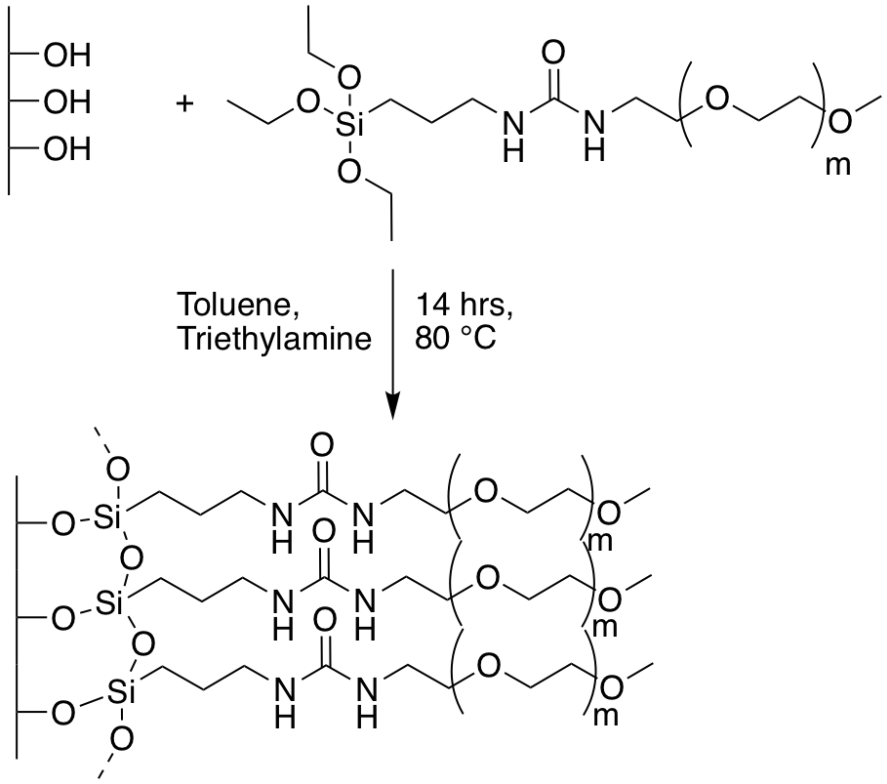

Figure 5.3 Passivation of gold nanostructered glass substrates. After activation of glass surfaces in hydrogen plasma, PEG2000 was covalently coupled to the substrate.

Table 5.3 Surface density of immobilized BMP-6. Gold NP = gold nanoparticle

Inter particle distance d [nm]	No. of gold NP per μm^2	No. of gold NP with iBMP-6 per μm^2	Density of BMP-6 on the surface [ng/cm^2]	Amount of BMP-6 per sample [ng]
32 ± 8	803 ± 54	723	3.3	19
63 ± 11	281 ± 17	253	1.1	6
107 ± 21	51 ± 12	46	0.2	1

The inter particle distance between the Au nanoparticles was used to determine the average number of gold nanoparticles per μm^2 to calculate the amount of immobilized BMP-6 (**Table 5.3**). The analysis of the SEM images served as the basis of the calculation (see

section 6.2.2.1). These took into account the order parameter and not the theoretical values, because this would assume a perfectly hexagonal order, what is impossible. Assuming a coverage of 90 % of the gold nanoparticles harbor at least one BMP-6 dimer, it was determined that the number of gold nanoparticles per μm^2 is equal to the number of iBMP-6.

These assumptions based on AFM measurements on passivated gold nanostructured substrates with covalently immobilized BMP-2 on the nanoparticles. Measurements and determination of the nanoparticle-BMP-2 binding ratio were performed by Dr. Theresa Pohl[96].

5.1.5 Dual functionalization of gold nanopatterned glass surfaces

The dual functionalization is an improved development of the gold nanostructured surfaces[83]. This allows the independent immobilization of a second single molecule on the surface. The space between the gold nanoparticles was coated with a PEG2000 and PEG3000-alkyne mixture. This enables to immobilize the second molecule through the copper(I)-actalyzed azide alkyne cycloaddtion (CuAAC), also known as the click reaction. K. Barry Sharpless introduced this term in 2001[97], naming a decisive development of a set of highly reliable and selective reactions, which allow for the covalent bonds between molecules having different functional groups.

5.1.5.1 Passivation with PEG2000 and PEG3000-alkyne

Nanopatterned substrates were activated in reactive oxygen plasma (p_{o2} = 0.4 mbar, 150 W) for 10 min. Afterwards the surfaces were immersed in a mixture of 250 μM PEG2000 and 2.50 μM PEG3000-alkyne in dry toluene (p.a., Merck) and 0.01 equivalents of triethylamine (≥99.5 %, Sigma Aldrich) at 80 °C for 14 h under argon atmosphere (**Figure 5.4**). The samples were sonicated in ethylacetate (p. a., Merck) and methanol (p. a., Sigma Aldrich) for 5 min each. The substrates were rinsed with methanol and dried in a stream of nitrogen to be processed immediately.

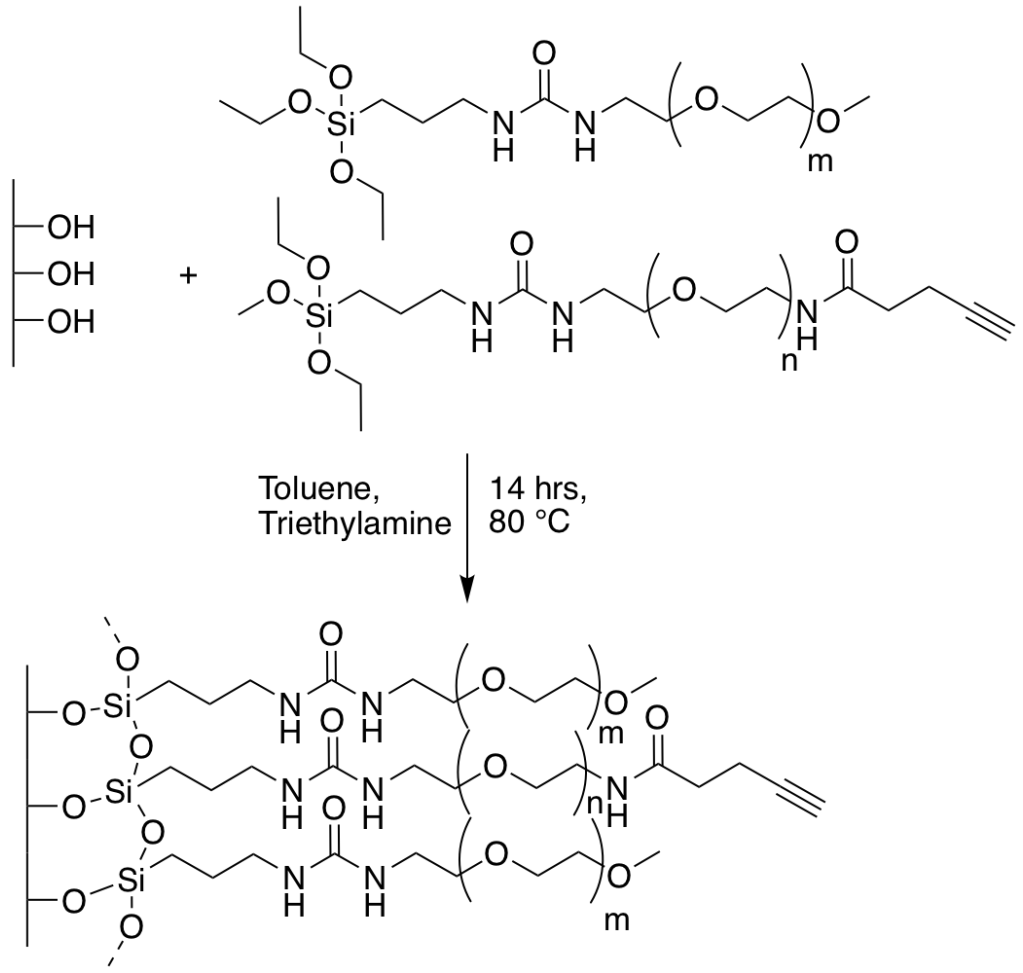

Figure 5.4 Passivation and functionalization of gold nanostructured glass substrates. After activation of glass surfaces in oxygen plasma, PEG2000 and PEG3000-alkyne were covalently bound to the substrate surface. Adapted and modified from Martin *et al*.[98]

5.1.5.2 Coupling of peptides by CuAAC

The copper(I)-catalyzed azide-alkyne cycloaddition can be performed at RT and in aqueous solvents. Furthermore, the wide pH range from 4 – 12, the enormous turnover rate (10^7 – 10^8) compared to the non-catalyzed click reaction and the tolerance of a wide spectra of functional groups make the CuAAc to one of the most favorable reactions. Sodium ascorbate reduces the Cu(II) species to the active Cu(I) catalyst.

Click reaction was performed according to Schenk *et al*.[83]. Glass substrates passivated with PEG3000-alkyne (section 5.1.5.1) were incubated with 50 μl of a freshly prepared reaction solution containing 100 mM L-ascorbic acid, 100 mM Tris HCl (pH 8.5), 0.15 mM azide-

containing molecule and 1 mM $CuSO_4$ in a humidity chamber at RT for 2 h. Samples were washed three times with MilliQ water, dried in a stream of nitrogen and immediately processed (**Figure 5.5**).

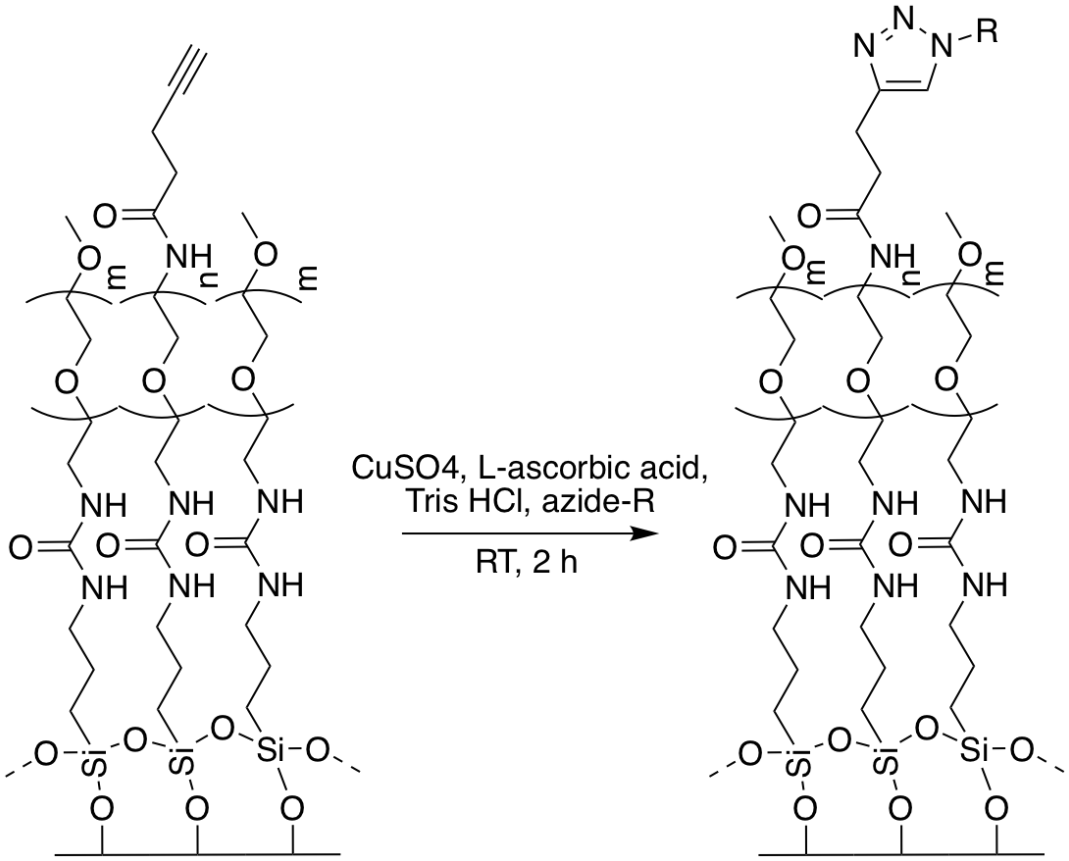

Figure 5.5 Functionalization of PEG passivated background by introduction of azide-containing peptides through azide-alkyne cycloaddition reaction.

In this work, two different adhesion molecules were coupled to the PEG3000-alkynethe by their azide moieties. The $\alpha_5\beta_1$-integrin-selective peptidomemetic (**Figure 5.6** A) is an artificial ligand, which binds strongly to integrin $\alpha_5\beta_1$ resulting in cell adhesion, that is selectively mediated by this specific integrin heterodimer[82]. The molecule was kindly provided by Prof. Dr. Horst Kessler (TU Munich). The tripeptide motif RGD, which is present in many ECM proteins, is known to induce cell adhesion[99-102]. The cyclic peptide c(RGDfE)K(N_3) (cRGD-azide) (PSL Peptide Specialty Laboratories GmbH, Heidelberg) contains this motif and serves as a ligand for several integrins (**Figure 5.6** B).

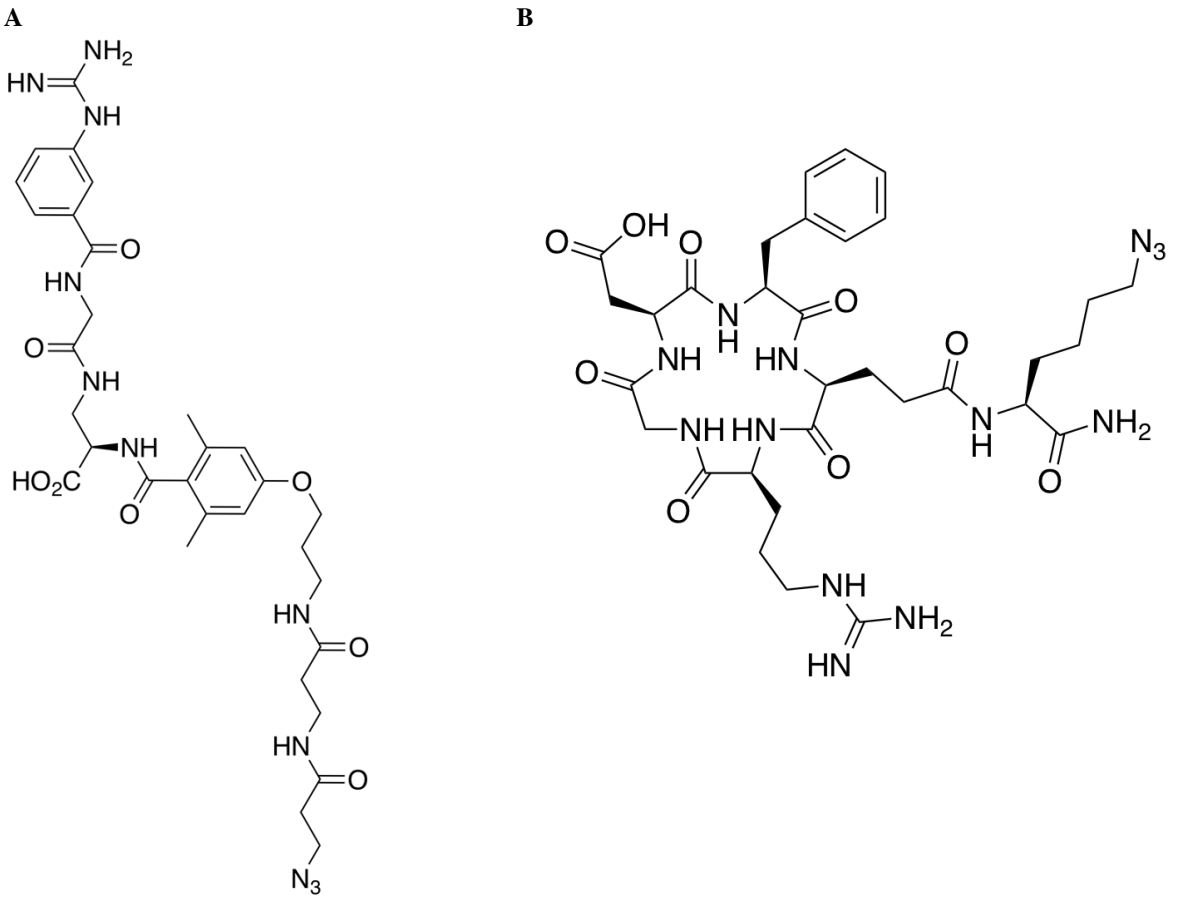

Figure 5.6 Chemical structure of $\alpha_5\beta_1$-integrin-selective peptidomimetic (A) and cyclic RGD (B). Functionalization of surfaces with the peptidomimetic (A) and cyclic RGD (B) results in cell adhesion, whereby cell adhesion, induced by A, is selectively mediated by integrin $\alpha_5\beta_1$.

5.1.6 Preparation and functionalization of gold nanostructured PEG-DA hydrogels

5.1.6.1 Synthesis of polyethylene glycol diacrylate (PEG10000-DA)

In this work polyethylene glycol-diacrylate with a molecular weight of 10000 g/mol was used and synthesized according to Elbert *et al.*[103] with the technical support of Radka Koelz (Max-Planck Institute for Intelligent Systems, Stuttgart) (**Figure 5.7**). PEG10000 (50 g, 5 mmol; Iris Biotech GmbH, Germany) was dissolved in dichloromethane (125 ml, Sigma Aldrich) and toluene (75 ml, Merck) under nitrogen atmosphere. Triethylamine (1.4 ml, 10 mmol, Sigma Aldrich) and acryloyl chloride (1.25 ml, 15 mmol, Sigma Aldrich) were added and the reaction mixture was stirred at RT for 16 h. The raw product was filtered

through Al_2O_3 (Roth). K_2CO_3 (12.5 g, 90.5 mmol, Roth) was added and the solution was stirred at RT for 1.5 h. The mixture was filtered again through Al_2O_3 and the solvent was removed under reduced pressure. The residue was dissolved in diethyl ether (400 ml, Roth) while stirring. The suspension was filtered and washed with diethyl ether. The PEG10000-DA was dried under vacuum.

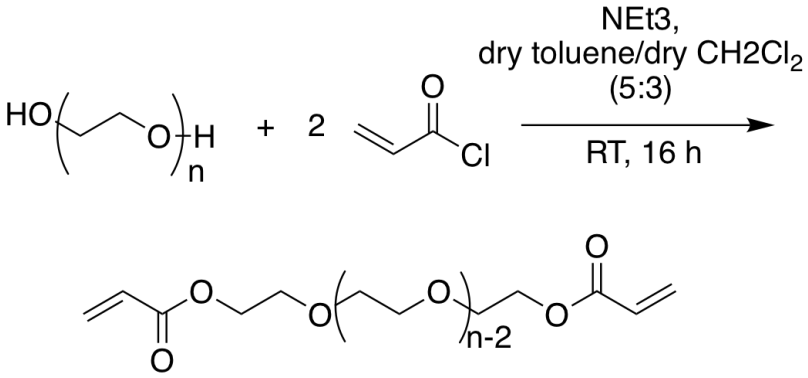

Figure 5.7 PEG-DA synthesis. Condensation of PEG10000 and acryloyl chlorid.

5.1.6.2 Preparation of gold nanostructured PEG-DA hydrogels

To optimize the handling during the experiments, the gold nanostructured hydrogels were prepared as glass-supported gels. For this, glass substrates were cleaned as described in section 5.1.2.1 and activated in reactive oxygen plasma (p_{o2} = 0.4 mbar, 150 W) for 10 min. Followings, the substrates were placed in a desiccator together with 1 ml (3-aminopropyl)triethoxysilane (APTES, Alfa Aesar) under vacuum. At the following day, the functionalized surfaces were removed from of the silane atmosphere. After the unbound APTES volatilized the substrates were used for the copolymerization to bind the hydrogels. The gold nanostructured glass substrates (section 5.1.2) were incubated in 2 mM solution of *N*,*N*-bis(acryloyl)-cystamine (Alfa Aesar, Karlsruhe) in pure ethanol at RT for 1 h. Afterwards unbound linker was removed by washing with pure methanol and substrates were dried under nitrogen stream. **Figure 5.8** shows the procedure of the hydrogel synthesis.

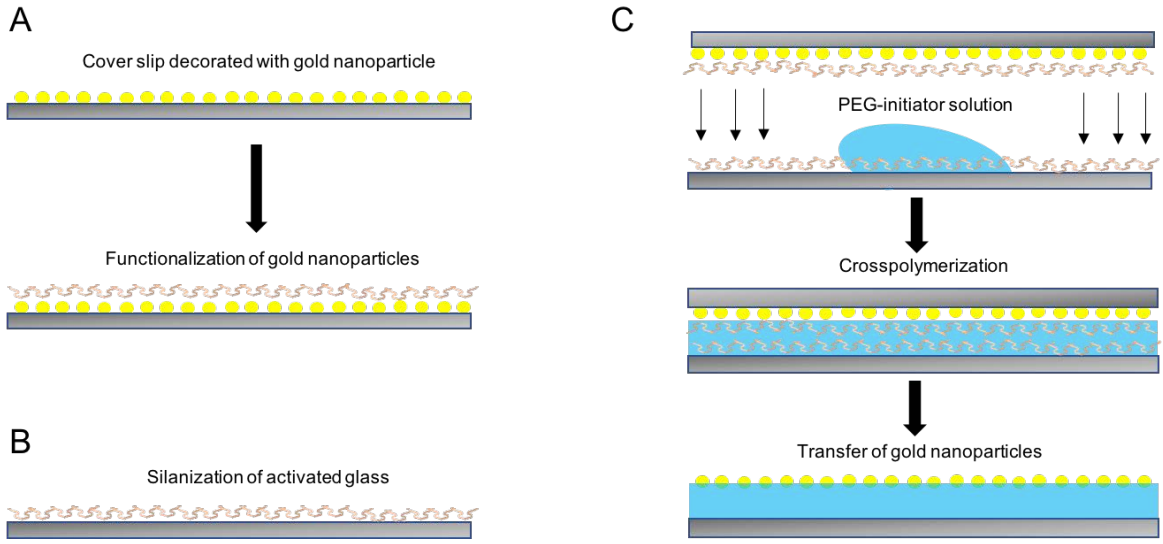

Figure 5.8 Preparation of gold nanostructured hydrogels bound to a glass surface. (A) The gold nanoparticles, which orientated in a quasi-hexagonal structure on the glass surface, were transferred to the hydrogel during the polymerization process by using (*N*,*N*-bis(acryloyl)cystamine) as crosslinker. (B) The glass substrate was functionalized with (3-aminopropyl)triethoxysilane after cleaning and activating. (C) The PEG-DA-solution, containing APS and TEMED, was pipetted onto the APTES functionalized glass substrate and covered by in (A) prepared surfaces. Since the polymerization started immediately after addition of APS and TEMED, the embedding needed to be done quickly. After 30 min in darkness, the substrate was placed in pure water. Here, the glass coverslip on top started detaching, induced by the swelling process of the hydrogel, while the gold nanoparticles remained attached to the hydrogel. Thus, the gold structure was transferred to the hydrogel surface, which was bound to the lower coverslip.

The PEG-DA (MW : 10000 g/mol) was dissolved in degassed water to obtain a final concentration of 150 mg/ml and stirred at RT for 30 min. Afterwards, a 10 % (w/v) solution of the polymerization initiator ammonium persulfate (APS) in degassed water and the polymerization catalyst tetramethylethylenediamine (TEMED) were added to the PEG mixture. APS was used in a concentration of 0.35 μl/mg PEG-DA and TEMED was used in a concentration of 0.05 μl/mg PEG-DA. This PEG-initiator solution was embedded between the gold nanostructured surface, functionalized with *N*,*N*-bis(acryloyl)cystamine linker, and the activated glass substrates containing APTES. By adding APS and TEMED the cross-polymerization between the unsaturated acrylate groups of each linker and the PEG solution was initiated. This results in chemical bonding of the hydrogel to the glass substrate and the transfer of the gold nanoparticle. The samples were covered with aluminum foil at RT for 30 min. The preparation was done in a custom-made Teflon™ form of 25 mm x 25 mm. The size of the synthesized hydrogels is determined by the used coverslips (24 mm x 24 mm).

The substrates were placed in either pure water or sterile PBS for 48 h in order to allows swelling to equilibrium. They were stored in the dark at 4 °C. In **Figure 5.9**, the mechanism of chain propagation during the cross-polymerization is shown. In this way, the gold nanoparticles are coupled covalently to the hydrogel surface and the hydrogel is tethered on the glass coverslip.

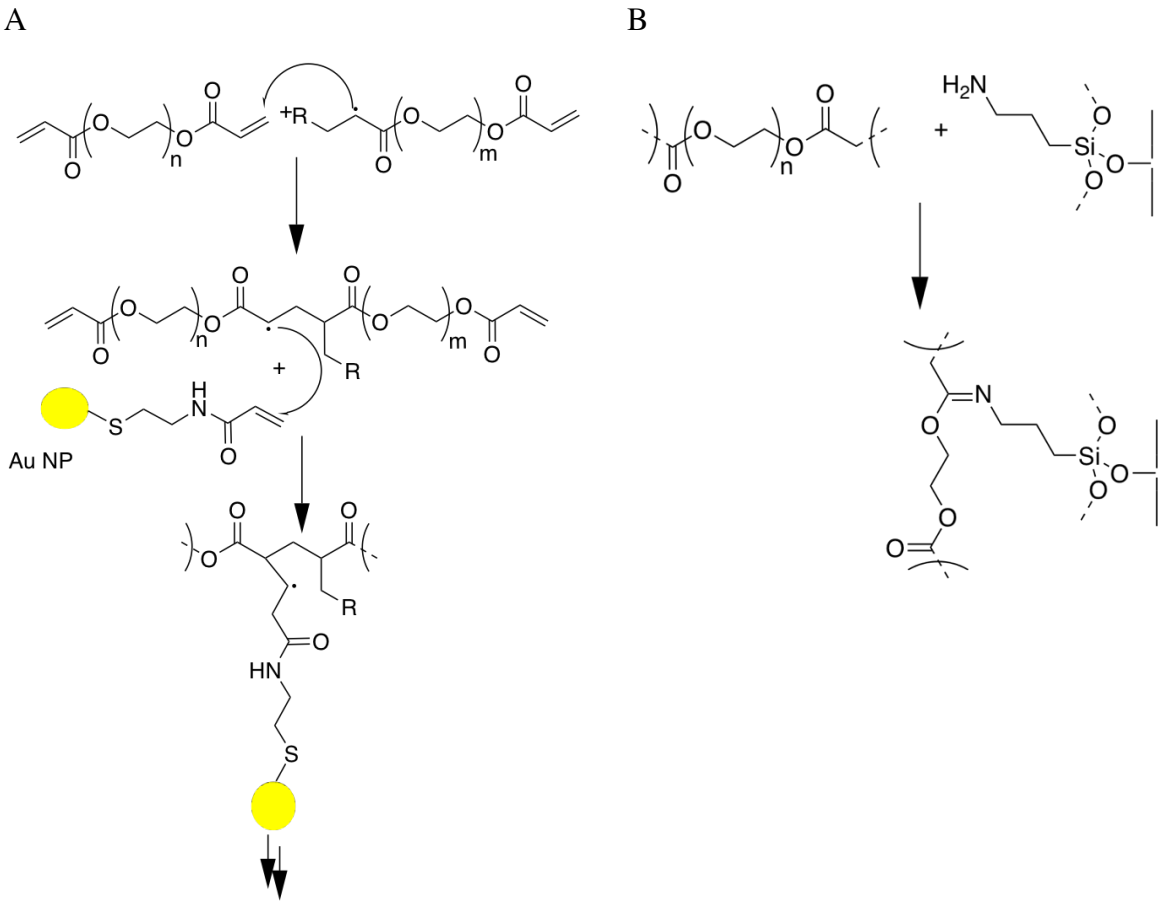

Figure 5.9 Mechanism of the cross polymerization. (A) Transfer of the gold nanoparticles by crosslinking of PEG-DA and the *N*,*N*-bis(acryloyl)cystamine linker. (B) Binding of the hydrogels to the glass substrates. The (3-aminopropyl)triethoxysilane, bound to the glass surface, reacts in a radical reaction with the polymerized PEG-DA.

The MU-NHS was dissolved in DMSO to obtain a final concentration of 100 mM. Then, this solution was diluted with water to a final concentration of 1 mM. The hydrogels with gold nanostructured surface were incubated in the diluted solution at RT for 4 h. After removing unreacted linker from the surfaces by sonicating in water for 2 min, the substrates

were rinsed with PBS. The covalent immobilization of BMP-6 was performed as described in section 5.1.3.2.

5.1.6.3 Generating an adhesive background on PEG-DA hydrogels

In order to induce cell adherence to hydrogels, different methods were used to generate an adhesive background on gold nanostructured PEG-DA hydrogels.

5.1.6.3.1 PLL coating

After BMP-6 immobilization, gels were incubated with a 0.1 mg/ml solution of Poly-L-lysine–FITC labeled (MW ~ 15000 – 30000, Sigma Aldrich) in MilliQ water at RT for 1 h. Before usage, the substrates were washed with MilliQ water three times on a shaker for 10 min.

5.1.6.3.2 Incorporation of cyclic peptide c(RGDfE)K(N_3) into hydrogels

To incorporate cRGD-azide into the hydrogel, cRGD was added to the PEG-DA polymer solution (section 5.1.6.2) in three different concentrations (1.5 mM, 0.15 mM and 0.015 mM). PEG-DA and cRGD were mixed before adding APS and TEMED. The polymerization was performed according to section 5.1.6.2.

5.2 Surface characterization

5.2.1 Characterization of functionalized substrates

5.2.1.1 Quartz crystal microbalance with dissipation (QCM-D)

Fundamentals:

The principles of a QCM-D are based on the inverse piezoelectric effect. An electric potential is generated in dielectric crystals with permanent dipoles and symmetric distribution of charges, if the charges are moved by mechanical stress. This effect can be observed in the opposite direction as well. By applying an external voltage, a deformation of the crystal structure is induced. By using alternating current voltage, the crystal starts oscillating. If the excitation frequency matches with the resonance frequency f_0, it results in

resonance. After turning off the alternating current voltage, the crystal continues to vibrate mechanically. This oscillation can be quantified by measuring the reducing electrical field. The decrease of the damped oscillation's energy compared to the total energy is called dissipation (*D*). In equation 5.3, the resulting oscillation is described.

$$A(t) = A_0 \exp(-\pi f D t) \sin(2\pi f t + \theta) \tag{5.3}$$

Here, A_0 is the start amplitude of vibration, f is the frequency and θ is the phase angle of f. Considering the dissipation conclusion about the properties of the adsorbed masses can be made. Soft and inert masses cause higher dissipation than rigid masses. In case of an elastic and soft adsorbate, the crystal slows down faster.

A quartz crystal can be used as mass sensor, since the oscillation frequency is decreased by coating with either a rigid or a soft and elastic mass. Besides the basic oscillation, the odd overtones (n=1, 3, 5,…13) are able to induce resonance vibration. The relation between the frequency modulation and the adsorbed mass is given by the Sauerbrey equation 5.4[104].

$$\Delta m = -\frac{\upsilon_q \rho_q}{2 f_0^2} \times \frac{\Delta f}{n} = -C \frac{\Delta f}{n} \tag{5.4}$$

The mass sensitivity constant C summarizes Δm = mass difference, Δf_n = frequency difference and the specific variables of the quartz, $\Delta \rho$ = quartz density (2.65 ng × cm^{-2}), υ_q = sound velocity in the crystal (3340 m × s^{-1}). The sensor of the E4 sensor system has a value of 17.7 ng × cm^{-2}Hz for the mass sensitivity constant C in liquid. To apply the Sauerbrey equation, the following conditions for the adsorbed masses need to be fulfilled: a) the mass must be rigid, b) the mass must not shift, c) the mass must be homogeneously distributed on the crystal and d) the mass must be small compared to the mass of the crystal. Therefore, deviations will appear in measurements of soft masses. To avoid these variations, there are different measuring methods like surface plasmon resonance (SPR)[105], reflectometry[106] and ellipsometry[107]. These methods can only be used for the analysis of dry masses, whereas in QCM-D measurements, only hydrated masses are measured. Since the experiments in this work were performed in liquid, the QCM-D was the method of choice.

The formation of a self-assembled monolayer (SAM) of MU-NHS linker on an Au surface and the subsequent immobilization of BMP-6 were observed by using a quartz crystal microbalance. The measurements were performed with the E4 sensor system from Q-Sense (Västra Frölunda, Sweden) in an open module at RT and the software QSoft401 (version 1.4.2). The analysis was done with QTools (version 2)

5.2.1.2 X-ray photoelectron spectroscopy (XPS)

X-ray photoelectron spectroscopy is a surface-sensitive, established method to analyze the chemical composition of solid substances and determine nondestructively their surfaces, respectively. Furthermore, it allows identification and quantification of chemical elements and their chemical environment (oxidation state) with a depth of max. 10 nm as well as information about the oxidation levels and binding states can be obtained. XPS belongs to the group of photoemission spectroscopy (PES) methods. PES in general and XPS in particular are based on the physical principle of Einstein's photoelectric effect. By irradiation of a surface with electromagnetic radiation, which has an energy hν higher than the work of emission Φ of the sample, the difference between the vacuum energy E_{vac} and the Fermi energy E_F, electrons are excited from occupied ground states to unoccupied, unbound end states of the sample (**Figure 5.10**)[108]. This means, that electrons are released from the sample, where their speed can be measured. The kinetic energy E_{kin} of an irradiated electron can be described by equation 5.5:

$$E_{kin} = h\upsilon - E_F - \Phi \qquad 5.5$$

XPS examines emissions of low-energy electrons in the range of 20 – 2000 eV. Aluminum (1486.7 eV) and magnesium (1253.6 eV) are typical X-ray sources. The binding energy E_B of a core electron in a solid refers to the Fermi energy E_F. Therefore, E_B can be determined by measuring E_{kin} and using equation 5.5. This leads to peak position of the referring chemical element[109]. The peak position can be shifted up to 10 eV caused by the chemical environment and the oxidation state, respectively. Core electrons don't have high possibility to scatter inelastically. For this reason, the kinetic energy of electrons, which scatter

inelastically, cannot be used for determination of binding energy and appear only in the background of the spectra[108, 110].

To determine the time, in which the NHS ester is stable in aqueous solvent, three conditions were chosen: 1st surfaces coated with homogenous gold were decorated with MU-NHS linker as described in section 5.1.3.1. 2nd Surfaces were incubated in PBS for 20 min at RT after decoration with MU-NHS. 3rd Surfaces were incubated with MU-NHS linker in DMF for only 20 min at RT. Substrates were shortly rinsed with MilliQ water, dried in nitrogen flow and analyzed by XPS MAX 200 photoelectron spectrometer (Leybold-Heraeus, Cologne) with Mg K_α radiation source (1253.6 eV) operated at 220 W and in ultra-high vacuum below 10^{-8} mbar. For the acquisition of the spectra emitted electrons were collected perpendicularly to the sample surface with a hemispherical electron energy analyzer at constant pass energy of 96 eV and 48 eV for overview spectra and detailed spectra, respectively.

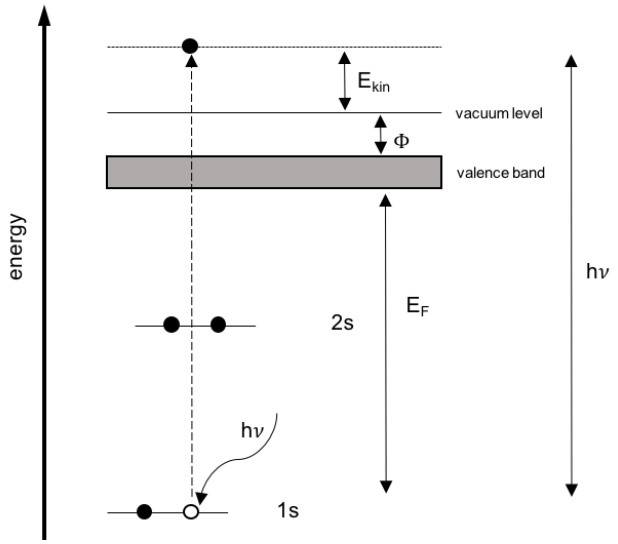

Figure 5.10 Scheme of the XPS functioning process. An atom emits an electron from the 1s energy level after photoionization by X-ray irradiation[108, 110].

The recorded spectra were normalized by the spectrometer specific transmission function, which is specific for the spectrometer. The binding energy was calibrated to 84.0 eV for elemental gold in order to compensate electrostatically charging of the samples[111]. The spectra were analyzed with the software XPS Peak 4.1[112]. Spectra were background corrected for signal quantification by subtracting the background according to Shirley and fitted by a

symmetric Voigt function with a variable Gauß-Lorentz product function. The spectra were plotted in Origin 8.5.

5.2.1.3 Infrared reflection absorption spectroscopy (IRRAS)

The IR spectroscopy is a qualitative spectroscopy method and based on the stimulation of vibrational energy states in molecules. In this method, the substrate is irradiated by mid infrared radiation (100 to a few 1000 cm^{-1}). Specific wavelengths are absorbed by the substance, because their energies stimulate the vibration of molecule groups. This results in absorption bands at the related wave numbers in the spectrum. The infrared spectrum is characteristic for every molecule and can be used to identify substrates.

In this work, surfaces coated with a homogeneous gold layer (section 5.1.1) and decorated with self-assembled monolayer (SAM) of MU-NHS linker (section 5.1.3.1) were analyzed by using a IFS 66v/S Vacuum FT-IR system (Bruker Optics, Billerica, USA). The substrates were rinsed with MeOH and dried in nitrogen flow before placing in the analytical chamber. The measuring time for both the sample and the background was 180 s each (200 scans). The scans were performed in reflection mode in vacuum (10^{-3} mbar) with a resolution of 4 cm^{-1}. The detector was a DTGS and the thermal light source was globar. The spectra were recorded in a range from 400 – 4000 cm^{-1}. The effective analyzed range was from 1000 – 3000 cm^{-1}.

5.2.1.4 Scanning electron microscope (SEM)

The scanning electron microscopy is a surface-sensitive, penetration depth imaging method, which uses electrons to analyze samples. During the process the sample is scanned line wise by a highly-focused electron beam and the intensity of the emitted secondary electrons is determined by a detector (**Figure 5.11**). For this reason, the SEM is also called secondary electron microscope.

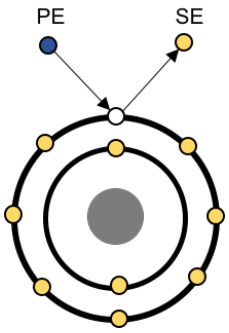

Figure 5.11 Mechanism of emission of a secondary electron. By interaction with the primary electron (PE), a valence electron is knocked out of orbital and detected as a secondary electron (SE)[113].

Since a primary electron is able to generate several secondary electrons by interaction with the sample, the sample needs to be conductive. Non-conductive samples can be sputtered with gold or graphite in order to analyze them by SEM. The working electron energy of a SEM is about 20 keV. Normally, a few keV are used to limit the maximum depth of SE to 10 μm. By using a primary energy < 1 keV, the maximum depth can be reduced to a few nanometers. Therefore, with SEM primarily the sample surface is visualized. Several detectors can be used during the scanning process.

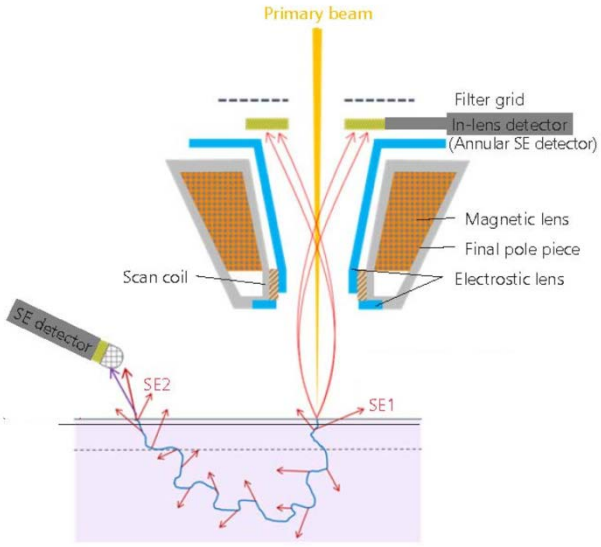

Figure 5.12 Scheme of a scanning electron microscope. The positions of the different detectors (SE1 and SE2 types) and the origin of the secondary electrons are shown. Modified and adapted from Kuo *et al.*[114]

Depending on the position of the detector, the images of the same sample can be visualized completely different, because the information is collected from different depths and angles of sample. The In-Lens-detector is perpendicular to the sample and it detects mainly electrons, which are refracted and reflected by elastic scattering with the atoms. Therefore, they are called backscattered electrons (BSE, type SE1) and origin from the upper layer of the sample. The SE2 detector is fixed in a 45 ° angle to the sample. The SE2 electrons are derived from deeper layers of the sample[113]. A scheme of an SEM is shown in **Figure 5.12**.

In this work, the gold nanopatterned surfaces were analyzed by SEM after plasma treatment and tempering. Since the surfaces are not sufficiently conductive, they were coated with a thin conductive layer of graphite (~ 5 nm) by using EM ACE200 sputter coating system (Leica, Wetzlar). Imaging was performed using a LEO 1530 (Carl Zeiss, Jena). The spacing and the order of the gold nanoparticles were measured by using amagbificatio of 50000x and 100000x and analyzed using the dot analyzer plug-in created by Dr. Phillipe Girard for ImageJ (Research Services Branch, Image Analysis Software Version 1.51h, NIH, USA). The average distance between neighboring gold nanoparticles was determined and averaged over N particles with this plug-in. The order parameter Φ ranges from 0 to 1, with 1 being a perfect hexagonal order. Only samples with an order parameter > 0.5, were used for experiments.

5.2.1.5 Atomic force microscopy (AFM)

To determine the elasticity of the hydrogels an atomic force microscope Nano Wizard I was used (JPK Instruments AG, Berlin). The device was installed on an inverted microscope (Axiovert 200, Carl Zeiss, Jena). The measurement of the hydrogels was performed by indentation of a CONT-Silicon-SPM-Sensor cantilever with colloidal particle (CP-CONT-BSG-A, sQUBE, Bickenbach, Germany). The cantilever had a thickness of 2.0 ± 1 μm, a length of 450 ± 10 μm and a width of 50 ± 7.5 μm. The force constant was determined by calibration with the thermal noise and was in the range of 0.02 – 0.77 N/m. The colloid particle consisted of borosilicate glass and had a diameter of 5 μm. The obtained data were analyzed with AtomicJ (Version 1.7.2_OS Independent)[115] and further edited with Microsoft Excel for Mac 2016. The AFM measurements of the PEG-DA hydrogels and the analysis

were done in cooperation with Dr. Carolina Diaz (Physical Chemical Institute, Heidelberg University).

5.2.2 Detection of iBMP-6

5.2.2.1 Chemiluminescence detection

Surfaces, either homogeneous gold coated or gold nanostructured, functionalized with iBMP-6 were prepared as described above (section 5.1.3.2). Samples were blocked in a solution of 3 % (w/v) BSA (Carl Roth) in PBS at RT for 1 h followed by incubation with 5 μg/ml anti rhBMP-6 mouse IgG (R&D Systems, Wiesbaden) in a solution of 1 % (w/v) BSA in PBS at RT for 1 h. After washing with PBS three times at RT for 10 min, the samples were incubated with 0.1 μg/ml secondary anti-mouse IgG conjugated with horseradish peroxidase (HRP) enzyme (Santa Cruz, Heidelberg) in a solution of 1 % (w/v) BSA in PBS at RT for 1 h. Finally, surfaces were washed with PBS three times at RT for 10 min. In order to reveal the specific signal, samples were incubated with ECL Plus Western Blotting Detection Kit (GE Healthcare, Little Chalfont, Great Britain) and imaged by using a luminescent imaging analyzer Amersham Imager 600 (GE Healthcare, Little Chalfont, Great Britain).

5.2.2.2 Indirect immunofluorescence

The preparation of the different surfaces was performed as described in section 5.2.2.1 until primary antibody incubation. After washing with PBS three times at RT for 10 min, the samples were incubated with secondary antibody Alexa Fluor 488 goat anti-mouse IgG (Invitrogen, Carlsbad, USA) in a final concentration of 1 μg/ml in a solution of 1 % (w/v) BSA in PBS at RT for 1 h. Then, samples were washed again three times in PBS at RT for 10 min followed by immunofluorescence microscopy with an upright wide field microscope Leica DM 6000B (Leica Microsystems, Wetzlar). Cells were examined with a 10x air objective lens (Leica). The images were adjusted in brightness and color with ImageJ software (Research Services Branch, Image Analysis Software, NIH, USA).

5.3 Cell culture

5.3.1 Cell lines and culture conditions

Mouse C2C12 myoblasts (CRL-1772, ATCC, Wesel, Germany) are a standard model system employed for the investigation of bone morphogenetic proteins and known to respond to BMP-6[32]. Cells were cultured as sub-confluent monolayers (~80 %) in growth medium (DMEM containing 4.5 g/l D-glucose, L-glutamine, pyruvate, phenol red; Thermo Fisher, Darmstadt) supplemented with 10 % (v/v) fetal bovine serum (FBS, Biochrom, Berlin) and 1 % (v/v) penicillin/streptomycin (Gibco, Life Technologies) at 37 °C and 5 % CO_2 in a water saturated atmosphere and the medium was renewed every 2 - 3 days. Upon reaching 70 – 80 % confluence, cells were detached by accutase treatment (Life Technologies) and subcultured at a dilution of 1:10. To exclude false positive results induced by possible traces of BMP in the FBS, cells were incubated 6 days in the presence of FBS to observe myotube formation by phase contrast microscopy.

The multiple myeloma cell line OPM-2, established from the peripheral blood of a woman aged 56 yearswith multiple myeloma (IgG lambda) in leukemic phase, are suspension cells and were purchased from DSMZ (German Collection of Microorganisms and Cell Cultures, Braunschweig). Cells were cultured in growth medium (RPMI 1640 containing 4.5 g/l D-glucose, L-glutamine, pyruvate, 2 g/l $NaHCO_3$; Biochrom, Berlin) supplemented with 10 % (v/v) FBS and 1 % (v/v) penicillin/streptomycin, 5 % CO_2-atmosphere at 37 °C in a water saturated atmosphere and the medium was renewed every 2 - 3 days.

5.3.2 Mycoplasma test

To detect contamination of mycoplasma, cells were tested after thawing. 5 x 10^4 cells were incubated in DMEM containing 10 % (v/v) FBS in cell culture flask for 24 h. Then, 2 ml of culture supernatant was collected and tested by using the MycoAlert Mycoplasma Detection Kit (Lonza, Basel, Switzerland). The samples were prepared according to the manufacturer's protocol and analyzed by a luminometer Infinite M200 (Tecan, Männedorf, Switzerland). Only cells which did not have any mycoplasma contamination were used in this study.

5.3.3 Cell experiments

For experiments with substrates coated with homogeneous gold (section 5.1.3) and gold nanostructured surfaces (section 5.1.4), cells were seeded in custom-made poly(dimethyl siloxane) (PDMS) chambers (Sylgard 184, silicone elastomer kit, Dow corning) with a density of $1x10^5$ cells/chamber under standard culture conditions. After 24 h cells were starved in serum-free DMEM for 5 h. Then, the medium was replaced by 50 μl of serum-free medium per chamber. Cells were stimulated either with substrates containing BMP-6 (iBMP-6, section 5.1.3.2), with soluble BMP-6 in DMEM, whereby the concentration is related to the amount of iBMP-6, (sBMP-6, as positive control) or with only a substrate without iBMP-6 (Ctrl, as negative control) (**Figure 5.13**). Cells were covered with the different substrates from top. After gently removing the substrates, cells were checked for integrity by using phase contrast microscopy (Axiovert 40C, Carl Zeiss).

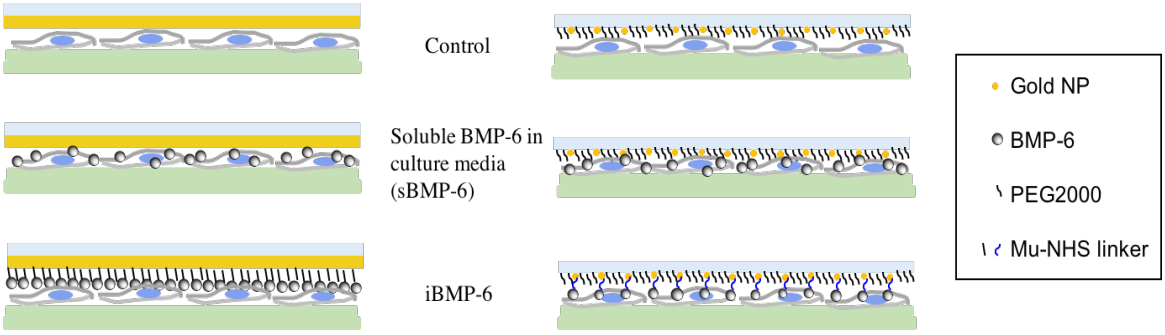

Figure 5.13 Scheme of cell stimulation from top by iBMP-6 substrates. Adherent cells were short-term stimulated from top either by surfaces coated with homogeneous gold (left) or by gold nanostructured surfaces (right); with soluble BMP-6 in culture medium (sBMP-6) or with immobilized BMP-6 (iBMP-6).

For experiments with dual functionalized substrates (section 5.1.5) and gold nanostructured PEG-DA hydrogel substrates (section 5.1.6), cells were starved in serum-free DMEM for 5 h. Substrates were placed in custom-made poly(dimethyl siloxane) (PDMS) chambers. Cells were washed with PBS, detached by using accutase (Life Technologies) and seeded on the substrates in a density of 1 x 10^5 cells/substrates (24 x 24 mm^2) in 2 ml of cell culture medium. As positive control, sBMP-6 was added in culture media right before seeding cells on substrates (**Figure 5.14**). Before lysing, cells were checked for integrity by using phase contrast microscope.

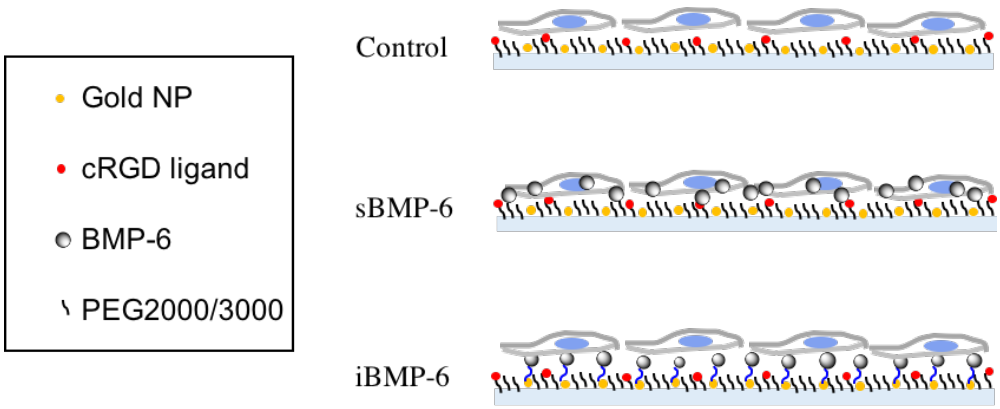

Figure 5.14 Scheme of cell stimulation from bottom by iBMP-6 substrates. Cells were seeded onto the substrates for long-term responses e.g. inhibition of myotube formation or alkaline phosphatase assay.

5.4 Molecular biological methods

5.4.1 Preparation of cell lysates

After removal of culture medium, cells were washed three times with cold PBS. Then, 50 μl of RIPA lysis buffer (Sigma Aldrich) complemented with Halt Protease Inhibitor Single-Use Cocktail (Thermo Fisher, Waltham, USA) and 5 mM EDTA (Thermo Fisher) was added per well. After incubation at 4 °C for 30 min, cells were detached from the culture well by using a cell scraper. Samples lysates were separated from cell debris by centrifugation in a precooled centrifuge at 14000 rpm (Centrifuge 5417R, Eppendorf, Hamburg) at 4 °C for 30 min. The cell supernatant was collected and used for further experiments. Protein lysates were stored in aliquots at -20 °C.

5.4.2 Protein quantification

By using the BCA (bicinchoninic acid) Protein Analysis Kit (Pierce, Thermo Fisher), the protein concentration of each sample was determined, so equal loading was acquired. The analysis was performed in a 96-well plate according to the manufacturer's protocol. BSA was dissolved in lysis buffer in 8 different concentrations (2 mg/ml, 1.5 mg/ml, 1 mg/ml, 0.75 mg/ml, 0.5 mg/ml, 0.25 mg/ml, 0.125 mg/ml and 0.0625 mg/ml) in order to measure a

standard curve. A blank control consisted of lysis buffer only. Afterwards, 25 μl of standards and samples were transferred into the wells and 200 μl of the working reagent (50 : 1 mixture of solution A and B) were added and mixed thoroughly. Then, the samples were shaken for 1 min and incubated at 37 °C for 30 min. The solutions' absorption was measured at 562 nm by using a microplate reader (Infinite M200, Tecan) three times. The resulting absorption data were analyzed with Microsoft Excel for MAC 2016. Protein concentration of the samples was determined by the measured standard curve.

5.4.3 Sodium dodecyl sulfate polyacrylamide gel electrophoresis (SDS-PAGE) and western blot (WB) analysis

The nomalized lysate samples (section 5.4.2) were mixed with sample buffer and reducing agent (Life Technologies) and heated up to 95 °C for 10 min. After cooling down, samples were loaded onto a 4 – 12 % BIS-Tris pre-cast gel (NuPage,Life Technologies) together with a Novex Sharp Pre-stained Protein Standard (Life Technologies), as a molecular weight marker. The electrophoresis was performed in MOPS (3-(*N*-morpholino)propanesulfonic acid) running buffer (Life Technologies) in a SDS-PAGE Chamber (Life Technologies) at 200 V for ~50 min for one gel.

The proteins, separated by using SDS-PAGE were transferred from the gel to a nitrocellulose membrane by wet blotting (X Cell II Blot Module, Life Technologies). The transfer by wet blotting system was performed in transfer buffer (Life Technologies) using power supply at 30 V for 90 min. After blocking with 3 % (w/v) BSA (Carl Roth) in TBS-T (50 mM Tris HCl (Carl Roth), 150 mM NaCl (Sigma), 1 % Tween-20 (Carl Roth), pH 7.5) at RT for 1 h, the nitrocellulose membrane was incubated with primary antibody (Table **5.4**) in a corresponding dilution in TBS-T containing 1 % (w/v) BSA at 4 °C overnight. The membrane was washed three times with TBS-T at RT for 10 min and incubated with secondary antibody conjugated with HRP enzyme (Table 5.5), diluted in TBS-T containing 1 % (w/v) BSA, at RT for 1 h. After washing three times with TBS-T for 10 min, the protein bands were detected by using luminescent imaging analyzer Amersham Imager 600 (GE Healthcare) and ECL Plus Western Blotting Detection Kit (GE Healthcare).

Table 5.4 List of primary antibodies. WB = Western blot, IF = Immunofluorescence, CL = Chemical luminescence

Epitope	Host	Company	Cat. No.	Application	µg/ml
β-actin	mouse	Sigma Aldrich	A1978	WB	2.5
Phospho-SMAD1/SMAD5 (Ser463, Ser465)	rabbit	Thermo Fisher	700047	WB	5
rhBMP-6	mouse	R&D Systems	MAB507	IF, CL	5
Myosin heavy chain (MHC)	mouse	Developmental Studies Hybridoma Bank	MF20	IF, WB	2

Table 5.5 List of secondary antibodies. HRP = Horseradish peroxidase, AF 488 = Alexa Fluor 488, ms = mouse, rb = rabbit.

Host & epitope	Conjugation	Company	Cat. No.	Application	Dilution
Goat anti-ms IgG	HRP	Santa Cruz	sc-2005	WB, CL	1:5000, 1:1000
Goat anti-rb IgG	HRP	Santa Cruz	Sc-2004	WB	1:1000
Goat anti-ms IgG	Alexa Fluor 488	Thermo Fisher	A-110011	IF	1:500

5.4.4 Alkaline phosphatase (ALP) colorimetric assay

Before seeding onto substrates (section 5.3.3), C2C12 myoblasts were starved for 5 h. Cells were either stimulated by iBMP-6 or sBMP-6 (corresponding amount) and cultured for 6 days in 2 % (w/v) FBS. The medium was refreshed after 3 days. After washing three times with PBS, cells were lysed with RIPA buffer (Sigma) without Halt Protease Inhibitor Single-Use Cocktail and without 5 mM EDTA. After incubation at 4 °C for 30 min, cells were detached from the culture well by using a cell scraper. Lysates were separated from cell debris by centrifugation in a precooled centrifuge at 14000 rpm at 4 °C for 30 min. The ALP

substrate p-nitrophenyl phosphate (pNPP, Sigma) was added to the lysates in a ratio of 2:1. Dephosphorylation of pNPP was observed by measuring absorbance at 405 nm in 10 min intervals for 60 min using a microplate reader (Infinite M200, Tecan). Data were analyzed with Microsoft Excel for MAC 2016.

5.5 Preparation of cells for imaging

5.5.1 Myosin heavy chain (MHC) staining and imaging

C2C12 cells were seeded on substrates as described in section 5.3.3. They were cultured on the surfaces for 6 days under low serum conditions (2 % FBS). The medium was refreshed after 3 days. After removing culture medium and washing three times with PBS, cells were fixed with 4 % (w/v) paraformaldehyde (PFA, Sigma) in PBS at RT for 15 min. Samples were washed three times with PBS and permeabilized with 0.1 % (v/v) Triton-X 100 (Sigma) in PBS at RT for 5 min. Then, cells were washed three times with PBS and blocked with 1 % (w/v) BSA in PBS for 1 h followed by incubation with primary antibody anti-myosin heavy chain (MHC) (see Table 5.4) in PBS with 1 % (w/v) BSA at RT for 1 h. Following washing three times with PBS containing 1 % (w/v) BSA, samples were incubated with the secondary antibody Alexa Fluor 488 goat anti-mouse IgG (see Table 5.5) in PBS with 1 % (w/v) BSA for 1 h at RT. After washing three times with PBS containing 1 % (w/v) BSA, samples were mounted with Mowiol (Sigma) supplemented with 1,4-diazabicyclo-[2,2,2]-octane (DABCO, Merck). The mounting reagent was mixed with DAPI (Sigma) at a final concentration 1 μg/ml in order to stain the cell nuclei. Fluorescence images were acquired with an upright widefield fluorescence microscope (Leica DM6000B; software LAS AF 3.2.0.9652, Leica Microsystems CAS). The following air objectives were used: HCX PL Apo 10x/0.4, HCX PL Apo 20x/0.7 and HCX PL Apo 40x/0.85 (all Leica).

5.5.2 Image processing, data and statistical analysis

Data were analyzed and quantified with Microsoft Excel for MAC 2016 and graphics were plotted either with Origin 8.5 software (OriginLab Corporation, Northampton, USA) or with GraphPad Prism 7.0 for Mac OS (GraphPad Software, La Jolla, USA) and further edited

with Microsoft PowerPoint for MAC 2016 or Adobe Illustrator, if not stated otherwise. Statistical analysis was done with GraphPad Prism software. Groups were compared using t-test with p-values < 0.05 considered as statistically significant. ImageJ (Research Services Branch, Image Analysis Software Version 1.51h, NIH, USA) was used to process images. Brightness and contrast of microscopy images were adjusted for the presentation. Western blot bands and myotubes area were quantified by ImageJ as well[116]. All plotted data show mean values with standard deviations calculated from at least three independent experiments (samples in duplicates or triplicates), if not otherwise stated.

5.6 Experiments with multiple myeloma cell line OPM-2

5.6.1 Cell adhesion on dual functionalized surfaces

OPM-2 cells were seeded onto dual functionalized surfaces at a density of 1 x 10^5 per surfaces (24 x 24 mm^2) in 2 ml RPMI medium supplemented with 10 % (v/v) FBS and 1 % (v/v) penicillin/ streptomycin. Since OPM-2 are suspension cells, surfaces were washed with PBS in order to detect adherent cells. Before and after washing, images were taken by using phase contrast microscope (Axiovert 40C, Zeiss).

5.6.2 Viability assays

5.6.2.1 Trypan blue staining

Multiple myeloma cells OPM-2 were seeded in a 12-well plate at a density of 2 x 10^5 cells/well in 1 ml culture medium. The cells were stimulated with either 19 ng BMP-6, 0.133 μM BMP-6 or 160 μM HCl. After 3 days under standard culture conditions, 1 ml fresh medium was added. After 1 day, 2 days, 3 days, 4 days and 7 days, live and dead cells were counted by staining with trypan blue (Carl Roth) (9 : 1) using a haemocytometer and phase contrast microscope (Axiovert 40C, Zeiss).

5.6.2.2 Water soluble tetrazolium-1 (WST-1) assay

As described in section 5.3.3, 5 x 10^4 cells were seeded onto substrates containing iBMP-6 in 1 ml RPMI and stimulated with either iBMP-6 (19 ng) or sBMP-6 (19ng) and $\alpha_5\beta_1$-

integrin-selective ligand under standard culture conditions. 1 ml fresh culture medium was added after 3 days. After 1day, 3days and 7 days, WST-1 reagent (Roche Diagnostics, Mannheim) was added (1 : 10) to the cells, followed by incubation at 37 °C for 30 min. After 1 min shaking, 100 μl of sample mixture was transferred into a 96-well plate in triplicates. The absorbance was measured at 450 nm with Tecan plate reader. By using samples with known cell number (8×10^5, 4×10^5, 2×10^5, 1×10^5, 5×10^4, 2.5×10^4, 1.25×10^4) a standard curve was prepared for every sampleand data were analyzed with Microsoft Excel for MAC 2016.

5.6.2.3 Fluorescence-activated cell sorting (FACS) measurement

Cells were seeded at a density of 5×10^4 cells/surface in 1 ml medium, followed by stimulation with either sBMP-6 or sBMP-2. 1 ml fresh culture medium was added after 3 days. After 5 days and 7 days, suspension cells were scrubbed from the surfaces, transferred in Eppendorf tubes (Eppendorf, Hamburg) and washed with PBS. Prior to FACS measurement, 1 μl of propidium iodide (Thermo Fisher) in a concentration of 1 mg/ml was added to a 300 μl cell suspension in PBS. The fluorescence-activated cell scanning (FACS) was performed in cooperation with Dr. Monika Langlotz (Flow Cytometry & FACS Core Facility, ZMBH Heidelberg University).

6 Results

The goal of this project was to investigate the influence of the growth factor BMP-6, immobilized on different surfaces, on cell signaling and differentiation. A linker system, which was established by Dr. Theresa Pohl[96] and further developed by Dr. Elisabeth Baha-Schwab[88], was used in this work for covalent immobilization of the growth factor on homogeneous gold, gold nanostructured glass and gold nanostructured PEG-DA hydrogel surfaces. First, the linker system was characterized by different surface analysis methods and biochemical techniques. The bioactivity of the immobilized BMP-6 was proven by examining short-term (< 4 h) signaling in BMP-responsive cells. Furthermore, the long-term stimulation effects were analyzed by determining cell differentiation.

6.1 Characterization of the linker system for the covalent immobilization of BMP-6

6.1.1 Infrared measurements prove NHS activity

Glass coverslips were coated with homogeneous layer of gold with a thickness of 50 nm, supported by an adhesive chromium layer (thickness of 15 nm), generated by physical vapor deposition (section 5.1.1). Afterwards the substrates were functionalized with a self-assembled monolayer (SAM) of the heterobifunctional linker 11-mercaptoundecanoyl-*N*-hydroxysuccinimide ester (MU-NHS). Since the ester is instable against hydrolysis, forming the SAM is a critical step in the preparation. In order to prove the successful SAM formation on the one hand and the stability of the NHS ester on the other hand, infrared reflection absorption spectroscopy (IRAS) was utilized to detect the characteristic groups of the MU-NHS linker. **Figure 6.1** displays the IR spectrum of the reactive groups of interests. The methylene asymmetric and symmetric vibrations of the alkane chain can be assigned to the weak signals at 2930 cm^{-1} and at 2850 cm^{-1}. The strong band at 1750 cm^{-1} can be attributed to the three carbonyl groups. The weak signal at 1590 cm^{-1} and the medium signal at 1350 cm^{-1} belong to the N-O asymmetric and symmetric vibrations, respectively. The C-N

vibration corresponds to the strong peak at 1250 cm^{-1}. Due to the detection limit of the used IR spectrometer, the intensity at wave numbers < 1000 cm^{-1} could not be determined.

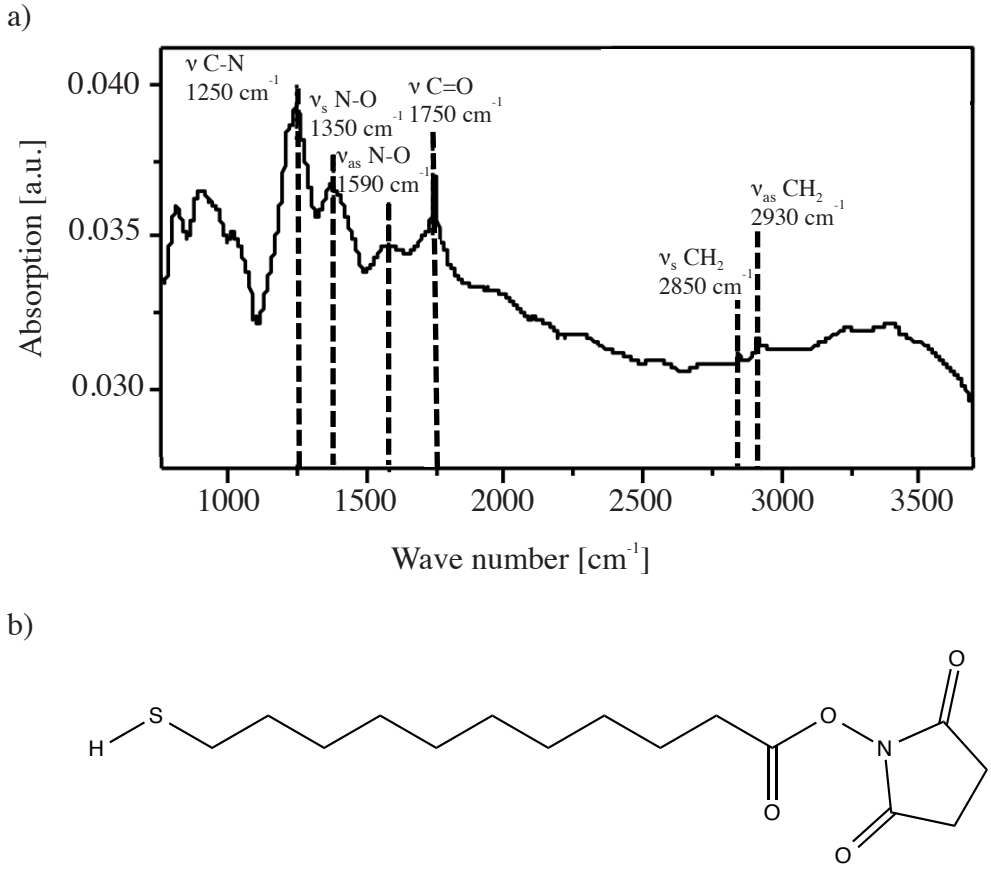

Figure 6.1 IRAS spectrum and chemical structure of the linker. a) The absorbance of the functional groups belonging to the heterobifunctional MU-NHS linker, bond to the gold surface. The absorbance intensity is plotted against the wave numbers. b) Chemical structure of MU-NHS.

The results show that all relevant signals could be detected and assigned to the related groups of the molecule. Furthermore, it can be concluded that the NHS ester maintains intact. If it was deactivated by hydrolyzation, the three signals for nitrogen at 1250 cm^{-1}, 1350 cm^{-1} and 1590 cm^{-1} would not have been detected due to the release of the nitrogen as *N*-hydroxysuccinimide (NHS). Moreover, additional signals of the free carboxylic acid were not detected, which would be indicated by the O-H (wide peak at 3000 cm^{-1}) in case of ester hydrolysis. In summary, it can be stated that the binding of the MU-NHS linker onto the

gold surface was successful and the activity of the NHS ester could be preserved during the adsorption process.

6.1.2 X-ray photoelectron spectroscopy measurement proves NHS stability in aqueous conditions

Due to the need to perform the linker binding in aqueous conditions for usage on hydrogels (see section 6.2.2), the MU-NHS linker was decorated on gold surface, treated in different conditions and analyzed by using XPS (section 5.2.1.2). For the comparison of the film quality depending on the immersion time the film thickness and the packing density was calculated. In addition, the exposure of NHS ester in PBS was tested.

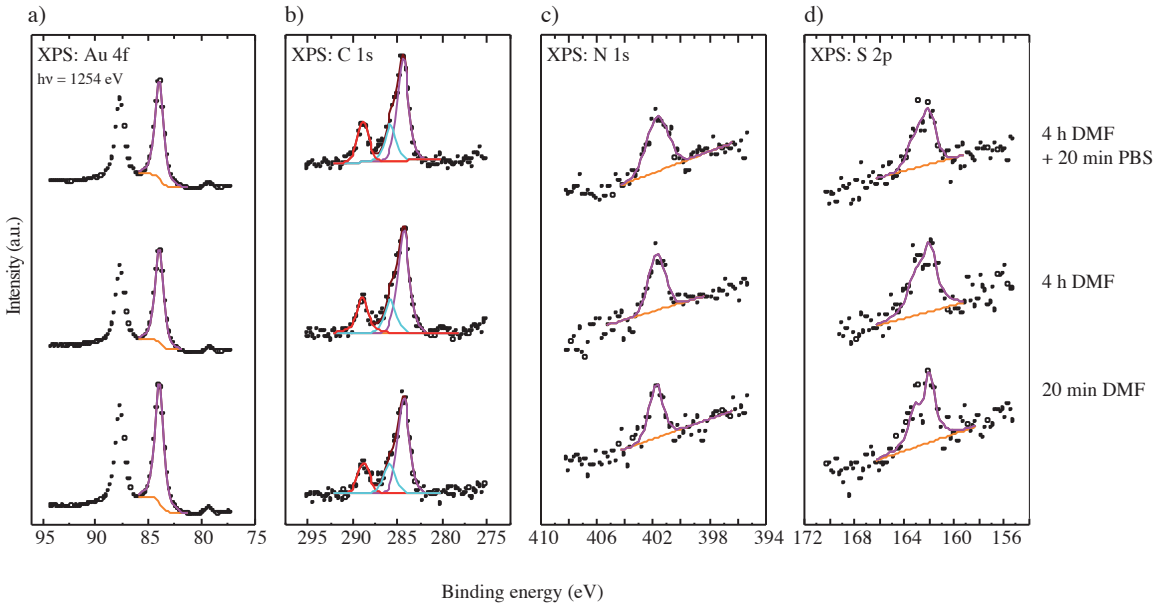

Figure 6.2 XPS spectra of the MU-NHS linker on gold surfaces in different conditions. a) Au 4f signal, b) C 1s signal, c) N 1s signal, d) S 2p signal. Obtained spectra for distinct atoms are displayed as intensity values, plotted against binding energy (BE). Plots: measured signals (…), peak sum (brown), background (orange), fitted peaks (magenta, red, cyan).

The XPS spectra of the pristine films exhibit the peaks and doublets characteristic of the well-defined SAMs with no traces of contamination or oxidative products. For a reasonable comparison between the films the surface, which was incubated for 4 h in DMF, was used as a standard. The C 1s, S 2p, and N 1s XPS spectra of the films are presented in **Figure 6.2**, which behave all similarly.

The C 1s spectrum of the standard **Figure 6.2** exhibits three peaks, which can be tentatively assigned into a main component peak at 284.29 eV corresponding to the CH_2 chain moiety as well as a weaker component peak at ~285.09 eV associated with the CH_2 moiety of the five-membered ring, as well as a peak at 288.89 eV which relates to carbonyl component. The S 2p XPS spectrum of all spectra exhibits a characteristic S 2p3/2,1/2 doublet at a BE position of ~162.0 eV (S 2p3/2) corresponding to the thiolate species bound to noble metal surfaces with no traces of atomic sulfur, disulfide, unbound sulfur, or oxidized species. The gold signal was used as internal reference for each sample in order to normalize the area under the curve of each signal. The surfaces, which were prepared in 20 min, showed all carbon, nitrogen and sulfur signals, which were also detected on the control surface. The sample, which was incubated in PBS, displayed also all important signals including the nitrogen signal. The normalized intensities of the different conditions are listed in **Table 6.1**.

Table 6.1 Table shows the intensities of carbon (b), nitrogen (c) and sulfur (d) of the different samples. In order to compare the two conditions with the standard sample, the intensities were normalized to the corresponding gold signal (a).

	4 h DMF	4h DMF + 20 min PBS	20 min DMF
C1	0.170	0.148	0.112
S2p	0.016	0.013	0.011
N1s	0.012	0.013	0.007

The normalized results for the standard samples were (C1s), (S2p) and (N1s). The results of the standard sample and the PBS sample were comparable, especially the nitrogen signal was almost identical. This indicates that the ester was not hydrolyzed during 20 min PBS incubation. The 20 min sample's results were lower than the standard with at least 60 % of the correlated standard's signal intensity, which leads to the assumption that a minimum of 60 % of the surface was covered by MU-NHS-linker within the first 20 min of incubation time. According to the spectroscopic data, the presented linker is stable in aqueous conditions for more than 20 min. Furthermore, the adsorption time of the linker is rather fast, with a more than 60 % coverage of the surface after incubation for 20 min. This means that the MU-NHS linker could be used for the fast and effective immobilization on gold nanostructured hydrogels in aqueous environment.

6.2 Characterization of covalent immobilization of BMP-6 on surfaces

In this chapter, the linker system was bound to the three different types of surfaces (homogeneously coated gold surface, gold nanostructured glass coverslips and gold nanostructured hydrogels) in order to verify the successful BMP-6 immobilization. Furthermore, it was investigated, whether BMP-6 remained immobilized on the surface after cell contact.

6.2.1 Immobilization of BMP-6 on homogeneous gold

6.2.1.1 BMP-6 was successfully immobilized to gold

The following control experiments were carried out to exclude false positive results by proving the SAM formation and the non-specific binding affinity of the anti-BMP-6 IgG. Then, the successful immobilized BMP-6 was detected on the gold surface by QCM-D and by chemiluminescence experiments independently.

Control experiments

The first control experiment was performed to analyze the SAM formation of the linker in aqueous solution and to determine the required time by measuring the frequency change during incubation and washing. Comparing normalized frequencies allows a statement about SAM formation. The reaction was performed on a quartz crystal of an open module (QCM-D). For the PEG-DA experiments (section 6.2.3) it is necessary to perform the reaction in aqueous solution because other solvents would interact with the hydrogel and damage it. The detailed protocol is described in section 5.1.6. Since the MU-NHS linker is poorly soluble in water, a 100 mM linker stock solution in DMSO was prepared and diluted with water in a ratio 1:100 prior to use. **Figure 6.3** shows the frequency and dissipation change during the reaction. After calibration with the two buffers PBS (B_1) and PBS with 1 M NaCl (B_2), the MU-NHS linker (1) was added on the gold coated sensors. After approximately 30 min, the frequency (blue line) and the dissipation (red line) stopped changing, what indicates the full

coverage of the surface with linker molecules. While washing with buffer B_2, neither the frequency nor the dissipation changed. This means that there is no release of linker molecules from the surface. To see the binding to the linker, the sensor was washed with buffer B_1. Only a small amount of BSA was released from the surface, while the rest remained bond to the surface. However, it could not be distinguished whether BSA was bound to the linker or physisorbed onto the surface. To sum up, the QCM-D measurements show that the MU-NHS linker also forms a self-assembled monolayer in aqueous conditions.

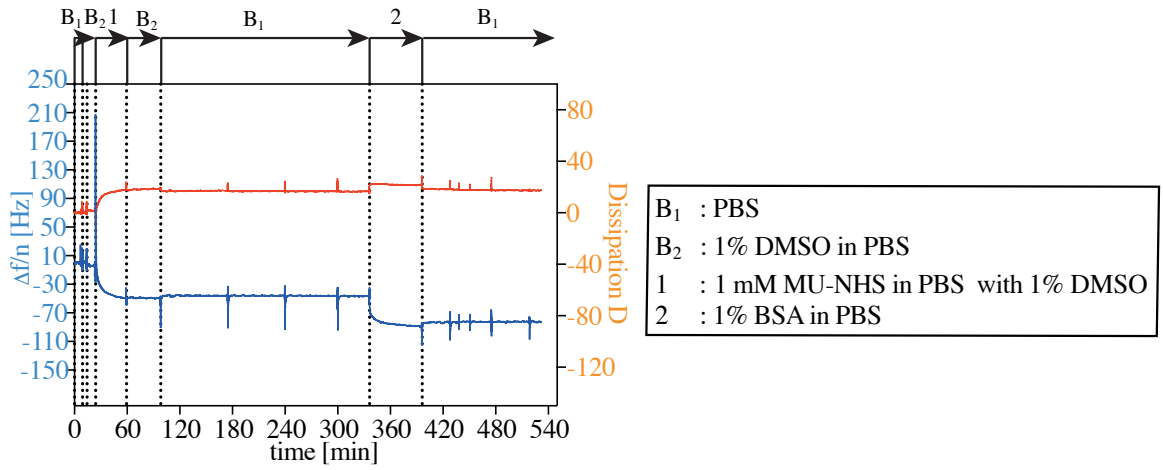

Figure 6.3 The QCM-D diagram shows the successful binding of the linker to the surface and the binding of BSA. The frequency is displayed in blue and the dissipation in red. The vertical outliers are caused by the exchange of the solutions during the measurement. After addition of MU-NHS linker, the frequency decreased and stayed at the same level, while washing with PBS. Blocking with BSA induced a further frequency decrease.

In the next control, the affinity of the anti-BMP-6 mouse IgG was investigated by using a QCM-D crystal, already decorated with a monolayer of MU-NHS linker in order to exclude non-specific binding to the MU-NHS linker. In **Figure 6.4** the change of frequency and dissipation during the antibody incubation is shown. After calibrating with buffer B_1, the crystal was incubated with anti-BMP-6 mouse IgG. During the 30 min incubation, both frequency and dissipation did not change at all. Afterwards the crystal was washed with PBS. There was no change in frequency and dissipation.

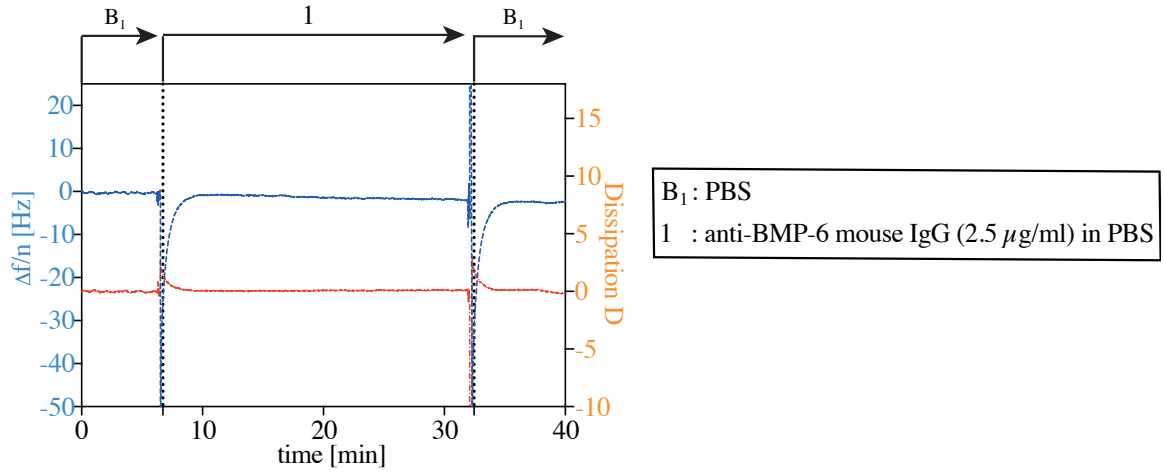

Figure 6.4 The QCM-D diagram shows no shift in frequency and dissipation indicating the non-absorption of anti-BMP-6 mouse IgG antibody. The frequency is displayed in blue and the dissipation in red. The frequency did not change during the incubation with PBS nor with anti-BMP-6 mouse IgG antibody.

In the second experiment, it could be shown that anti-BMP-6 mouse IgG did not unspecifically bind to the surface. It was important to investigate the binding behavior of the antibody to exclude false positive results.

Validation of the BMP-6 immobilization on homogeneous gold

After the control experiments were successfully completed, the immobilization of BMP-6 was observed by QCM-D (**Figure 6.5**). The BMP-6 incubation induced a frequency decrease, which did not change back to the starting point after rinsing. This indicates that BMP-6 bound to the surfaces. In order to validate this result, the immobilized BMP-6 was detected via indirect immunochemiluminescence. During the incubation of the primary antibody, there was a change in the frequency, which was enhanced after secondary antibody incubation. Finally, the QCM-D crystals were revealed in order to detect the immobilized BMP-6 with indirect immunochemiluminescnece. As can be seen in **Figure 6.5**, the crystal treated with BMP-6 showed a high and almost homogeneous signal, indicating the presence of BMP-6. Moreover, the control surface showed no specific signal.

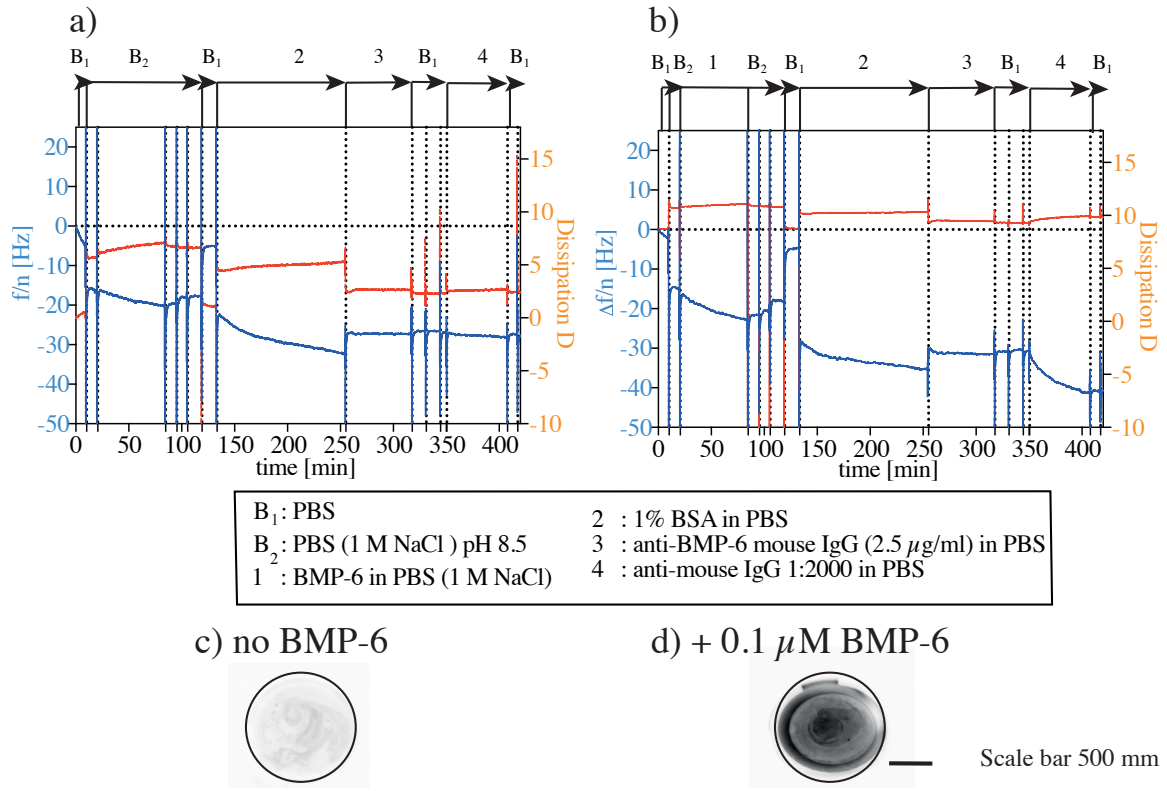

Figure 6.5 The successful immobilization process of BMP-6 is displayed by QCM-D and chemiluminescent detection with antibodies. The QCM-D showed the binding of BMP-6 to the linker followed by antibody binding (b), while there was no binding of antibodies to the control surface (a). The immobilized BMP-6 could be detected by a clear chemiluminescence signal (d). The control surface showed only background signal (c). Adapted and modified from Martin *et al.*[98]

Summing up, the successful immobilization of BMP-6 could be shown and it was evidenced on the surface by direct and indirect detection.

6.2.1.2 BMP-6 binds to the surface through primary amines

After showing the successful immobilization of BMP-6 to the surfaces, it needed to be proven whether the protein binds to the MU-NHS ester through its primary amine group or was physisorbed non-specifically. In order to validate the immobilization, the primary amine groups were acetylated in order to block it for the NHS ester. Furthermore, the green fluorescence protein (GFP) was used as control, because it can be directly detected by fluorescence microscope.

Validation by QCM-D

As it could be shown, the MU-NHS linker generated a monolayer. Therefore, the only interaction took place between BMP-6 and the linker. This means that the protein could bind to the linker in both manners, specifically and non-specifically. By acetylation of the BMP-6's primary amines (Ac-BMP-6), specific immobilization was excluded, because the NHS ester of the linker cannot react with the protein anylonger. If Ac-BMP-6 still binds to the surface, the interaction was unspecific. If Ac-BMP-6 does not bind, the immobilization is mediated by the primary amines.

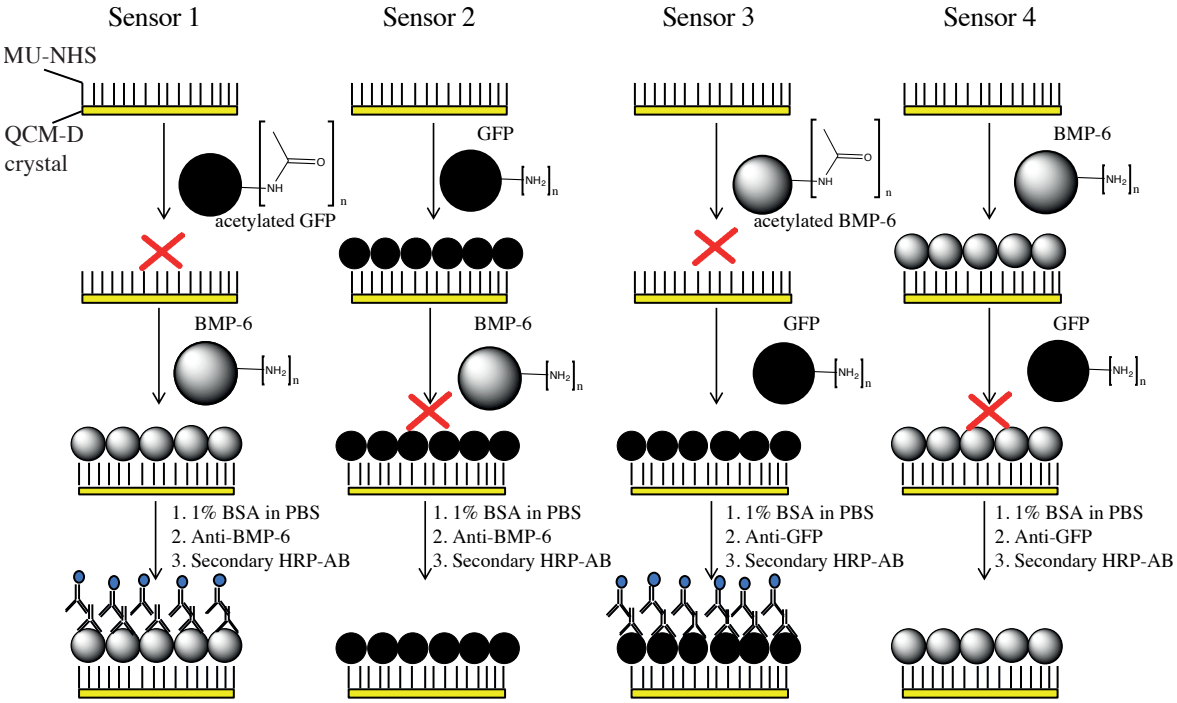

Figure 6.6 Scheme of the setup for the QCM-D experiment with four different conditions. Sensor 1 and Sensor 2 were used as control for the acetylation of the primary amine groups. Sensor 3 proved the immobilization through primary amine groups and Sensor 4 was used as control for the acetylation of BMP-6.

In **Figure 6.6**, the experimental scheme is shown. After incubation with acetylated GFP, the BMP-6 could bind to the surface (Sensor 1), whereas it could not bind after incubation with normal GFP (Sensor 2). Sensor 1 served as positive and Sensor 2 served as negative control, since GFP also contains primary amine groups. In order to prove the specific immobilization, Sensor 3 was incubated with acetylated BMP-6, which could not bind, in contrast to the GFP, which was incubated afterwards. By incubation with untreated BMP-6, the wafers

were completely occupied, so that no GFP was able to bind to the surface (Sensor 4). Sensor 4 served as control for the acetylation of BMP-6.

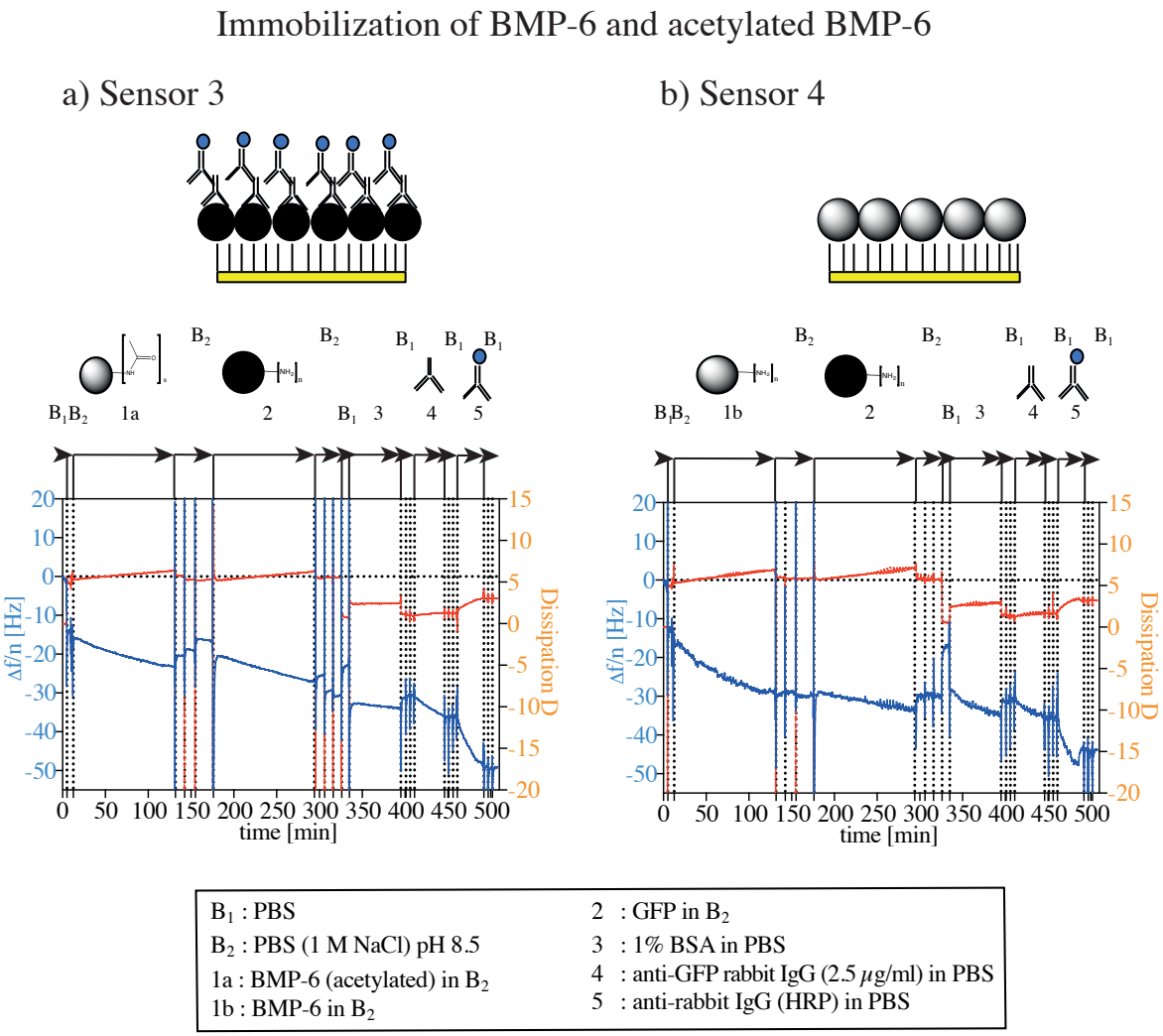

Figure 6.7 The non-binding of Ac-BMP-6 and the successful immobilization of BMP-6 are shown in the QCM-D diagram. a) Ac-BMP-6 did not bind to the surfaces, indicated by the return of the frequency back to the starting point, in contrast to GFP, which could bind to the surfaces showed by frequency change and antibody binding. b) The frequency shift displayed the successful immobilization of BMP-6. Adapted and modified from Martin *et al*.[98]

The experiment showed that acetylated BMP-6 was not able to bind to the MU-NHS linker (**Figure 6.7** a), in contrast to the native BMP-6 (**Figure 6.7** b). Moreover, GFP could bind to the surface after incubation with acetylated BMP-6, but not after incubation with native BMP-6.

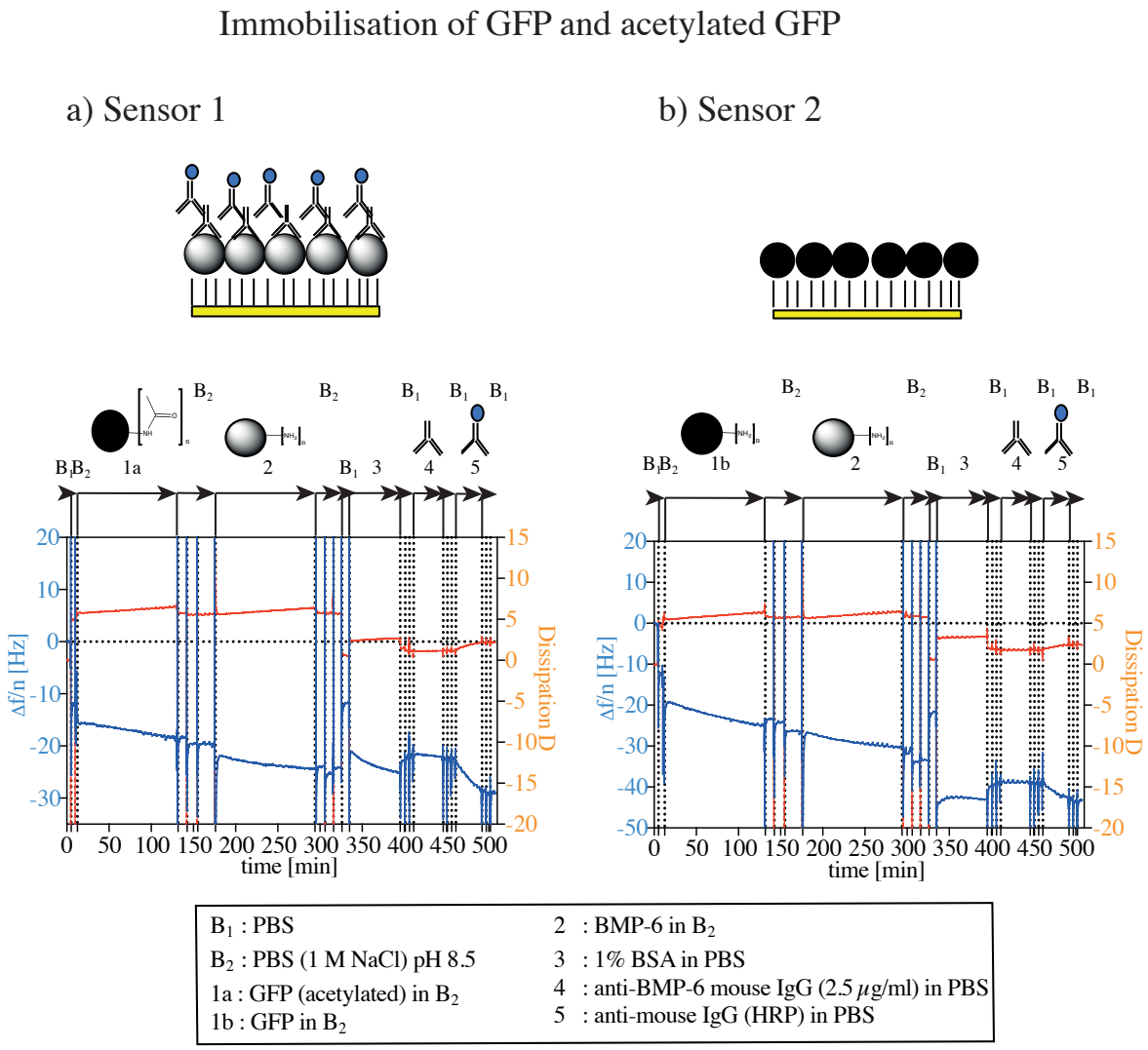

Figure 6.8 QCM-D diagram shows the immobilization of GFP and acetylated GFP. a) The frequency decreased slightly during incubation with acetylated GFP and remained below its starting point level after washing. After incubation with BMP-6 and washing, the frequency did not change back, but remained at a lower point. Then, the frequency decreased further strongly during blocking with BSA. The incubation with first anti-BMP-6 antibody did not affect much the frequency, contrary to the incubation with secondary HRP-conjugated antibody. It changed to a lower level. b) After incubation with GFP, the frequency decreased and did not return while washing. The incubation of BMP-6 and the following washing led to a shift of the frequency. After blocking, the frequency did not change while incubating with first anti-BMP-6 antibody. But while incubating with secondary HRP-conjugated antibody, the frequency reached a lower level than before.

In the second experiment, in which GFP instead of BMP-6 was acetylated, the acetylated GFP (**Figure 6.8** a) showed a lower binding affinity than the non-acetylated GFP (**Figure 6.8** b). Nevertheless, the affinity was higher than the affinity of acetylated BMP-6. This indicates, that the GFP was not completely acetylated, whereas BMP-6 was.

Conclusively, the QCM-D results showed that BMP-6 is immobilized to the surface by binding through its primary amine groups to the MU-NHS linker. Since the Ac-BMP-6 showed a significant lower binding affinity to the linker coated surface than the untreated BMP-6, a non-specific binding interaction can be excluded as main type of binding. But the experiment also showed that GFP was not completely acetylated.

Validation by fluorescence microscopy

To further validate the results, two QCM-D crystals were treated like Sensor 3 and Sensor 4 described in **Figure 6.6**. But instead of incubating with primary and secondary antibody, the substrates were removed from the QCM-D and GFP was imaged with fluorescence microscope.

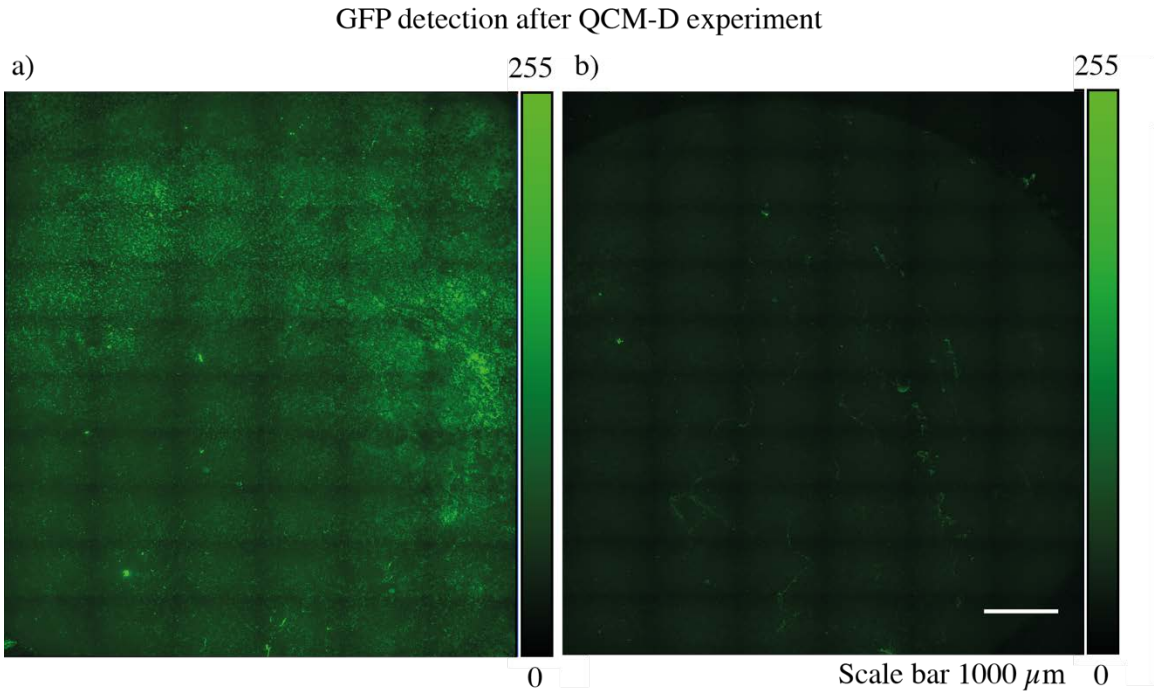

Figure 6.9 Fluorescence microscopy images of the QCM-D crystals. The fluorescence of GFP is shown in green. a) The crystal, decorated with MU-NHS linker, was first incubated with Ac-BMP-6 followed by GFP, which could be clearly detected. b) The sensor was incubated with BMP-6 followed by GFP incubation. The intensity of the GFP signal was significant lower.

In **Figure 6.9**, the fluorescence images are shown. The substrate, incubated with acetylated BMP-6, showed a strong signal (**Figure 6.9** a). This indicates that BMP-6 did not bind to the surface and neither reacted with the NHS ester, what allowed GFP to bind to the surface. The intensity of the crystal, which was incubated with BMP-6, was significantly lower

(**Figure 6.9** b). This matches with the previous QCM-D results, in which it was shown that BMP-6 occupied the surface, when it could bind to the MU-NHS linker.

The following experiment aims at investigating BMP-6's binding ability to different surfaces. Therefore, a glass cover slip was treated to give four different areas, namely homogeneous gold surface, glass surface, PEG passivated surface and PEG2000 passivated nanopatterned surface. GFP served as control. After immobilization of BMP-6, it was labeled by using Alexa488 conjugated secondary antibody. In **Figure 6.10**, fluorescence images are shown. Both proteins did not bind to the passivated surface. While BMP-6 and GFP binding homogeneously distributed on the passivated nanopatterned surface coated with MU-NHS linker, they bound non-specifically to the glass surface. On the gold surface, decorated with MU-NHS linker, the fluorescence signal of BMP-6 and GFP were more homogeneously distributed, but not as even as on the passivated nanopatterned surface.

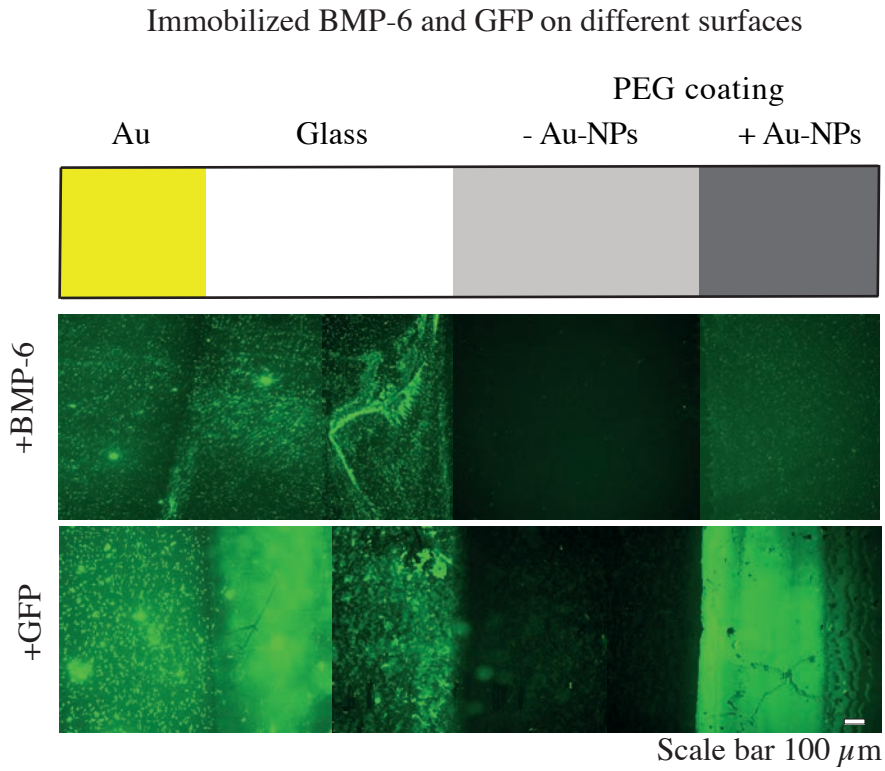

Figure 6.10 Fluorescence images of immobilized BMP-6 and GFP on four different surfaces. The glass cover slips, containing four different areas on the surface, were first incubated with the MU-NHS linker followed by the immobilization of BMP-6 and GFP, respectively. BMP-6 was detected of Alexa488. The fluorescence signal of the proteins showed different distributions on the four areas. Image was adapted and modified from Martin *et. al*.[98]

In conclusion, it could be proven that BMP-6 binds specifically to the MU-NHS ester. Furthermore, it does not bind to the PEG2000 passivated surface in a non-specific interaction.

6.2.2 Successful immobilization of BMP-6 on gold nanostructured surfaces

This chapter deals with the immobilization of BMP-6 on gold nanostructured surfaces by using MU-NHS linked to the gold particles. The inter particle area was passivated with the protein repellent PEG2000.

6.2.2.1 Surface characterization by SEM

The particle distance (**Figure 6.11**) was varied by employing different block copolymer chain lengths resulting in the following particle spacings of (32 ± 8) nm, (63 ± 11) nm and (107 ± 21) nm.

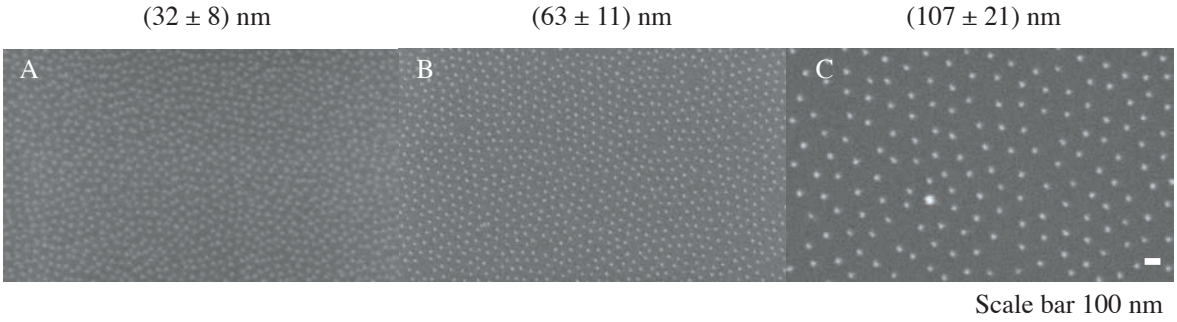

Figure 6.11 SEM images of gold nanostructured arrays prepared from different diblock copolymer solutions on glass. Substrates were imaged with a 50000x (A – C) magnification in order to analyze the inter particle distance and order parameter. The order parameter ϕ was calculated to be 0.51 (A), 0.54 (B) and 0.59 (C), respectively. The mean inter particle distances are indicated above each picture.

6.2.2.2 Detection of immobilized BMP-6 by chemiluminecence immunoassay

The gold nanostructured substrates with different inter particle distances were prepared as described in subsection 5.1.2. The inter particle space was passivated with a protein repellent PEG2000 monolayer (section 5.1.4.2). BMP-6 was immobilized on the gold particles

through the MU-NHS linker. Since only one BMP-6 homodimer was bound per gold nanoparticle, an increased spacing of the gold particles caused a decrease in the amount of surface-bound protein.

Figure 6.12 shows surfaces with a spacing of 32 nm, 63 nm and 107 nm. The immobilized BMP-6 was detected with anti-BMP-6 antibody and HRP conjugated secondary antibodies. The binding of BMP-6 was visualized via chemiluminescence.

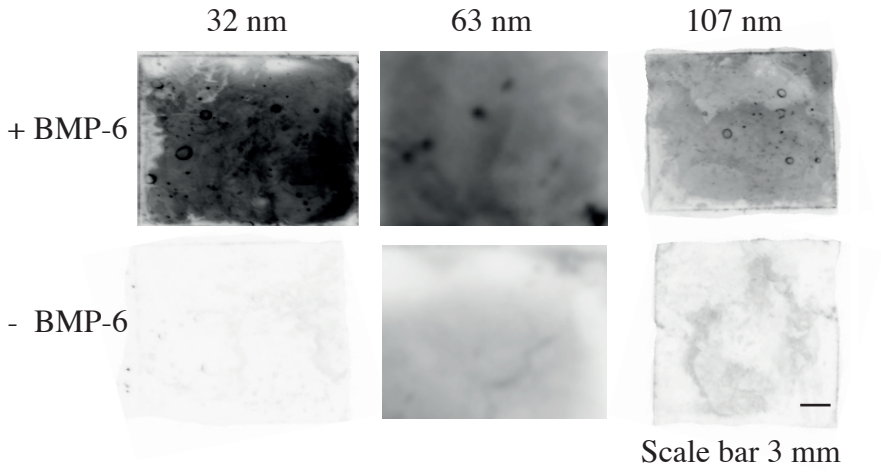

Figure 6.12 Chemiluminescence detection of iBMP-6 on gold nanostructured surfaces with different inter particle spacing. The signal indicated the successful BMP-6 immobilization. The smaller the distance between the particles the stronger the signal on the surfaces treated with MU-NHS and BMP-6 (+ BMP-6) whereas there was almost no signal or only background detectable on control surfaces (- BMP-6).

The substrates treated with MU-NHS and BMP-6 showed a clear chemiluminescent signal (+BMP-6) whereas the negative controls (-BMP-6) displayed almost no signal or background noise. Due to the different spacing, the signal intensity decreased (from left to right). The increased spacing caused a reduced signal. As the results in section 6.2.1.1 showed, the BMP-6 did not bind to the PEG layer.

To further investigate the stability of iBMP-6 (5.1.4), C2C12 cells were exposed to the surfaces from the top of the cells for 60 min and presence of iBMP-6 was assessed prior and after cell contact. The approach is shown in **Figure 5.13**. BMP-6 was detected using chemiluminescence on all surfaces (see **Figure 6.13**).

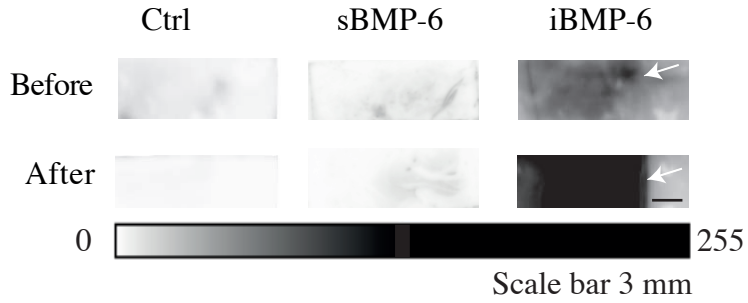

Figure 6.13 Chemiluminescence detection of iBMP-6 before and after cell stimulation. The surfaces, containing iBMP-6 showed a clear signal before and after cell stimulation. Note, the dipping edge (white arrow). The substrate with soluble BMP-6 (sBMP-6) and the control surface did not display any signal neither before nor after cell contact. Image was adapted and modified from Martin *et al.*[98]

iBMP-6 could be detected before as well as after cell stimulation (**Figure 6.13**). Both surfaces showed a strong signal, while on the control surfaces and the surface with sBMP-6 no BMP-6 was detectable. sBMP-6 was used to prove that BMP-6 bound specifically. The dipping edge (see arrow in **Figure 6.13**) marks the border between the area with and without nanoparticles and is due to the preparation.

Additionally, the stability of the immobilization was verified for longer time periods of 120 min and 240 min, respectively. The experimental setup was the same as described above. The sBMP-6 condition was left out, because it could be already proven that it did not bind unspecifically. The surfaces were not parted in order to detect iBMP-6 before cell contact.

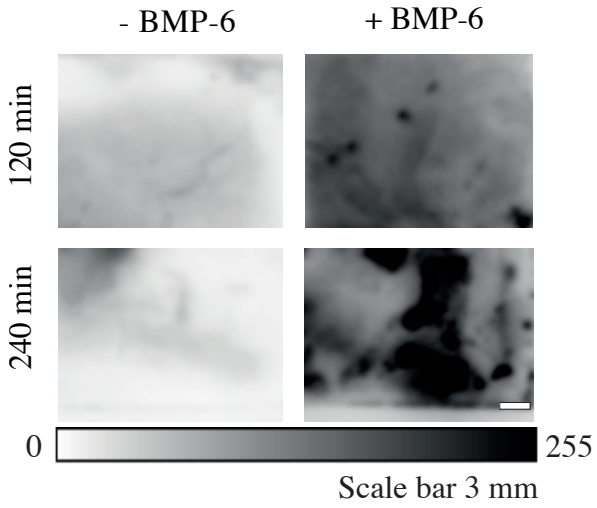

Figure 6.14 Chemiluminescence detection of iBMP-6 after 120 min and 240 min cell stimulation. The surfaces containing iBMP-6 showed high intensities after 120 min and 240 min, while the control surfaces without BMP-6 only displayed low background signal.

The comparable signal intensity after 120 min and 240 min of the iBMP-6 substrates verified the binding stability (**Figure 6.14**). The high stability of iBMP-6 allowed the usage for longer periods of cell stimulation.

It can be summarized that the density of iBMP-6 on the surface could be controlled by varying the inter particle distance. Furthermore, the binding of BMP-6 to the nanopatterned via the MU-NHS linker surface was stable for more than 240 min.

6.2.3 BMP-6 binds successfully to gold nanostructured hydrogel surfaces

In this chapter, gold nanostructured hydrogels were prepared and characterized by using cryo-SEM and AFM. Afterwards, BMP-6 was immobilized to the gold particles through the MU-NHS linker as described earlier (section 5.1.4) and consequently detected by chemiluminescence.

6.2.3.1 Nanoparticle transfer to PEG-DA hydrogels

Gold nanostructured hydrogels were prepared as described in subsection 5.1.6. Prior to the analysis by cryo-SEM, the gels were removed from the glass coverslip, frozen in liquid nitrogen and coated with a carbon layer. Images were taken from at least three different positions.

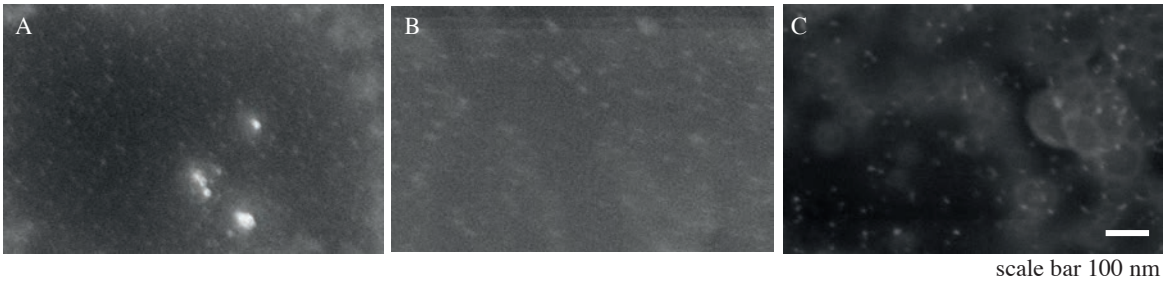

Figure 6.15 Cryo-SEM images of nanopatterned hydrogel surfaces after different preparation steps. A) The hydrogel surfaces were imaged directly after polymerization and transfer of the gold particles. B) After linking the MU-NHS to the gold particles and C) after coupling of BMP-6 to the linker images of the surfaces were taken. The differences in intensity were caused by the varying electrostatic charges.

The MU-NHS ester was coupled to the gold particles on the hydrogel surface and BMP-6 was immobilized on the surface as described in subsection 5.1.6.2. Directly after the polymerization of the PEG-DA and gold particle transfer, the surfaces were imaged by cryo-SEM (A). It can be clearly seen that the particle transfer from the glass coverslip to the hydrogel worked. Image B shows the surface after connecting the linker to the gold particles. The linker binding did not affect the order of the gold particles, since there was no big difference between the first images recognizable. However, after the coupling of BMP-6 to the NHS linker, the image of the surfaces changed. There were less particles on the surfaces with reduced order and increased inter particle distance.

6.2.3.2 Verification of BMP-6 immobilization by chemiluminescence immunoassay

In order the verify the successful immobilization of BMP-6 to the hydrogel surface, BMP-6 was detected by indirect-chemiluminescence assay Four different conditions were used to perform the assay: a gel with nanoparticles, a gel with nanoparticles decorated with MU-NHS linker, a gel with sBMP-6 and a gel consisting of iBMP-6.

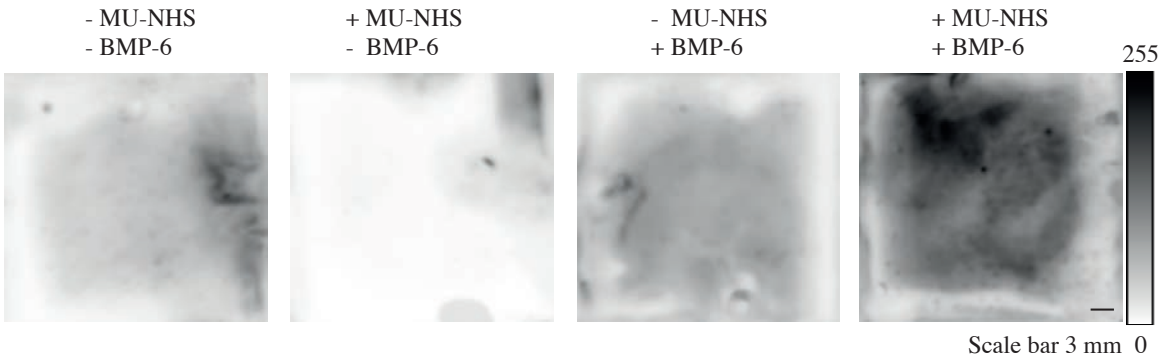

Figure 6.16 Chemiluminescence detection of BMP-6 on gold nanostructured hydrogels. The gel consisting of iBMP-6 showed a clear signal, while the MU-NHS decorated surface showed almost no signal. The surfaces with sBMP-6 and no BMP-6, respectively, showed a low background noise.

Figure 6.16 showes that BMP-6 could be successfully immobilized to the hydrogel via the MU-NHS (**Figure 6.16**, right image). The very low signal of the MU-NHS decorated hydrogel displayed that the linker passivated the surfaces, so that there was no non-specific

binding of the antibodies. This was the case for the untreated surface and the surface containing sBMP-6. But even their signals were only a background signal, since they were weaker than the iBMP-6 signal.

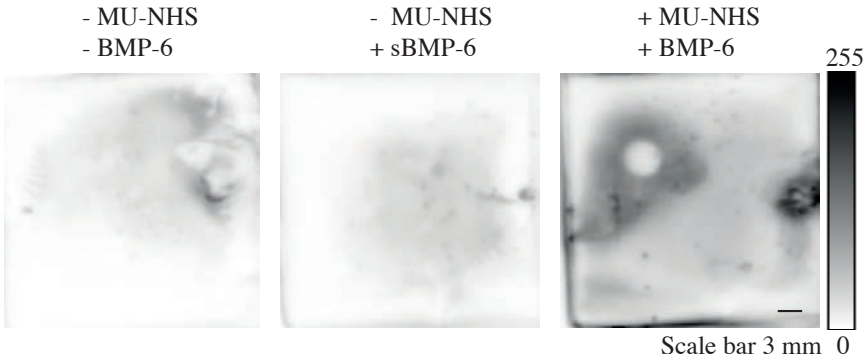

Figure 6.17 Chemiluminescence detection of BMP-6 on gold nanostructured hydrogels after 60 min of cell contact. The iBMP-6 hydrogel showed a significant higher signal than gels with sBMP-6 or no BMP-6.

In order to test the binding stability, the hydrogels were exposed to C2C12 cells as described in subsection 5.3.3 and removed after 60 min. Afterwards, the same assay was used to visualize the iBMP-6. **Figure 6.17** shows the chemiluminescence images of the hydrogels after 60 min cell stimulation. While the control gel and the gel with sBMP-6 showed almost no signal, the iBMP-6 surface displayed a significant higher signal. In conclusion, the immobilization method for glass coverslips could be successfully transferred to gold nanostructured hydrogels. The stability of the binding was also comparable to the substrates prepared on glass (see section 6.2.2).

6.3 iBMP-6 maintains its biological activity upon immobilization to different surfaces

In chapter 6.2, the successful immobilization of BMP-6 to different surfaces through its primary amine groups could be shown. In this chapter, I focused on validating the biological activity of iBMP-6 on the different surfaces. For this reason, short-term and long-term cell responses of C2C12 cells to iBMP-6 were investigated. Furthermore, the results were compared to sBMP-6 as positive control.

6.3.1 Activity of immobilized BMP-6 (iBMP-6) on homogeneous gold

As calculated in section 5.1.3.2, the theoretical amount of BMP-6, which can be immobilized on a (24 x 24) mm surface is 460 ng. This amount of BMP-6 was used in soluble form as positive control (sBMP-6) in order to compare the results of the iBMP-6.

6.3.1.1 Stimulation of SMAD phosphorylation by iBMP-6

The phosphorylation of SMAD 1/5, downstream reporters of the BMP-6, signaling pathway stimulated by iBMP-6 was analyzed by western blot analysis. For this reason, C2C12 cells were incubated either with iBMP-6, sBMP-6 or negative control surface from the top as described in section 5.3.3. As shown in **Figure 6.18** A, SMAD 1/5 phosphorylation was observed after 60 min stimulation with either iBMP-6 or sBMP-6, while SMAD 1/5 activation is absent in C2C12 cells exposed to negative control samples.

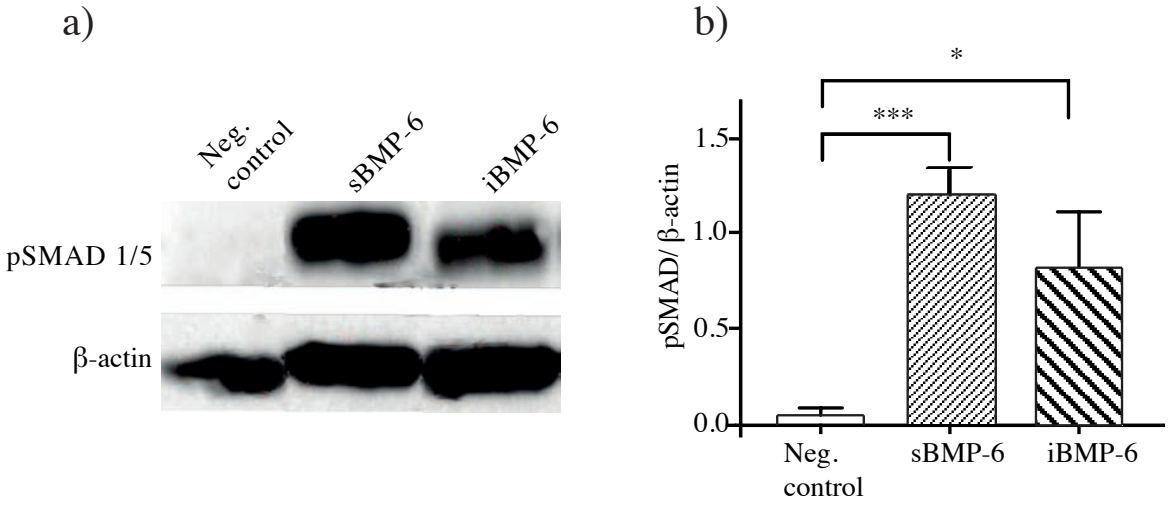

Figure 6.18 Immobilized BMP-6 maintains its biological activity and induces SMAD signaling. a) C2C12 cells were stimulated from the top with gold surfaces (control), with gold surface in presence of sBMP-6 and iBMP-6 for 60 min. After cell lysis, samples were immunoblotted for phospho-SMAD 1/5 and β-actin. b) Phospho-SMAD 1/5 intensities were normalized to β-actin. Error bars represent standard deviation, n = 3, *p < 0.05, ***p < 0.0001. Images were adapted and modified from Martin *et al.*[98]

The quantification of the Western Blot showed, that the immobilization of BMP-6 did not have any significant effect on BMP-6's short-term activity. The iBMP-6 showed a slightly

reduced biological activity like sBMP-6 (**Figure 6.18** b). These results validated that iBMP-6 maintained its biological short-term activity and the ability to trigger early steps in SMAD signaling like SMAD 1/5 phosphorylation.

6.3.1.2 Inhibition of myotube formation by BMP-6

C2C12 cells are known to undergo myogenic differentiation to form myotubes and produce characteristic muscle proteins. However, treatment with BMP-6 causes a shift in the differentiation pathway from myoblastic to osteoblastic, therefore suppressing the formation of myotubes. To investigate the effect of iBMP-6 on myogenesis C2C12 cells were cultured for 6 days under differentiation (low serum) conditions. Microscopy studies were performed to show myotube formation and to detect myosin heavy chain (MHC).

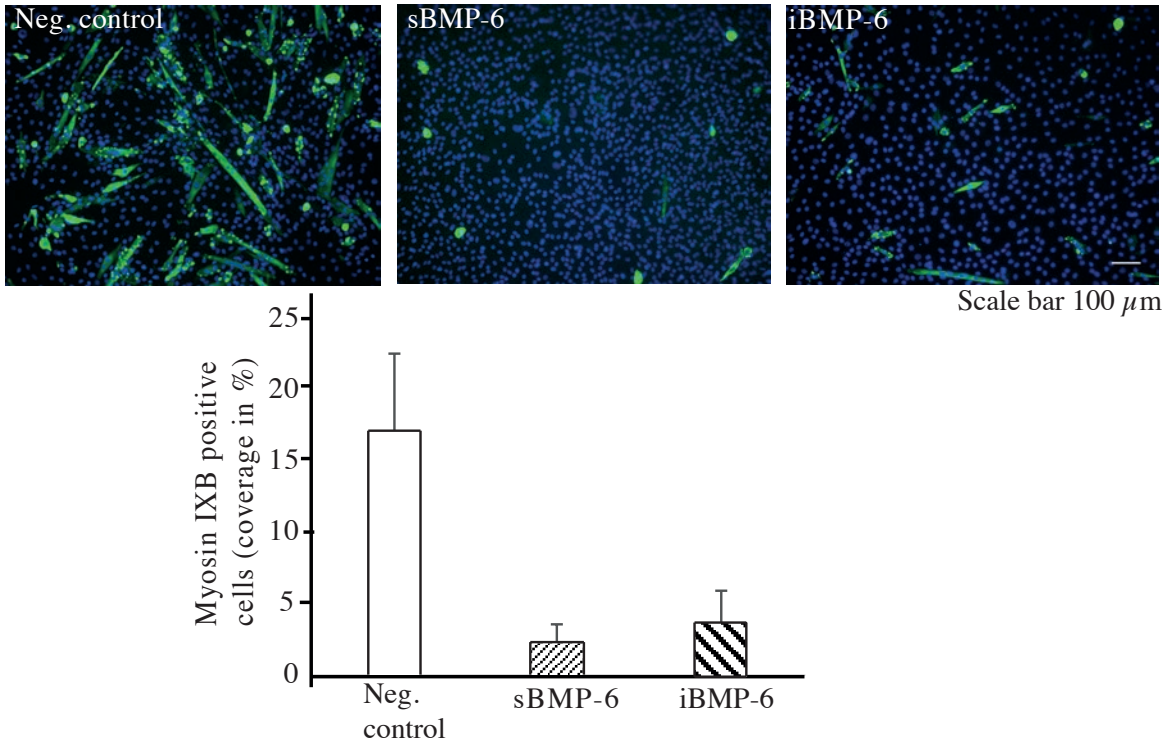

Figure 6.19 Fluorescence images show the inhibition of C2C12 myotube formation by iBMP-6 and sBMP-6. C2C12 cells were cultured for 6 days under low serum conditions to allow myogenesis. Images show myosin heavy chain (MHC IXB) staining of multinucleated myotubes (green) and DAPI nuclei staining (blue). The area covered by myosine IXB positive cells was plotted. Error bars indicate the standard deviation, n = 5. Images were adapted and modified from Martin *et al.*[98]

After six days in culture (see section 5.3.3), cells were fixed and stained. The negative control showed a high number of myosin IXB positive cells whereas on the surfaces with iBMP-6 and sBMP-6 almost no positive cells were found (**Figure 6.19**). The differences between the negative control surfaces and sBMP-6 and iBMP-6 in coverage of myosin IXB positive cells can be clearly seen. In summary, the iBMP-6 on homogeneous gold surfaces showed stable long-term activity which was comparable to the soluble form, by inhibition of myotube formation.

6.3.2 Activity of iBMP-6 on gold nanostructured surfaces

This chapter deals with nanopatterned surfaces with three different inter particle distances (32 nm, 63 nm and 107 nm), containing iBMP-6, which were prepared according to section 5.1.4. Due to the fact that cells cannot adhere on the passivated nanostructured surfaces, only on top stimulation was possible, allowing investigation of the short-term signaling activity of iBMP-6, but not the long-term activity.

6.3.2.1 Stimulation of SMAD phosphorylation by iBMP-6

As calculated in section 5.1.4.2, the amount of BMP-6, which could be immobilized to the surfaces, was 19 ng on 32 nm surfaces, 6 ng on 63 nm surfaces and 1 ng on 107 nm surfaces. These amounts were used in soluble form as positive control in order to compare them with the iBMP-6 results. The experiments were performed as described in section 6.3.1.1. C2C12 cells were on top stimulated by either iBMP-6, sBMP-6 or negative control surfaces. After 30 min, 60 min, 120 min and 240 min cells were lysed and the samples were immunoblotted for pSMAD 1/5 and β-actin. **Figure 6.20** shows the results for different BMP-6 concentrations.

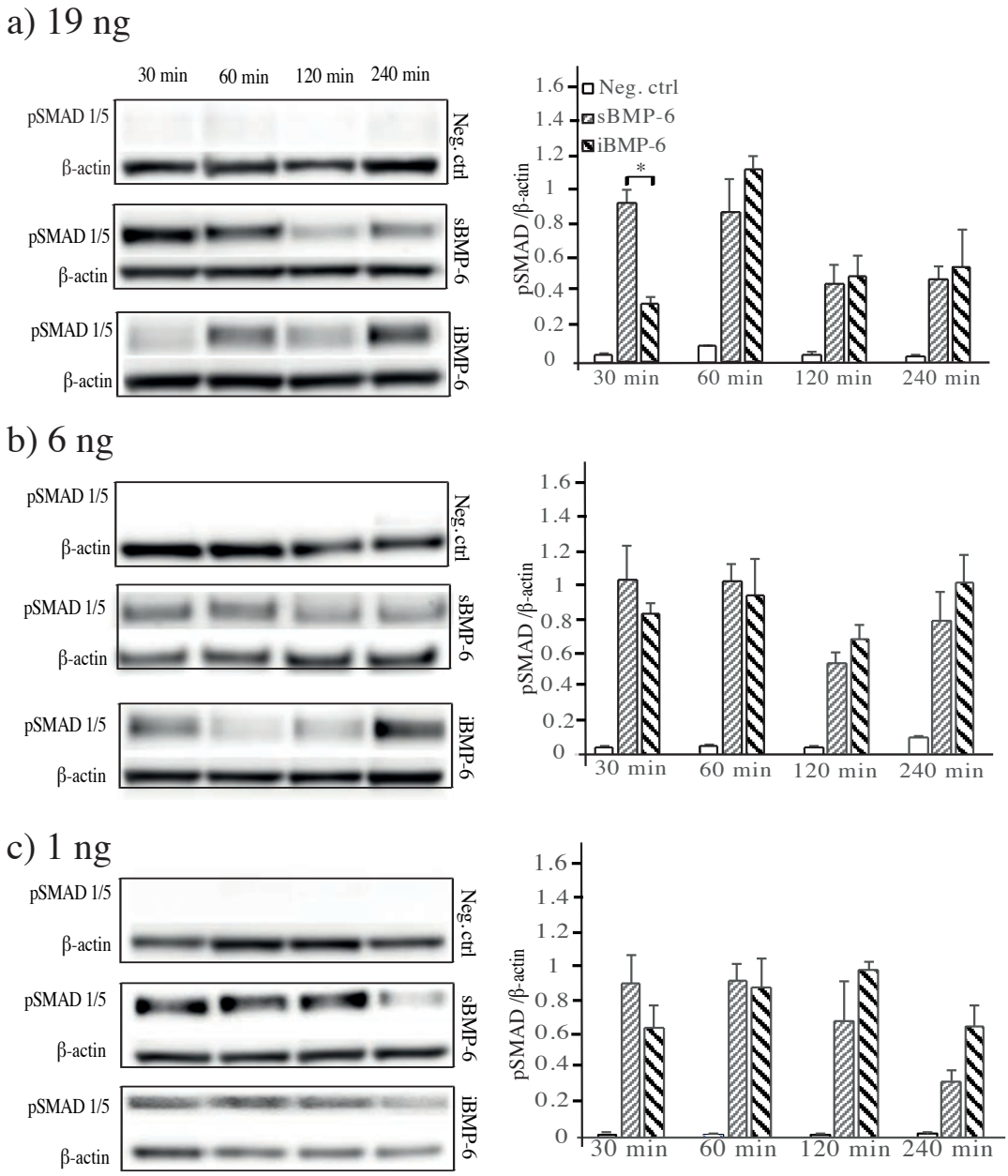

Figure 6.20 Western Blot analysis and quantification of C2C12 cell lysate stimulated by 19 ng (A), 6 ng (B) and 1 ng (C) BMP-6. Error bars represent standard error of the mean, n = 5, *p < 0.05. Adapted and modified from Martin *et al.*[98]

For the highest concentration, 19 ng BMP-6, iBMP-6 showed the highest activity after 60 min. Then it decreased and started increasing again after 240 min, while sBMP-6 showed the highest activity after 30 min and decreased until it reached a stable activity after 120 min (A). In comparison, the 6 ng sBMP-6 displayed the maximum after 30 min as well, but it started increasing after 240 min (B). Furthermore, the activity progress of the 6 ng iBMP-6

was similar to the 19 ng iBMP-6, but even more pronounced. The lowest concentration of BMP-6, 1 ng, showed a similar behavior for sBMP-6 as for 19 ng. For iBMP-6, the maximum was shifted to 120 min after increasing and then it started decreasing.
The results displayed that BMP-6 maintained its biological activity also after immobilization on nanopatterned surfaces. Furthermore, it could be shown that BMP-6 is still active in very low concentration (1 ng) in immobilized and soluble form. Both iBMP-6 and sBMP-6 showed a different activity. Moreover, the iBMP-6 showed always a higher activity after 120 min for all concentrations, although it was not significant.

6.4 Dual functionalized surfaces containing BMP-6 and adhesive ligand

In this chapter, gold nanostructured surfaces were dual functionalized in order to immobilize adhesive ligands on the PEG layer by click chemistry. This allowed using the substrates for long-term stimulations of cells with iBMP-6. For this reason, the effect of iBMP-6 on myogenesis and on stimulation of alkaline phosphatase (ALP) activity in C2C12 cells were investigated.

6.4.1 Dual functionalization of gold nanostructured glass surfaces

The dual functionalized surfaces were prepared as described in section 5.1.5 using integrin $\alpha_5\beta_1$ selective ligand and cRGD. The adhesive effect was investigated by seeding C2C12 on the surfaces. Furthermore, the short-term and long-term activity of iBMP-6 was determined.

6.4.1.1 Validation of ligand's adhesive effect

Cells were seeded on surfaces containing integrin $\alpha_5\beta_1$ selective ligand and cRGD ligand, respectively, and on non-functionalized surfaces, which were used as negtive control. After seeding the C2C12 cells on the surfaces, cell adhesion was observed at different time points by using phase contrast microscope. Cells seeded on substrates which were decorated with $\alpha_5\beta_1$ specific ligand ($+\alpha_5\beta_1$), started adhering to surface after 30 min (**Figure 6.21**). After 90 min, most of the cells were adhered and started to spread, indicated by change of shape.

After 18 h, all cells adhered and spread on the surface, while most of the cells on control were still round shaped.

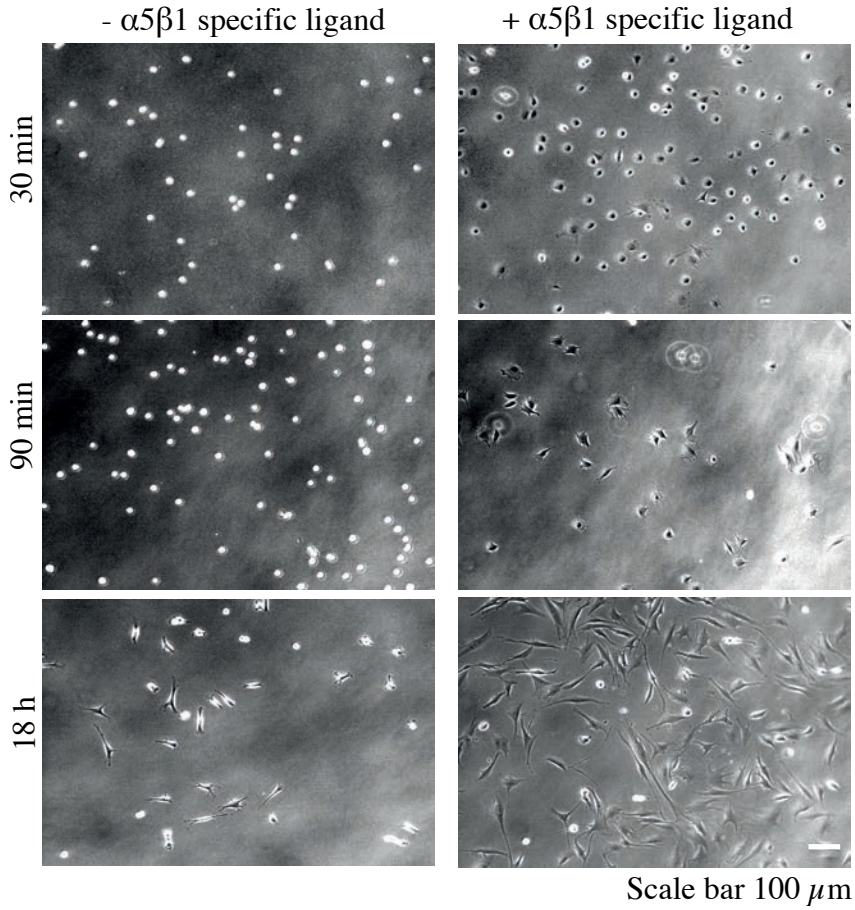

Figure 6.21 C2C12 cells adhesion induced by $\alpha_5\beta_1$ specific ligand. Cells were seeded on substrates and phase contrast images were taken after 30 min, 90 min and 18 h. Round cells presented non-adherent cells.

The tri-peptide motif RGD, which is present in many ECM proteins, is established and known to induce cell adhesion. For this reason, it was used as comparison for cell adhesion. C2C12 cells were seeded on surfaces coated with cRGD ligand. In **Figure 6.22**, phase contrast images can be seen, which show cell adhesion on the substrates containing cRGD after 60 min and 240 min.

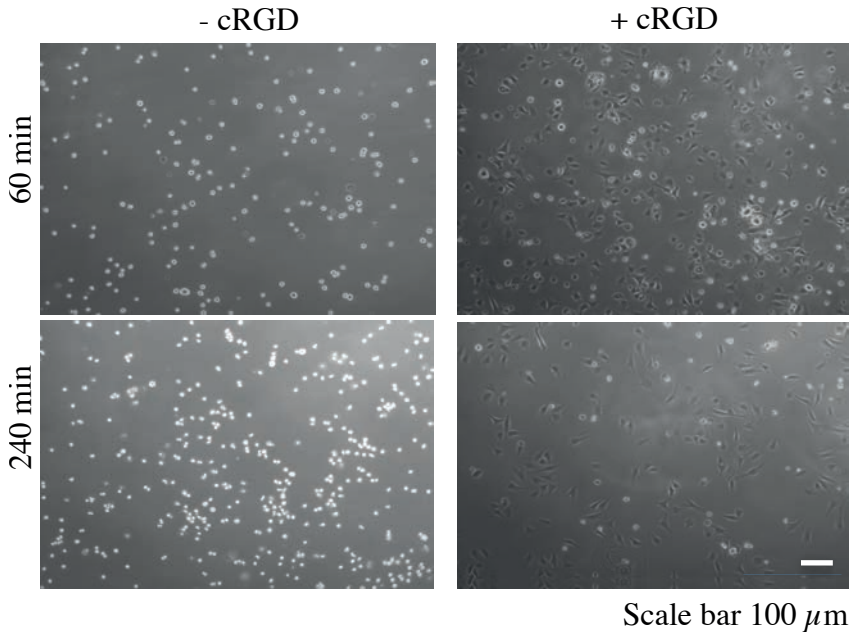

Figure 6.22 C2C12 cells adhered on the surfaces with and without cRGD ligand. Cells were seeded on substrates with and without cRGD and phase contarst images were taken after 60 min and 240 min. Adapted and modiefied from Martin *et al*.[98]

After 60 min, many cells started adhering to the surfaces decorated with cRGD (+ cRGD), while cells on the negative control surface were still round (- cRGD). After 240 min almost all cells adhered to the cRGD surface in contrast to control.

In conclusion, it could be shown that the $\alpha_5\beta_1$ selective ligand as well as cRGD induced cell adhesion of C2C12 cells.

6.4.1.2 iBMP-6 has a higher biological activity by bottom stimulation

The biological activity of iBMP-6 on gold nanostructured surface was already proven in section 6.3.2. There the cells were stimulated from top by iBMP-6. In this chapter, the bottom stimulation was performed as described in section 5.3.3.

Stimulation of SMAD phosphorylation by iBMP-6

C2C12 cells were seeded on nanostructured surfaces (107 nm) containing cRGD and 1 ng iBMP-6. After 60 min and 240 min, cells were lysed to analyze the short-term stimulation of the SMAD 1/5 phosphorylation as described previously. After 60 min, iBMP-6 showed

the highest activity of on top stimulation (see section 6.3.2.1). Furthermore, it was investigated whether iBMP-6 and sBMP-6, respectively, still showed an activity after 240 min.

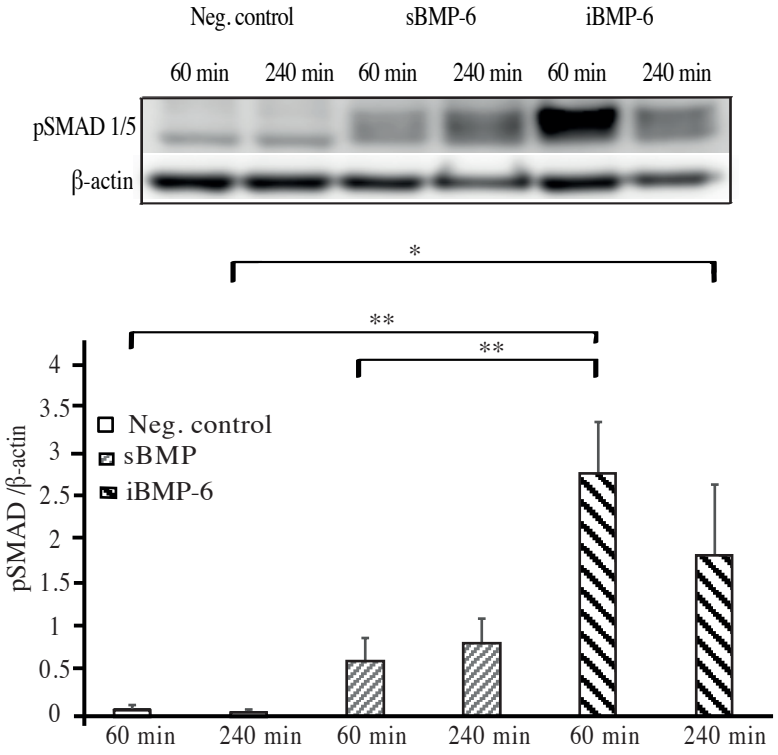

Figure 6.23 iBMP-6 showed a higher biological activity than sBMP-6 in bottom stimulation of SMAD 1/5 phosphorylation in C2C12 cells. Cells were stimulated with 1 ng BMP-6 in immobilized and soluble form. Lysates were immunoblotted for pSMAD 1/5 and β-actin. The pSMAD signals were normalized to β-actin signal. Error bars represent standard error of the mean, n = 5, *p < 0.05, **p < 0.001. Images were adapted and modified from Martin *et al.*[98]

Previous experiments (see section 6.3.2.1) could show that already 1 ng BMP-6 was sufficient to stimulate C2C12 cells. Therefore, 1 ng BMP-6 was used for the bottom stimulation. As it can be seen in **Figure 6.23**, iBMP-6 showed a very high activity after 60 min as well as after 240 min. It was significantly higher than the sBMP-6 and control samples, respectively.

Inhibition of myotube formation by iBMP-6

In order to investigate the long-term activity in bottom stimulation by iBMP-6, cells were seeded on surfaces containing $\alpha_5\beta_1$ selective ligand and cRGD, respectively. Three different concentrations of BMP-6 were used: 19 ng, 6 ng and 1 ng. Fluorescence images were taken to show myotube formation and to detect myosin heavy chain (MHC subunit IXB). The cells were cultured on the surfaces according to section 5.3.3.

In **Figure 6.24** A, the fluorescence images of cells seeded on surfaces containing $\alpha_5\beta_1$ selective ligand and different concentration of BMP-6 are shown. It can be clearly seen that iBMP-6 could inhibit myotube formation on all surfaces, while sBMP-6 could only inhibit myotube formation with high BMP-6 doses. The quantification of the myosin IXB positive cell supports the impression of the images (**Figure 6.24** B).

Figure 6.25 shows the same experimental setup but the $\alpha_5\beta_1$ selective ligand was replaced by the cRGD ligand. Instead of three different concentrations only two concentrations were used to investigate, whether there were any differences in the effect of the highest amount (19 ng) and the lowest (1 ng). Besides, the experimental procedures were similar. The results were comparable to the $\alpha_5\beta_1$ selective ligand samples. 19 ng of iBMP-6 and sBMP-6 were capable to inhibit myotube formation sufficiently. Furthermore, 1 ng of iBMP-6 could still trigger the inhibition, while the samples of 1 ng sBMP-6 looked comparable to the control surface. The quantification of the coverage matched with these results.

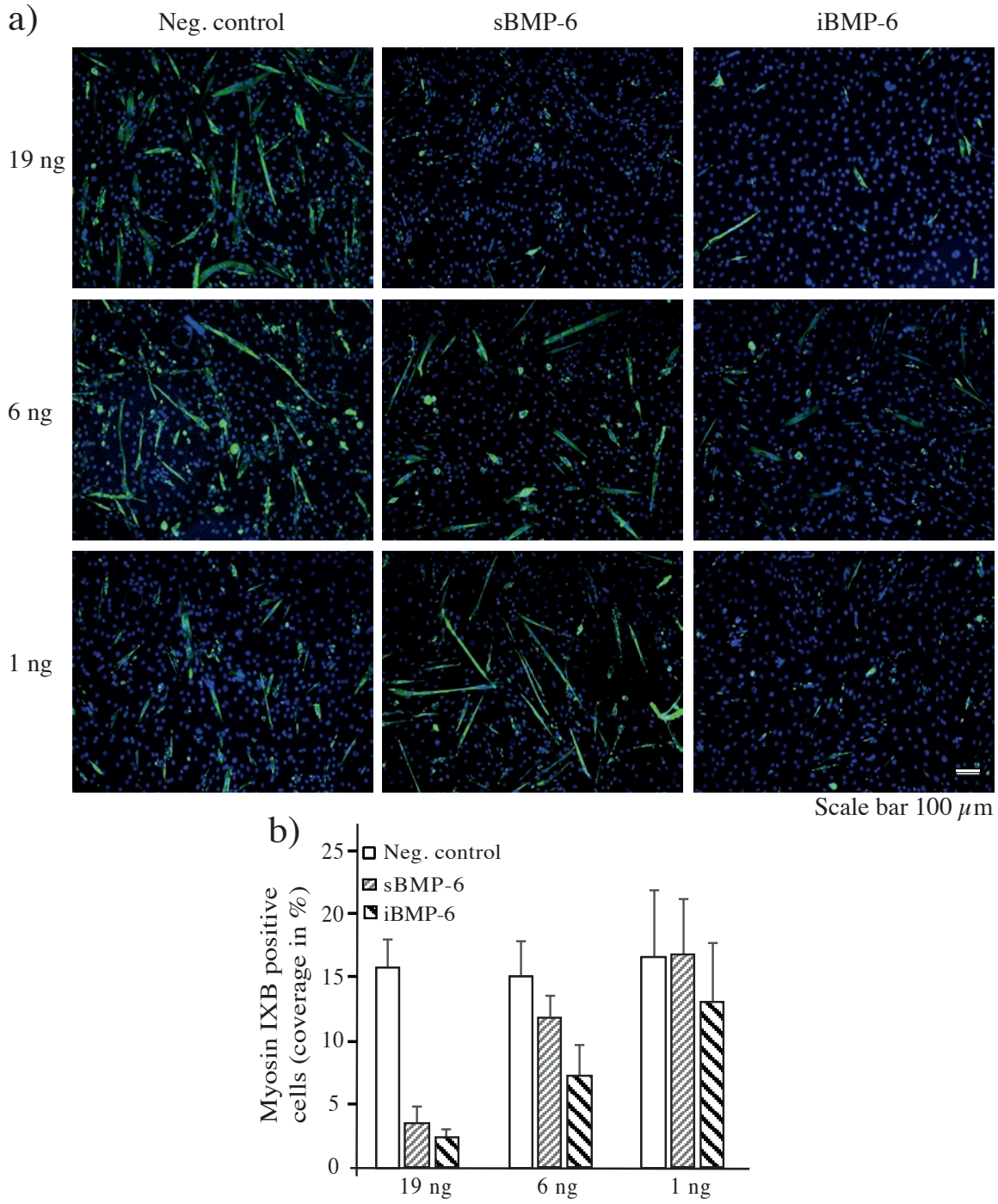

Figure 6.24 Fluorescence images show myosine IXB positive C2C12 cells upon iBMP-6 and sBMP-6. a) C2C12 cells were seeded on surfaces containing $\alpha_5\beta_1$ selective ligand and stimulated from bottom by 19 ng, 6 ng and 1 ng BMP-6 for 6 days under low serum conditions to trigger myogenesis. Images show myosin heavy chain (MHC subunit IXB) staining of myotubes (green) and DAPI nuclei staining (blue). b) By measuring the area, covered by myosine IXB positive cells, quantification was done and the results were plotted. Error bars indicate standard deviation, n = 5.

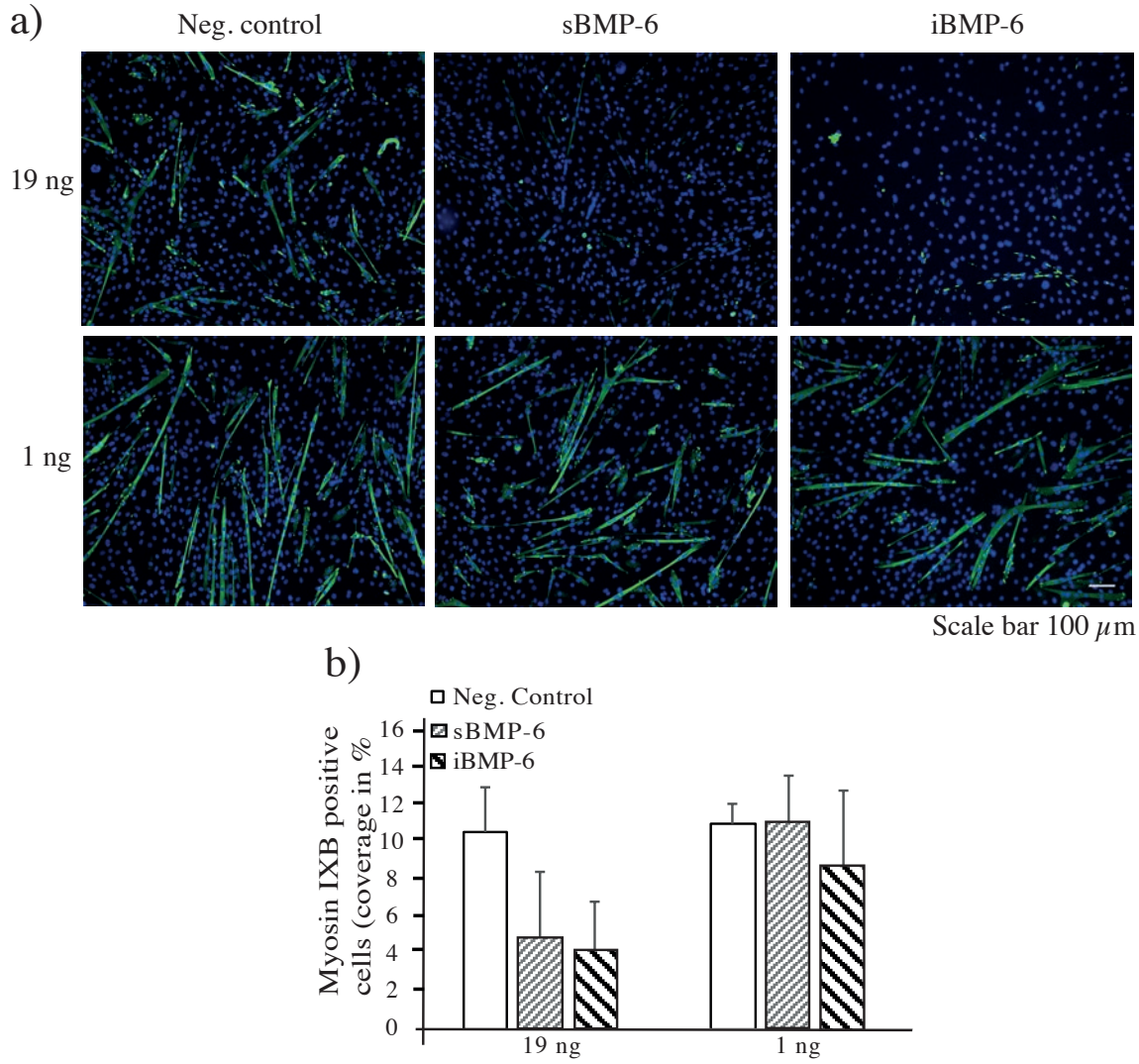

Figure 6.25 Fluorescence images show myosine IXB positive C2C12 cells upon iBMP-6 and sBMP-6 on cRGD decorated surfaces. a) C2C12 cells were stimulated from bottom by 19 ng and 1 ng BMP-6, respectively, under low serum conditions for 6 days to allow myogenesis. Images show myosin heavy chain (MHC) staining of multinucleated myotubes (green) and DAPI nuclei staining (blue). b) By measuring the area covered by positive cells, and relating to the total area, a quantification was done and the results were plotted in percentage. Error bars indicate standard deviation, n = 5. Images were adapted and modified from Martin *et al.*[98]

Stimulation of alkaline phosphatase (ALP) activity

The role of ALP as a marker for osteogenic activity has been consistently solidified. To determine whether iBMP-6 affects long-term osteogenic differentiation response, alkaline phosphatase (ALP) activity of C2C12 cells was measured after a 6-day incubation period.

Cells were seeded on surfaces functionalized with $\alpha_5\beta_1$ selective ligand and cRGD ligand, respectively.

ALP activity in lysates of cells cultured on surfaces with $\alpha_5\beta_1$ selective ligand was measured as described in section 5.4.4 (**Figure 6.26**). Lysates of cells cultured on iBMP-6 and sBMP-6 surfaces (19 ng) showed a higher enzymatic activity than negative control. While the 6 ng samples still induced a higher ALP activity than the control, the 1 ng iBMP-6 and sBMP-6 showed no increase of absorption compared to control sample.

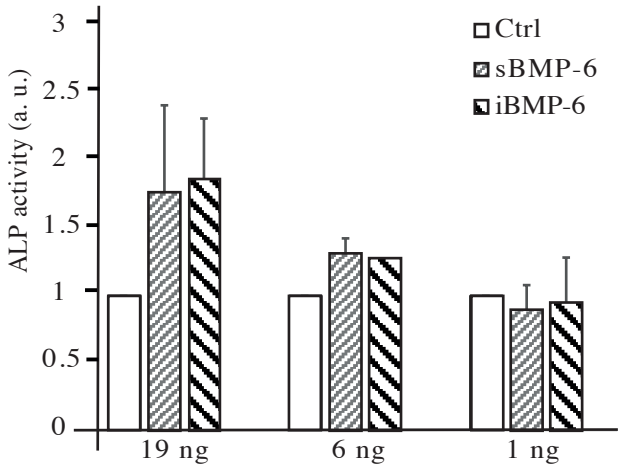

Figure 6.26 Immobilized BMP-6 stimulated osteogenic differentiation of C2C12 cells on surfaces decorated with $\alpha_5\beta_1$ selective ligand. The enzymatic activity of alkaline phosphatase (ALP) indicates osteogenic differentiation of C2C12 cells. ALP activity was measured as absorbance at 405 nm. The bar graph shows data normalized to corresponding control sample. The error bars indicate the standard deviation, n = 3.

Figure 6.27 shows the results of the experiments, which were performed with cRGD functionalized surfaces. Here, BMP-6 was used in two concentrations of 19 ng and 1 ng. The absorption of the 19 ng samples were comparable to the corresponding $\alpha_5\beta_1$ selective ligand samples. The difference appeared in the 1 ng iBMP-6 sample. It showed a higher ALP activity in comparison to the control and sBMP-6 sample with cRGD and was also higher than the 1 ng iBMP-6 samples with $\alpha_5\beta_1$ selective ligand.

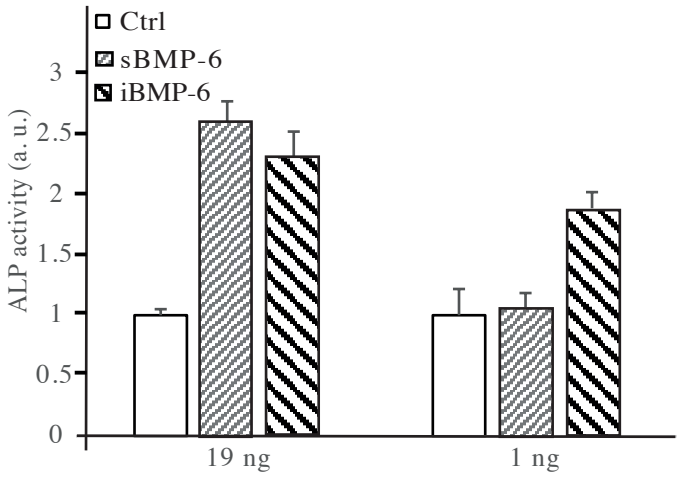

Figure 6.27 Immobilized BMP-6 stimulated also osteogenic differentiation of C2C12 cells on surfaces decorated with cRGD ligand even better. The enzymatic activity of alkaline phosphatase (ALP) indicates osteogenic differentiation of C2C12 cells. ALP activity was measured as absorbance at 405 nm. The bar graph shows data normalized to corresponding control sample. The error bars indicate the standard deviation, n = 3. Adapted and modified from Martin *et al*.[98]

To summarize the chapter 6.4, it could be shown that iBMP-6 was able to stimulate cells more efficiently than sBMP-6 in both short- and long-term basal stimulation. In general, differences in the adhesion mediation between $\alpha_5\beta_1$ ligand and cRGD ligand could not be noticed. Only in the ALP assay, the 1 ng iBMP-6 with cRGD induced higher ALP activity than the corresponding sample on $\alpha_5\beta_1$ selective ligand functionalized surface.

6.5 Applications

This chapter outlines the medical application of the prepared surfaces. Dr. Anja Seckinger and Dr. Dirk Hose (Multiple myeloma division, National Centre for Tumor Diseases (NCT) Heidelberg), our cooperation partner, discovered that BMP-6 can be used to induce cell death in multiple myeloma cells[53]. Since BMP-6 had to be used in high concentration when applied in soluble form, the aim was to reduce the required amount by immobilizing BMP-6. The ability for long-term stimulation should help to achieve the desired effect also with lower concentration of BMP-6. Therefore, the viability of multiple myeloma OPM-2 cells was determined before and after BMP-6 exposure using gold nanostructured glass surfaces containing iBMP-6 and $\alpha_5\beta_1$ selective ligand.

6.5.1 Validation of ligand's adhesive effect

The multiple myeloma cell line OPM-2 are suspension cells, which normally do not adhere on surfaces. In order to expose these cells to the immobilized BMP-6, dual functionalized surfaces with adhesive ligands were employed to force the cells to adhere. The cells were seeded on surfaces decorated with $\alpha_5\beta_1$ selective ligand. **Figure 6.28** shows the phase contrast images displaying cells adhesion on different surfaces.

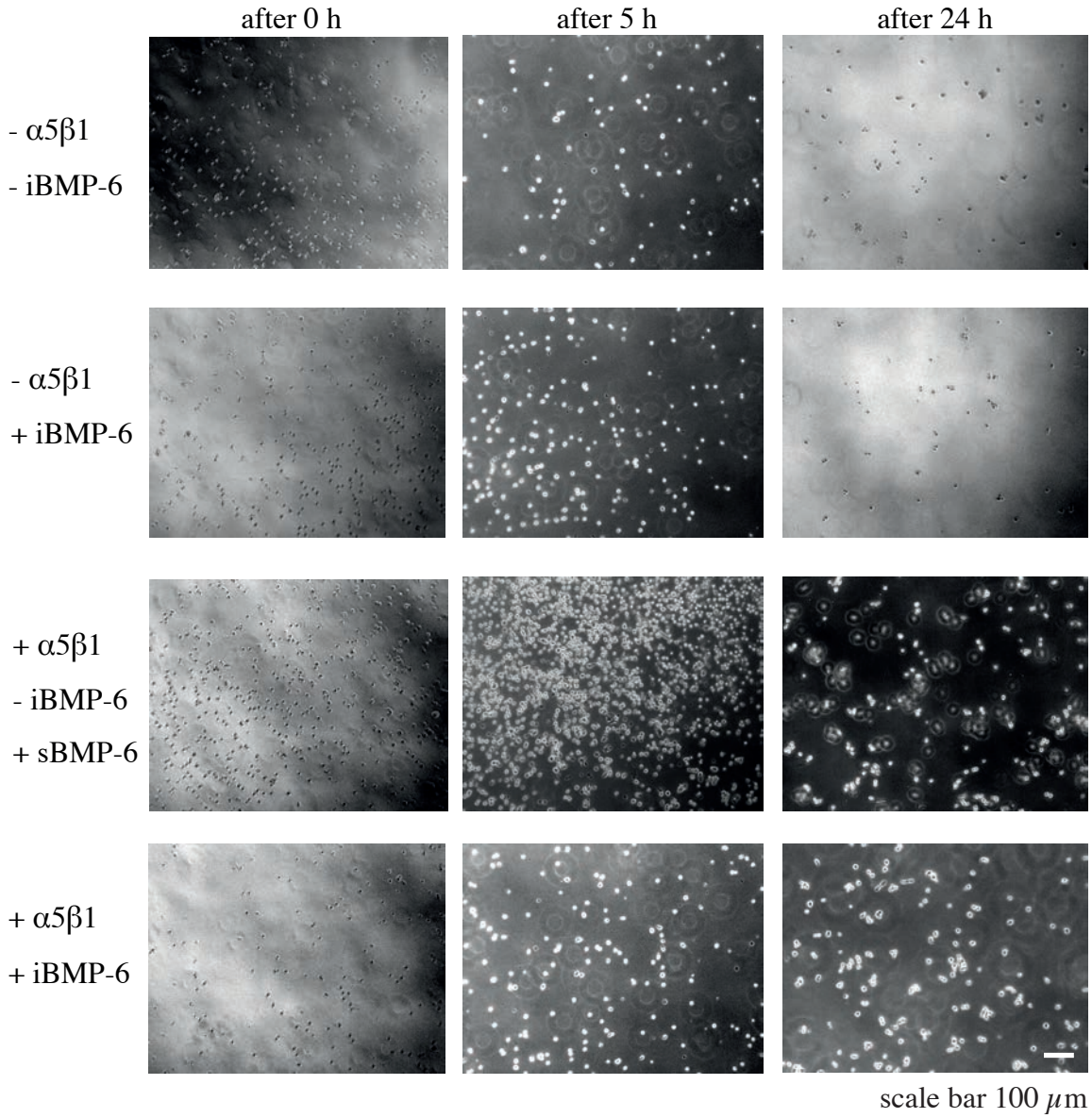

Figure 6.28 OPM-2 cells adhering on surfaces decorated with $\alpha_5\beta_1$ specific ligand. Cells were seeded on four different surfaces: passivated surface, passivated surface with iBMP-6, passivated surface decorated with $\alpha_5\beta_1$ specific ligand in presence of sBMP-6 in culture medium and passivated surface with $\alpha_5\beta_1$ specific ligand and iBMP-6. Phase contrast images were taken directly after seeding (0 h), after 5 h and after 24 h, respectively.

In order to visualize adhesion of the OPM-2 cells to $\alpha_5\beta_1$ specific ligands, the surfaces were washed with PBS after 54 h. Before and after washing, images were taken from different areas of the surfaces. In **Figure 6.29**, the differences between surfaces with and without $\alpha_5\beta_1$ specific ligand can be clearly seen. On surfaces without the ligands the cells were almost completely removed by the washing, while on the other ones the cell number did not changed much. This indicated the successful adhesion of OPM-2 cells to the ligand.

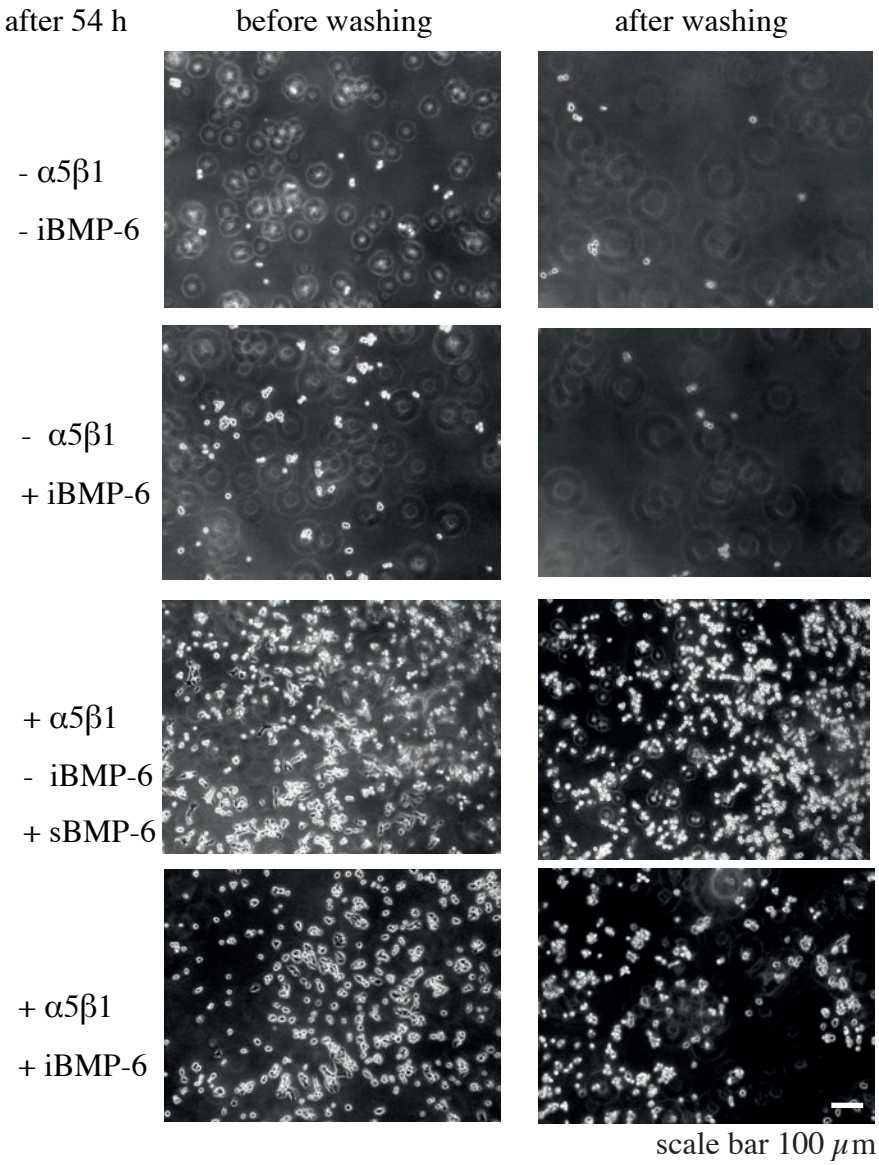

Figure 6.29 Washing did not remove OPM-2 cells from surfaces decorated with $\alpha_5\beta_1$. Surfaces were washed with PBS in order to remove non-adherent cells. Images were taken before and after washing.

In conclusion, it could be shown that the $\alpha_5\beta_1$ selective ligand induced cell adhesion of OPM-2 cells. Moreover, the adhesion was independent from presence of iBMP-6 and sBMP-6.

6.5.2 Initiation of cell death in myeloma cells

To investigate the effect of BMP-6 on multiple myeloma cells, BMP-6 was compared to BMP-2, which also belongs to the TGF-β superfamily, in order to use it as a control. OPM-2 cells were treated with BMP-6 or BMP-2, respectively, and cell viability was determined after 5 and 7 days by FACS measurement (see section 5.6.2.3). Furthermore, the negative control sample (indicated as Ctrl) was not treated. In **Figure 6.30**, it can be clearly seen that BMP-6 decreased the cell viability compared to the negative control sample, while there was no detectable effect upon BMP-2 stimulation.

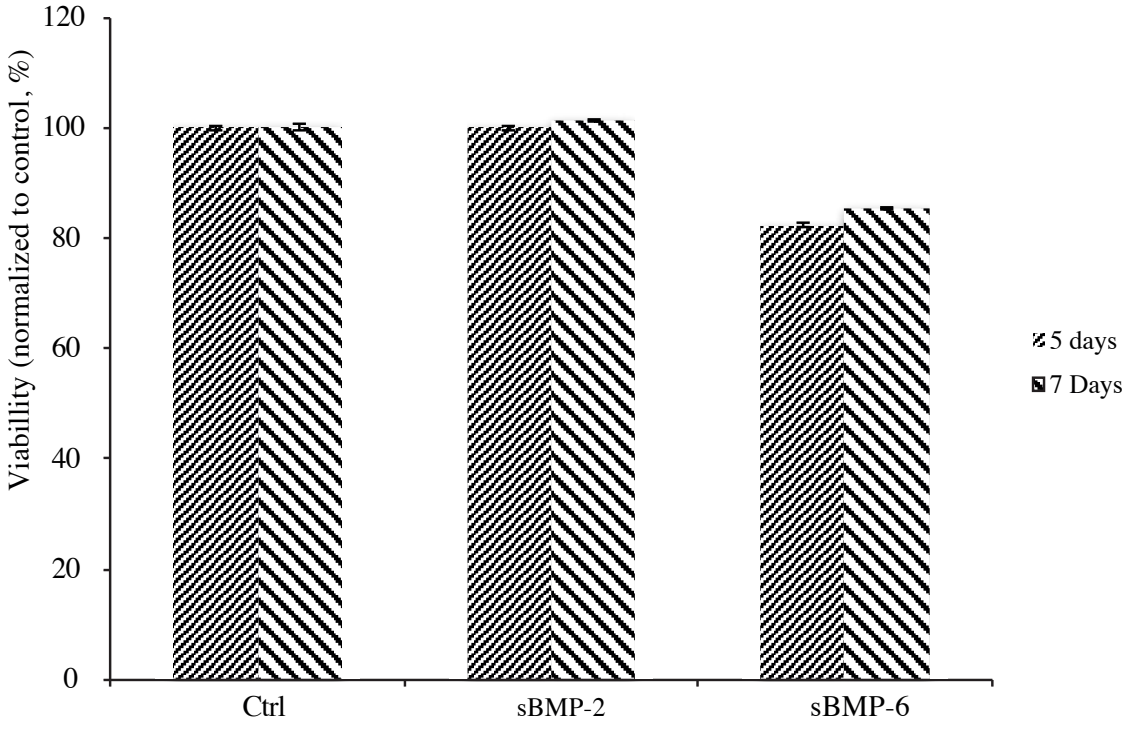

Figure 6.30 The effect of sBMP-2 and sBMP-6 on OPM-2 cell viability after five and seven days stimulation. OPM-2 cells were stimulated with either 1 μg/ml sBMP-2 or 1 μg/ml sBMP-6, which is equal to 1 μg. After five and seven days, cell viability was determined by FACS. The error bars indicate standard deviation, n = 3.

After the successful prove of BMP-6 effect on myeloma cells, the maximum amount of BMP-6 (19 ng), which could be immobilized on gold nanostructured surfaces (inter particle distance of 32 nm), was compared to the concentration (4 μg/ml), which was used by the cooperation partner.

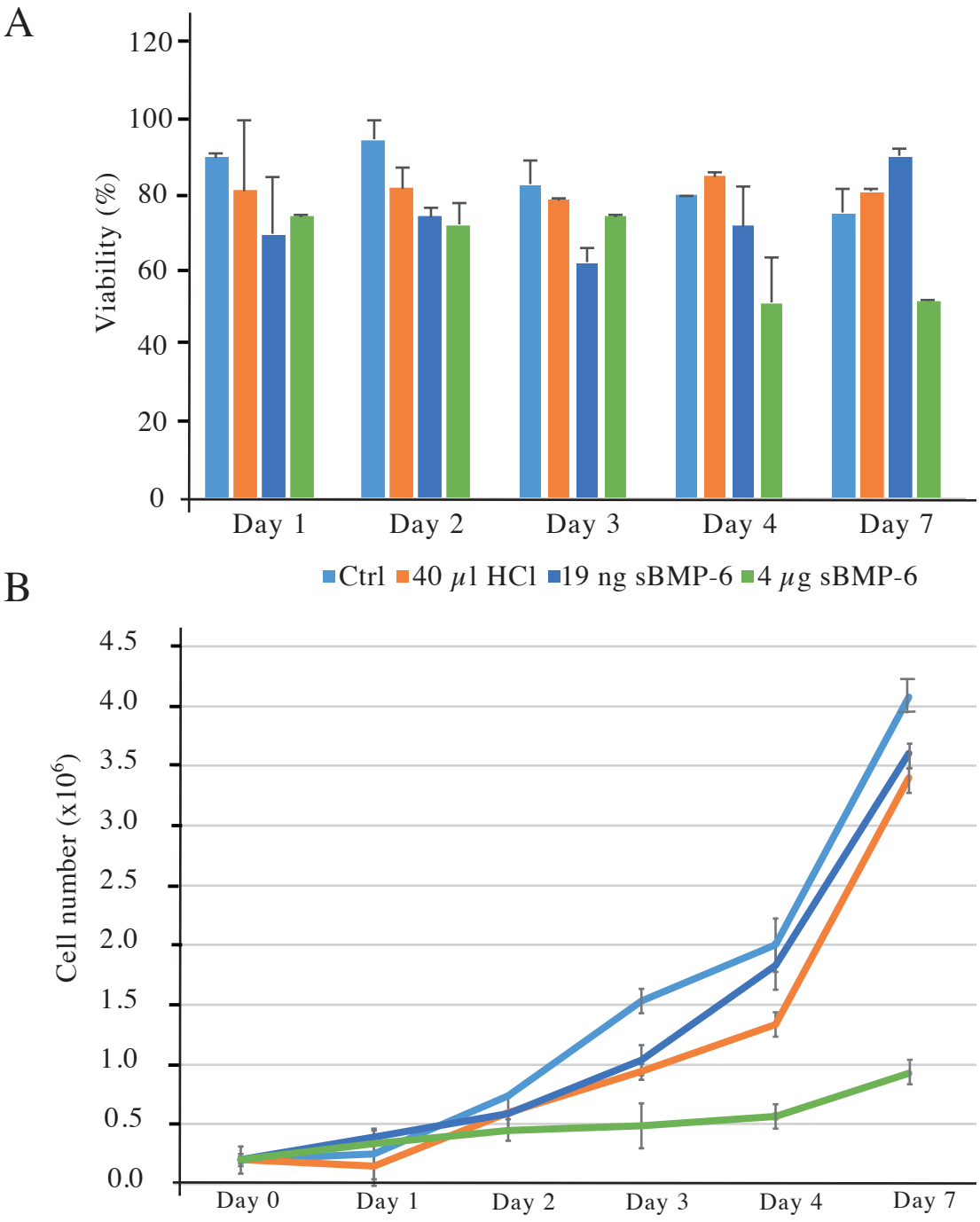

Figure 6.31 Determination of the viability and the cell number of OPM-2 cells after stimulation with different concentrations of sBMP-6. 200000 OPM-2 cells were treated by sBMP-6 (4 μg and 19 ng) and 40 μl of 4 mM HCl for seven days. Fresh medium was added after 3 days. A) The cell viability was determined by using trypan blue after 1, 2, 3, 4 and 7 days. B) The cell number was assessed by using a haemocytometer.

Cell viability was determined by using trypan blue staining and a haemocytometer. Furthermore, 40 μl of 4 mM HCl was included as control to avoid false positive results coming from the vehicle substance, since BMP-6 was dissolved in 4 mM HCl (section 5.1.3.2). Fresh culture medium was added after 3 days. sBMP-6 (4 μg) clearly reduced the cell viability to 50 % after seven days (**Figure 6.31** A), whereas 19 ng sBMP-6 reduced it until day 3 and then the viability increased again. The effect of HCl was not significantly different to the control, so that it could be neglected. **Figure 6.31** B shows the total cell number after different days. The doubling time for OPM-2 cells is about 50 – 60 h. If the total cell number is 200000 in the beginning, it increases to 3.2 x 10^6. The cell number of the sBMP-6 (4 μg) sample increased more slowly than the other samples. After 7 days, the cell number was determined to be 925000. This was a clearly smaller number than the control sample (4.1 x 10^6) and the HCl sample (3.4 x 10^6). That means 4 μg sBMP-6 significantly receded the doubling time. Furthermore, the 19 ng BMP-6 sample showed a smaller cell growth than the control samples (3.0 x 10^6).

Dual functionalized surfaces to induce myeloma cell death

In the previous experiment, 4 μg of sBMP-6 reduced cell viability and receded the doubling time of OPM-2 cells. sBMP-6 in a smaller dose (19 ng) showed also an effect on OPM-2 cells less than with 4 μg. Therefore, the gold nanostructured surfaces containing $\alpha_5\beta_1$ specific ligand and an inter particle distance of 32 nm were used in order to stimulate multiple myeloma cells with either iBMP-6. Because of the immobilization, BMP-6 should be protected from internalization into the cell, so that the lower amount might be able to have an similar effect on OPM-2 cells like 4 μg BMP-6. As negative control, gold nanostructured surfaces containing $\alpha_5\beta_1$ specific ligand were used. sBMP-6 was used in the same amount (19 ng) like iBMP-6. As it can be seen in **Figure 6.32**, the iBMP-6 did not show the desired effect on OPM-2 cells. Moreover, the results looked as if both BMP-6 substrates would stimulate the growth of the cells compared to the control surface.

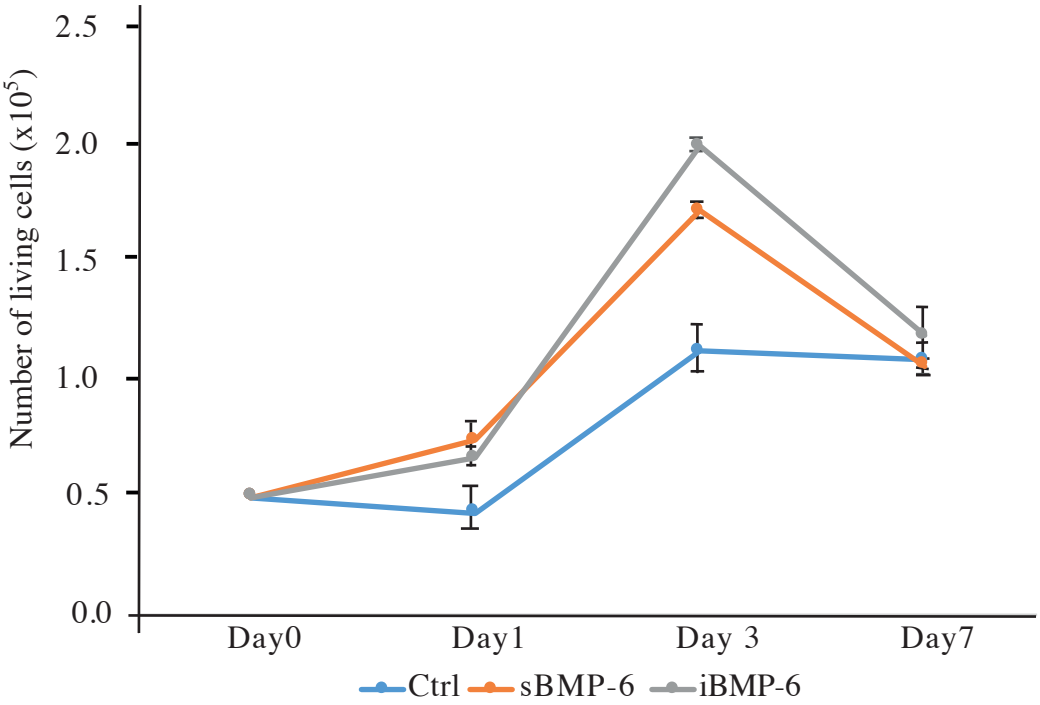

Figure 6.32 The diagram shows the number of living cells after treatment with iBMP-6 and sBMP-6. OPM-2 cells were stimulated with 19 ng of iBMP-6 and sBMP-6. After Day 1, Day 3 and Day 7 the number of living cells was assessed by using the WST-1 assay. The error bars indicate standard deviation, n = 3.

Conclusively, BMP-6 in high concentration showed a clear effect on multiple myeloma cells also compared to BMP-2. However, neither sBMP-6 nor iBMP-6 in low concentration showed an effect in reducing cell viability, moreover it seemed as if BMP-6 stimulated the cell growth.

7 Discussion and Outlook

The objective of this work was to engineer dual functionalized glass surfaces and PEG-DA hydrogels exhibiting both covalently coupled BMP-6 and adhesive ligands in order to investigate the effects of immobilized BMP-6 on BMP-mediated signaling and osteogenic differentiation in C2C12 cells. Furthermore, this approach was adapted to determine the effects of these engineered substrates on the proliferation of multiple myeloma cells.
For this purpose, a covalent immobilization strategy for BMP-6 was chosen in order to avoid uncontrolled release and diffusion of the growth factor. By using gold nanostructured surfaces, it was possible to control the amount and density of immobilized BMP-6. With this it was possible to reduce the amount of BMP-6 by a factor of 600. Recently, the successful immobilization of BMP-2 was shown using alkane thiols containing an NHS moiety as linker (Pohl *et al.*[70] and Schwab *et. al.*[72]).

7.1 Characterization of the linker system and adhesive ligands

Anderson *et al.*[117-119] proposed the *N*-hydroxysuccinimide (NHS) for the synthesis of active esters more than 50 years ago. In theory, NHS esters are relatively stable and can be stored for months under water-free conditions. However, the main reason for a suboptimal conjugation yield is the premature hydrolysis of the NHS ester[120]. The heterobifunctional linker 11-mercaptoundecanoyl-*N*-hydroxysuccinimide (MU-NHS), which was used to immobilize BMP-6 to the surface, maintained its activity after SAM formation on gold surfaces in dry DMF, as was proven by IR spectroscopy. The detected signals correlated with documented signals in literature[121]. The region in the spectra between 1200 cm^{-1} and 400 cm^{-1}, which is also called fingerprint region, was not further analyzed. In this range, many vibrations do not show an ideal behavior and display a shift by more than 100 wave numbers[122]. Due to electronic effects in the molecule, most of the structure and bend vibrancies are affected by this shift and the spectrum can have several hundred absorption bands. Therefore, the analysis of this region is challenging and not exact.

Due to the need of using aqueous solvents for the immobilization of BMP-6 on gold nanostructured PEG-DA hydrogels, the NHS ester's stability in aqueous solvent could be determined by XPS (see section 6.1.2). In recent studies, it was shown that the stability against hydrolysis was reduced by increasing the pH [123]. In pH conditions below 7.5, the ester showed its highest stability[124]. This is in agreement with the results, which were obtained in an almost neutral pH of 6.8. Furthermore, the required time for SAM formation of the MU-NHS linker was determined to be 20 min, what is even quicker than the results published in literature. The adsorption time of thiol alkane depends on its nature. Long chain alkanethiols (> C5) form well-ordered SAM during 2-24 h. In comparison, short chain alkanethiols (< C6) need to be incubated for at least 24 h[125]. The order of the SAM is increased by longer incubation time. In conclusion, the NHS linker can be immobilized in 20 min through SAM formation in aqueous solvents without losing its activity.

Cell adhesion promoted by adhesive ligands

The most important receptors for cell adhesion and adhesion mediated cell signaling are represented by the integrin family[75]. These proteins play an important role in the interaction between cells and the extracellular matrix (ECM) proteins. Due to their function, they are bidirectional and heterodimeric cell surface receptors[73]. Although it was possible to perform long-term (up to seven days) studies with surfaces, bearing gold and SAM of MU-NHS linkers coupled with BMP-6, cell adhesion to the surfaces was rather unspecific and guided by deposition of cell own matrix. This can mediate further signaling modulation of SMAD pathway (see section 3.1.2), as also reported for other systems[65, 126-127]. In this work, the integrin selective ligand $\alpha_5\beta_1$[82] and cyclic RGD were used to functionalize the PEG passivation layer between the gold nanoparticles by click-chemistry[83] to create an adhesive background while preserving the setup for the covalent immobilization of BMP-6. Successful cell adhesion and spreading of C2C12 cells could be shown on surfaces coated with cyclic RGD and $\alpha_5\beta_1$ selective ligands. Cell adhesion already started after 30 min and 60 min, respectively. These results match with the times of cell adhesion promoted by adhesive ligands which are published in literature[75, 128-129]. This approach accelerates cell adhesion and allows bottom stimulation by immobilized BMP-6.

Furthermore, the functionalization of the surfaces with $\alpha_5\beta_1$ selective ligand successfully promoted the adhesion of the OPM-2 suspension cells. In multiple myeloma, the bone

marrow is the preferred microenvironment for the proliferation and differentiation of the malignant plasma cells which rarely disseminate out of the bone marrow. ECM components within this microenvironment may play an important role in the specific adhesion and retention of the myeloma cells. Kibler *et al*.[130] published the strong expression of β_1 integrin subunit in OPM-2 cells. This explains the strong cell adhesion to the $\alpha_5\beta_1$ selective ligand coated surface.

7.2 Stiffness of artificial biomaterials

One of the major challenges in engineering of synthetic tissues for implantation is the development of a soft transition between the artificial and native tissue, especially in musculoskeletal tissues, where the function of the tissue comprises the production or transmission of forces[131]. The most crucial point is the stiffness of the artificial material, which influences cell adhesion and cell signaling[132].

7.2.1 Incorporation of adhesive ligand influences the hydrogels' stiffness

PEG-DA hydrogels containing gold nanostructured surfaces were prepared as described in section 5.1.6.3 and the Young's modulus was determined by AFM (**Figure 7.1**).

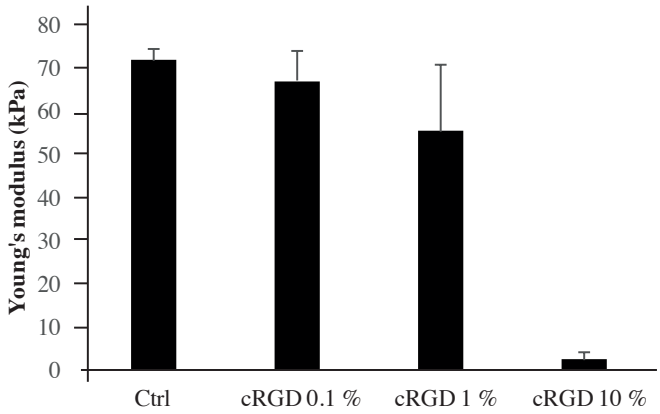

Figure 7.1 Young's modulus of the PEG-DA hydrogels with different cRGD concentration. The stiffness was measured by AFM on five different positions with ten repetitions each. The error bars show the standard deviation, n = 50.

The control sample, which did not contain any cRGD, had a stiffness of 70 kPa, while the stiffness of the PEG-DA hydrogels was reduced by increasing the concentration of incorporated cRGD, following a linear decrease except the highest concentration of cRGD. However, the stiffness dramatically decreased in gels containing 10 % (w/w) cRGD to 4 kPa, whereas gels with 1 % (w/w) cRGD had a stiffness of 54 kPa.

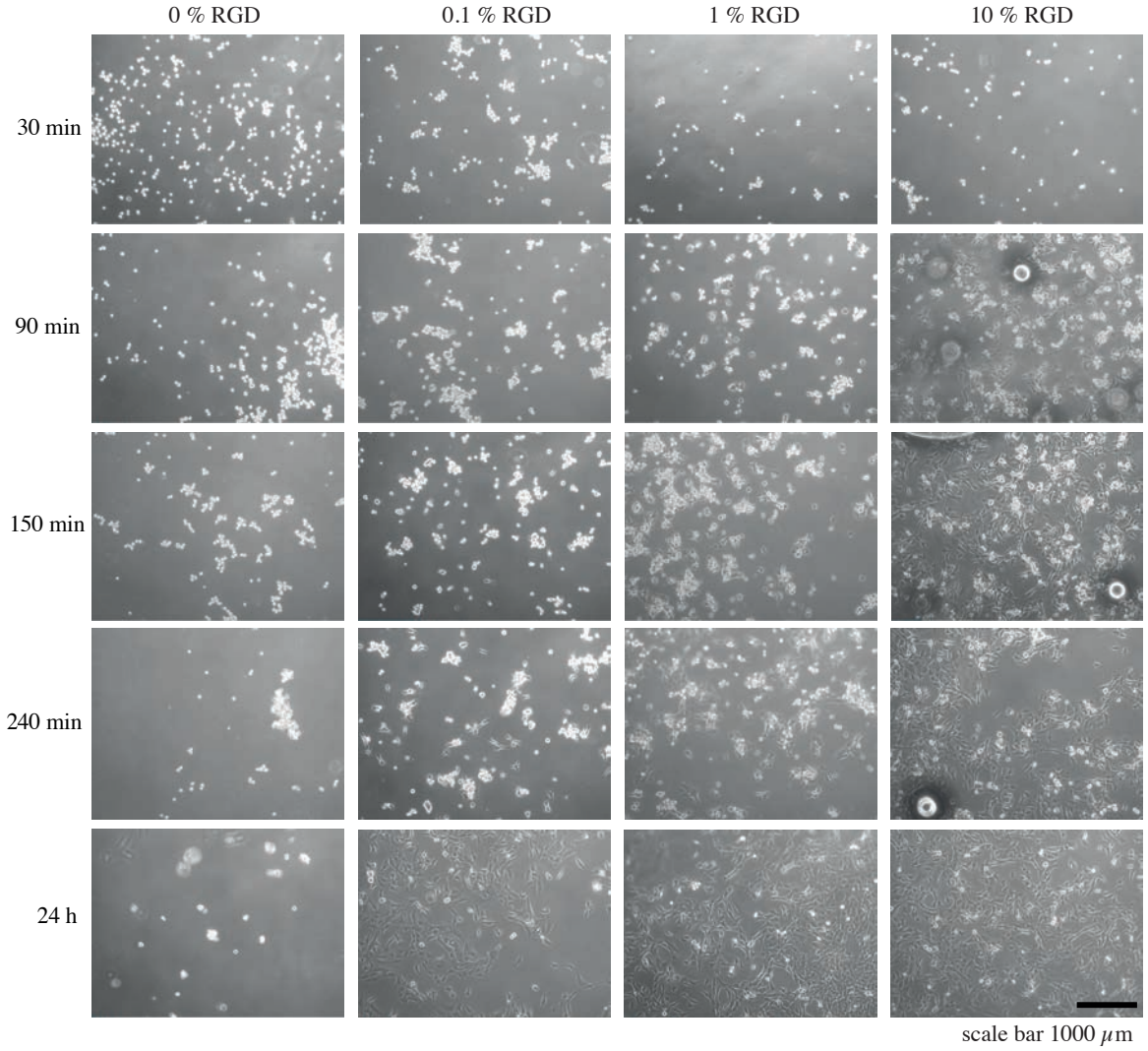

Figure 7.2 C2C12 cell adhesion on PEG-DA hydrogels containing cRGD. Cells were seeded on substrates with cRGD with concentrations ranging from 0.0 % to 10 % (w/w) related to the PEG-DA concentration. Images were taken after 30 min, 90 min, 150 min, 240 min and 24 h. Round cells presented non-adherent cells.

Paxton *et al*.[133] showed the influence of incorporated hydroxyapatite and acrylated GRGDS on the stiffness of PEG-DA hydrogels. They observed that the stiffness was reduced from

15 kPa to 5 kPa by incorporation of acrylated GRGDS, while the stiffness was increased to 32 kPa by incorporating hydroxyapatite. This is in accordance with the obtained results. Phase contrast images clearly show the effect of the cRGD concentration on cell adhesion (**Figure 7.2**). Most of the C2C12 cells started adhering already after 90 min and were completely adherent on 10 % (w/w) cRGD substrate after 240 min. In comparison, a few cells adhered on 1 % (w/w) cRGD after 90 min, while on 0.1 % and control substrate no adhesion could be observed at all. After 24 h on the cRGD functionalized hydrogels cells adhered and spread on the surface, while on control hydrogels no cell adhesion and cell spreading could be observed.

Taken together, by incorporation of cRGD into the hydrogel, the stiffness of the hydrogels was decreased by increasing the cRGD concentration. Furthermore, it was possible to easily introduce a cell adhesion mediated background, which allowed to investigate long-term stimulation of cells.

7.2.2 Influence of stiffness on cell signaling in C2C12 cells

Many cells alter their proliferation and differentiation state depending on the mechanical stiffness of the substrate, e.g. the ECM[134-135]. In order to investigate the influence of the material's stiffness on BMP-mediated cell signaling in long- and short-term BMP-6 stimulation of C2C12 cells, gold nanostructured hydrogels with an interparticle distance of 32 nm, containing iBMP-6, were prepared according to section 5.1.6. $cRGDN_3$ was incorporated into PEG-DA hydrogels in concentrations of 10 %, 1 % and 0.1 % (w/w) (see section 7.2.1), respectively. After successful establishment of an adhesive background (see **Figure 7.2**), the capability of iBMP-6 to stimulate C2C12 cells from bottom in short- (up to 4 h) and long-term (up to 7 days) was investigated.

Inhibition of myotube formation and stimulation of ALP activity by iBMP-6

Here, preliminary results of long-term stimulation of C2C12 cells by iBMP-6 are shown in (**Figure 7.3**). On the one hand, iBMP-6 (19 ng) was able to inhibit myotube formation as well as sBMP-6 (19 ng) compared to control (gold nanostructured hydrogel surface without BMP-6) on hydrogel (A and B), which contained 0.1 % (w/w) cRGD resulting in a stiffness

of 65 kPa (see **Figure 7.1**). These first results were comparable to the results obtained with glass surfaces (see section 6.3.1.2 and 6.4.1.2), which had a higher stiffness. This is in accordance with Engler *et al.*[136], who prepared polyacrylamide hydrogels with a stiffness ranging from 2 kPa to 27 kPa and observed myotube formation using glass surfaces as control. They demonstrated that the optimal elastic modulus for myotube formation is 12 kPa, what matches stiffness of muscle tissue. Moreover, their gels with the highest stiffness (27 kPa) showed comparable results like glass surfaces. Furthermore, they observed that the myotube's morphology is affected by the stiffness. They were more round shaped than elongated compared to the myotube formed on glass surfaces. This observation matches with the results from Ren *et al.*[137] who showed that stiffness modulates deeply adhesion, proliferation and differentiation. They concluded that each of these processes has its own stiffness requirement.

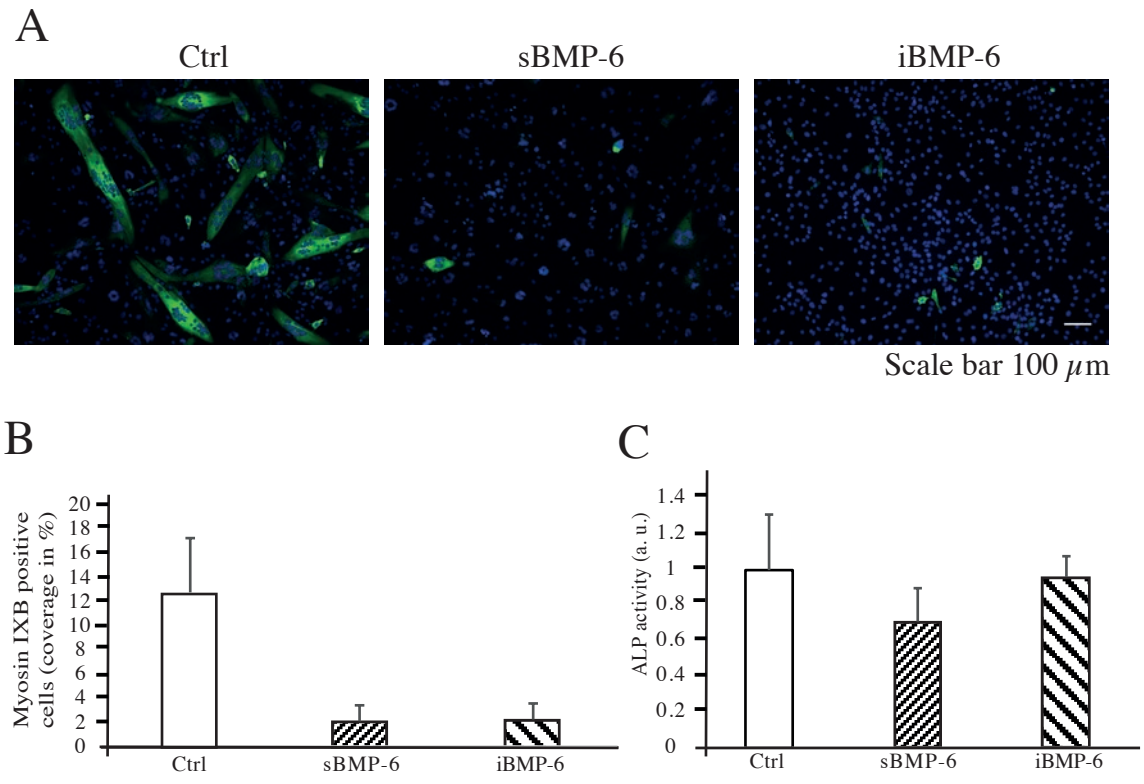

Figure 7.3 Immobilized BMP-6 supressed myotube formation, but did not stimulate osteogenic differentiation of C2C12 cells. A) C2C12 cells were seeded on indicated surfaces and cultured for 6 days under low serum conditions to allow myotube formation. Images show myosin heavy chain (myosin IXB) staining of multinucleated myotubes (green) and DAPI nuclei staining (blue). Image magnification 20x. B) By measuring the area, covered by positive cells, and relating to the total area, a quantification was done and the results were plotted in percentage. Error bars indicate standard deviation, n = 5 repetitions of images. C) The enzymatic activity of alkaline phosphatase (ALP) indicates osteogenic differentiation of C2C12 cells. ALP activity was determined via absorbance at 405 nm. Bar graph shows data acquired after 60 min reaction. The error bars indicate standard deviation, n = 3.

On the other hand, there was no observable difference in ALP activity between iBMP-6 and sBMP-6 stimulation compared to control sample. C2C12 cells were cultured on PEG-DA hydrogels, which contained 1 % cRGD resulting in a stiffness of 54 kPa (see **Figure 7.1**). In comparison with results in section 6.4.1.2, it seemed as if iBMP-6 and sBMP-6 could not stimulate the ALP activity and that the osteogenic differentiation was influenced by the stiffness of the biomaterial. This is in contrast to Gilde *et al.*[138], who showed that the ALP activity is dependent in a manner that the activity is increased by decreasing the substrate's stiffness. They prepared different surfaces with a stiffness ranging from 100 kPa to 400 kPa. However, the here used range of stiffness was different than to Gilde *et al*. Therefore, the influence of the stiffness on ALP activity was different, what complicates a comparison.

SMAD 1/5 phosphorylation by iBMP-6

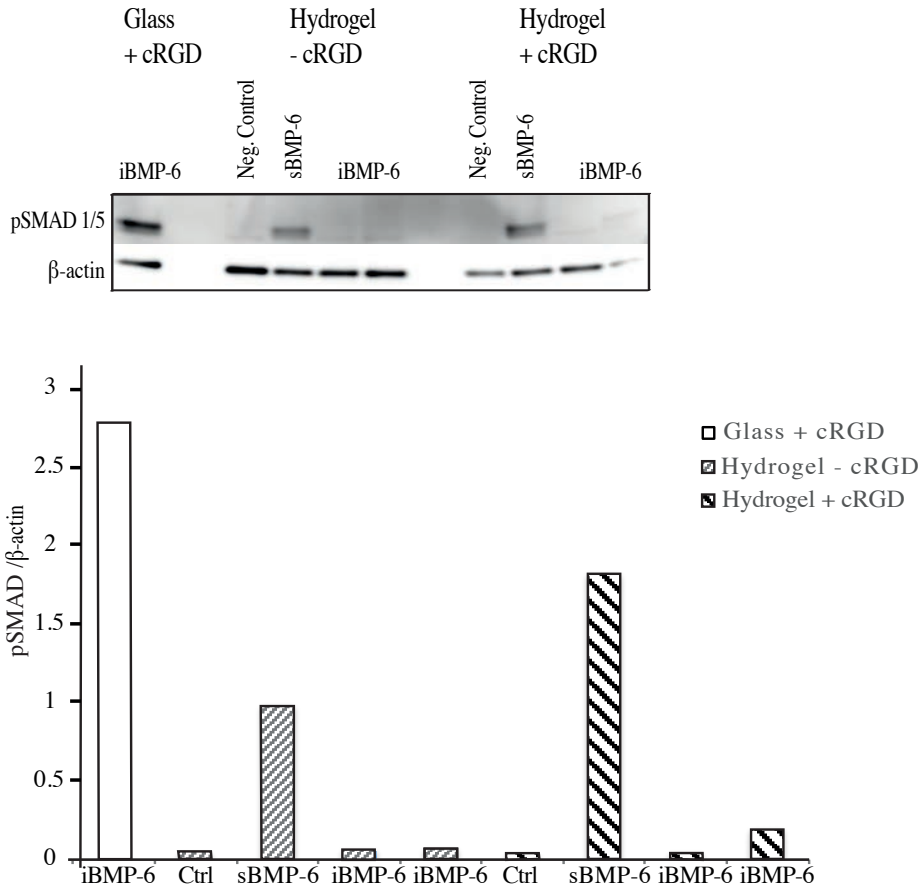

Figure 7.4 Western Blot analysis and quantification of C2C12 cells stimulated by 19 ng iBMP-6 and sBMP-6 on hydrogels with and without cRGD. After 90 min, cells were lysed and samples were immunoblotted for phospho-SMAD 1/5 and β-actin. iBMP-6 on gold nanostructured glass surfacse co-functionalized with cRGD was used as positive control.

In this experiment, two different kinds of PEG-DA hydrogels were used. One contained cRGD in a concentration of 10 % resulting in a stiffness of 4 kPa and one was without cRGD resulting in a stiffness of 74 kPa. The preliminary results, shown in **Figure 7.4**, indicated that iBMP-6 on both hydrogels was not able to stimulate the SMAD1/5 phosphorylation successfully compared to control surface, while sBMP-6 on both hydrogels stimulated the phosphorylation of SMAD 1/5. iBMP-6 on glass surface showed a clear signal for pSMAD 1/5.

In summary, the presented preliminary results showed the cells' differentiation dependence on the material's stiffness. Results need to be further investigated to prove the reproducibility and to further study the relation between differentiation and surface stiffness.

7.3 Immobilization of growth factors

For the first time, it was shown in this work that BMP-6 was covalently immobilized via the heterobifunctional linker mercaptoundecanoyl-N-hydroxysuccinimide ester (MU-NHS) to gold nanostructured glass surfaces and hydrogel. Furthermore, the covalent immobilization of BMP-6 was combined with the integrin $\alpha_5\beta_1$ selective ligand and cRGD which promoted cell adhesion resulting in the dual functionalization of surfaces. In this group, the covalent immobilization of BMP-2 a related growth factor via the MU-NHS linker as either self-assembled monolayer or bound to the gold nanoparticles have been successfully established[70-72]. Tabisz *et al*. recently showed the site-directed immobilization of BMP-2[139]. The protein was immobilized to neutravidin-agarose beads by modifying recombinant human BMP-2 site-specifically and using copper-catalyzed azide-alkyne cycloaddition (CuAAC) to bind it directly or via a short biotin-PEG linker. This method allows the immobilization of BMP-2 in a specific orientation in order to produce fully defined osteogenic surfaces. Although the strategy used in this work does not allow a precise control over the orientation of the protein, it enables to specifically immobilize the growth factor to the surface without further modifications of the molecule and control the density. This simplifies the preparation and avoids side and cross reaction between the active sites of the protein.

The currently available approaches of immobilization like encapsulation or adsorption to the scaffold require very high concentrations (100 μg/ml) of growth factors compared to the low

concentration in human blood[140-141]. This can cause an initial burst release phenomena[142], leading to a release of BMP2 from such scaffolds into extracellular environment where it affects surrounding tissues causing bone overgrowth, osteolysis, and inflammation[143]. To avoid these problems, Meinel *et al.*[144] presented a silk fibroin construct for controlled delivery of entrapped proteins or small molecule drugs. However, a controlled release into the human blood system only allows for growth factor stimulation for a specific time period. By using the covalent immobilization strategy, as presented in this work, undesired side reactions in the body can be circumvented. Additionally, the verified stability of the bond between the linker and the amine residues of the protein even after cell contact enables long-term stimulation of cells possible by using this approach. The effective immobilization of BMP-6 on surfaces, showing that the growth factor is still active even after a longer period of time, has not been reported so far.

Nevertheless, it should be noted that iBMP-6 was not homogeneously distributed on the surfaces, what can be clearly seen (refer to **Figure 6.12** and **Figure 6.13**). As a consequence, the produced substrates could never be equal, but varied in a small range resulting in a fluctuation of the obtained results. A quantitative comparison between the iBMP-6 and sBMP-6 is not entirely correct, but it indicates a tendency in the short- and long-term stimulation ability.

The phosphorylation kinetics and levels in cells, which were stimulated from top by iBMP-6 did not differ much from the ones exposed to sBMP-6 (refer to **Figure 6.20**). In comparison, cells adhering to cRGD surfaces stimulated by iBMP-6 showed significant faster and higher phosphorylation kinetics (stimulation over 4 h) levels than the cells exposed to sBMP-6. This indicated that the combination of immobilized BMP-6 and the adhesive ligand cRGD increased in the SMAD1/5 phosphorylation levels. Another advantage in comparison to other systems is the strongly reduced amount of BMP-6, which was used to obtain cellular response. With the introduced platform for growth factor immobilization combined with adhesive ligands, the required amount for short-term stimulation was 1 ng, which is equal to 0.033 nM. This is approximately 600-fold smaller than the typical amount of 20 nM, which is used in standard *in vitro* assays.

Furthermore, it could be shown that the BMP-6 capability of myotube suppression was not dependent in the mode of presentation without adhesive ligands, but dependent when it was

presented with the adhesive ligands cRGD and the $\alpha_5\beta_1$ selective ligand. iBMP-6 showed a higher efficiency than sBMP-6 even in very low amounts (1 ng). While the adhesive ligands did not have an influence on myotube suppression, cRGD seemed to influence positively the stimulation of ALP by iBMP-6 (1 ng, see **Figure 6.27**). In literature, it was published that BMP-6 induces high ALP activity already at low concentration and after 5 days[32, 41]. Since the amount, which can be immobilized to the surfaces, is limited, BMP-6 combining with adhesive ligands is a potent candidate for immobilization approaches in order to induce ontogenetic differentiation. The low required amount of BMP-6 also reduces the costs what makes it even more attractive.

On top stimulation vs. bottom stimulation

Differences between the on top and from bottom stimulation of C2C12 could be shown. The bottom stimulation with iBMP-6 showed higher phosphorylation activity than the on top stimulation. This can be caused by the fact that the space between the cells and iBMP-6 is filled with a few μl of culture medium, when cells are stimulated from the top. Therefore, the distance between cells and iBMP-6 cannot be controlled and this can cause non-contact of cells and iBMP-6. However, when cells are bottom stimulated, they sit and grow directly in contact with iBMP-6. On the one hand, this leads to total stimulation and not only partly stimulation. On the other hand, it also accelerates the stimulation compared to the soluble delivery of BMP-6. Therefore, the bottom stimulation is the preferred way of stimulation which can be performed with the dual functionalized surfaces.

The here presented approach allows the local and controlled delivery of BMP-6 in order to minimize adverse responses to make this technique applicable for therapeutic usage. Additionally, it reduces the required amount drastically, therefore optimizing costs and reducing side effects.

7.4 Initiation of cell death in multiple myeloma cells

One goal of this project was the medical application of the here presented approach. It is known that BMP-6 shows effects on multiple myeloma cells. Seckinger *et al.*[53] published the inhibition of proliferation in multiple myeloma cell lines. Their experiments proved that

BMP-6 showed its positive effect on myeloma cell death initiation in rather high concentrations (> 5.3 nM), when applied in soluble form. Moreover, 133 nM BMP-6 decreased cell viability to about 60 % and reduced the total cell number to 10 % compared to control after three days. However, it seemed that lower concentrations of BMP-6 on the contrary even stimulated the proliferation of multiple myeloma cells. This was also observed in experiments results shown in this work (compare **Figure 6.31**). The samples, treated with high concentrated BMP-6 (133 nM), showed 80 % less cells than the control after seven days. Furthermore, the cell viability was less than 60 %. During the first three days, there was no significant difference in cell viability detectable between 0.6 nM and 133 nM BMP-6. On later time points, the low dose did not show a significant effect on cell viability anymore. One reason could be the internalization and degradation of BMP-6 by the myeloma cells, so that it was depleted from the medium. Nevertheless, the proliferation was successfully reduced by the high dose, while the low dose did not show a significant effect on cell proliferation compared to control sample. As mentioned previously, high doses of grow factors in general and BMP-6 in special in human body can cause lot of side effects, which are supported by the systemic treatment. The here presented approach was used to reduce the required amount for cell death induction and to replace the systemic treatment with a local one. The fact that multiple myeloma cells are suspension cells makes the dual functionalized surfaces presenting BMP-6 and adhesive ligands as the method of choice. Besides, Kim *et al.*[145] published that BMP-6 is present in the kidney and potent to inhibit growth in human renal carcinoma cell lines. In other cancers such as prostate[146-147] or breast cancer[148] BMP-6 is supposed to promote tumor progression and development of metastasis. These results showed that BMP-6 should be applied in rather low doses to reduce and avoid side effects, respectively. In order to avoid BMP-6 internalization and to increase the effect on cell viability in multiple myeloma cells, iBMP-6 on the dual functionalized approach with $\alpha_5\beta_1$ selective ligand. The expression of integrin β_1 in multiple myeloma cells is known in literature[149-151] and was employed in this work to successfully promote cell adhesion via the $\alpha_5\beta_1$ selective ligand (compare **Figure 6.28**), whereas it was not possible to promote cell adhesion of multiple myeloma cells by using cRGD. The living cell number was determined after three and seven days, respectively (see **Figure 6.32**), whereby iBMP-6 and sBMP-6 did not comprise different results. However, both samples showed a higher number of living

cells than the control sample. The approach did not show the desired effect, means the low dose of BMP-6 seemed to be not insufficient to affect in the immobilized form either.
Until now, it is not known how BMP-6 induces cell death and inhibits proliferation in multiple myeloma. This needs to be further investigated in order to optimize the conditions of the BMP-6 application. Furthermore, the approach presented in this work can be further optimized in regards to the delivery form of BMP-6.

8 Summary and Conclusion

In this work, a novel platform copresenting growth factors, namely BMP-6, with cell adhesion promoting cues such as the $\alpha_5\beta_1$ integrin selective ligand or the integrin binding RGD peptide was presented. This setup was used to investigate the independence of growth factor cell signaling and integrin-mediated cell adhesion. BMP-6 was covalently immobilized to prevent internalization and therefore achieve their sustained presentation to cells. Moreover, on this approach, based on surface nanopatterning, BMP-6 and either of the two integrin selective ligands cRGD and $\alpha_5\beta_1$ selective ligand were immobilized, while maintaining their biological activity. By addressing the lysine residues and the N-terminus of the growth factor, BMP-6 was covalently immobilized to gold nanoparticles using MU-NHS linker. The adhesive ligands containing azide moisty were coupled to the PEG-alkyne by applying CuAAC click reaction. The presentation of factors using these platforms could be controlled independently by tuning the nanoparticle distances and the number of functional groups on the PEG to vary growth factor surface density and optimize cell attachment to the surface. This approach provides for the first time the presentation of active BMP-6 in small and defined amount on surfaces, while achieving controlled spatial resolution in combination with adhesive ligands. I showed that co-presentation of BMP-6 and either of the two adhesive ligands promoted SMAD 1/5 phosphorylation and osteogenic differentiation of mouse myoblastoma cells, at amounts as low as 1 ng, whereas addition of soluble BMP-6 in equal amounts was significantly less effective. I proved that a local control of ligands' density is crucial for modulating cell response. A potential medical application of the presented approach dealing with the initiation of cell death in multiple myeloma cells by iBMP-6 was also performed.

In future studies, the underlying molecular mechanisms are addressed, in particular regarding the regulation of lineage commitment and differentiation of cells to be able to make our approach suitable for clinical applications, e.g. scaffold functionalization and more in general tissue engineering. Furthermore, the transfer of the here presented approach on PEG based hydrogels allows the preparation of a platform, which enables the investigation of long-term cell signaling studies with controlled and covalently immobilized growth factors in combination with adhesive ligands. This setup is not limited to BMP-6 in particular and BMPs in general, but is applicable for any growth factors containing primary amine

groups, which can be addressed by the MU-NHS linker. Furthermore, other groups of the protein can be utilized by exchanging the NHS ester with appropriate reactive groups, e.g. nickel-nitrilotriacetic acid (NTA) addressing a polyhistidine-tag (His-tag) or a maleimide targeting cysteine residue. This makes the presented technique a versatile tool, since the dual functionalized linker only needs to contain a thiol group to bind to the gold nanoparticles. This allows for the investigation of short- and long-term signaling pathways stimulated by growth factors. This work can help to study cell pathways and interactions in order to understand the underlying mechanisms of various diseases paving the way towards new drugs and therapeutical treatments.

9 Appendix

9.1 Chemiluminescence detection of BMP-6 and GFP after QCM-D observation

While the surface treated with MU-NHS and BMP-6 showed a strong and intensive signal, the control surface without BMP-6 treatment displayed almost no signal. This confirmed the QCM-D results in the previous section and proved the immobilization of BMP-6 to the homogeneous gold surface.

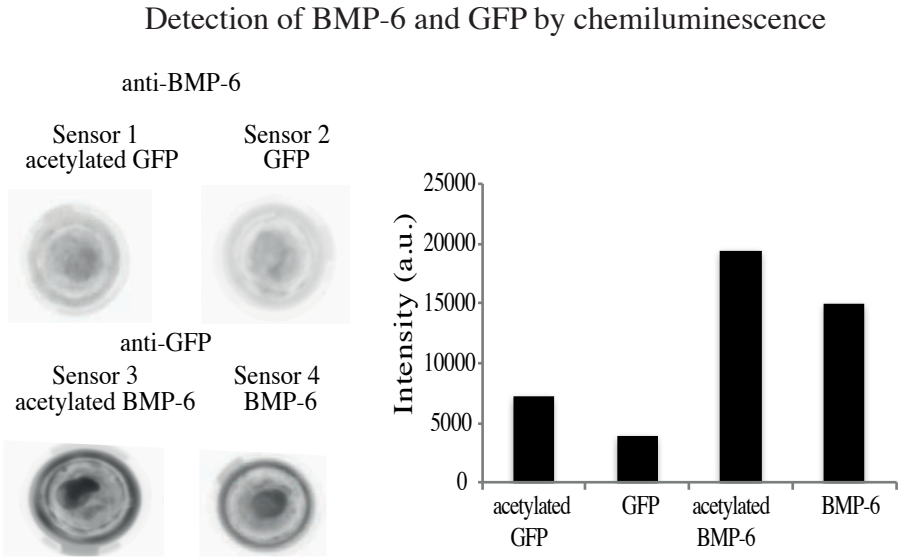

Figure 9.1 Chemiluminescence detection and quantification of BMP-6 and GFP on QCM-D crystals. The QCM-D sensors, which were first treated witch acetylated protein (sensor 1 and sensor 3), showed a higher signal than the other two sensors (sensor 2 and sensor 4). These results were supported by the intensity quantification supports.

The final chemiluminescence detection of BMP-6 and GFP on the QCM-D sensors (**Figure 9.1**) proved the results from the QCM-D experiment. The acetylated proteins bound weaker to the surfaces coated with MU-NHS linker than the untreated proteins.

9.2 BMP-6 detection on homogeneous gold surface by chemiluminescence

In order to validate the results and prove the reproducibility, glass coverslips were coated with homogeneous gold, supported by an adhesive chromium layer, generated by physical vapor deposition. Afterwards the substrates were functionalized with a SAM of MU-NHS ester, followed by immobilization of BMP-6 to the surface. Then, the surfaces were blocked with BSA and incubated with primary anti-BMP-6 mouse IgG antibody and secondary anti-mouse IgG antibody conjugated with HRP. The detection of BMP-6 was performed with luminescent imaging analyzer using ECL detection kit as described in section 5.2.2.1. **Figure 9.2** shows the successful immobilization of BMP-6 on gold substrates.

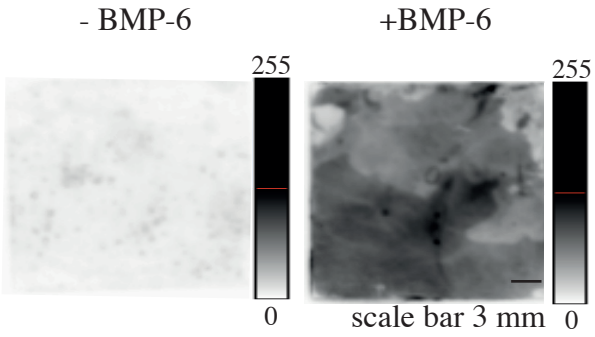

Figure 9.2 Chemiluminescence detection of BMP-6 on gold substrates. Surface bound BMP-6 was detected with indirect immunochemiluminescence. As control, a surface, which was not incubated with BMP-6, was used. Image was adapted and modified from Martin *et al*.[98]

10 Bibliography

1. Munk, K.; Abröll, C., Biochemie - Zellbiologie. *Thieme***:** Stuttgart [u.a.], **2008**; p XVI, 560 S.

2. Goldman, R., Growth factors and chronic wound healing: past, present, and future. *Advances in skin & wound care* **2004,** *17* (1), 24-35.

3. Steed, D. L., The role of growth factors in wound healing. *The Surgical clinics of North America* **1997,** *77* (3), 575-86.

4. Lind, M., Growth factors: possible new clinical tools. A review. *Acta orthopaedica Scandinavica* **1996,** *67* (4), 407-17.

5. Smith, P. C.; Martinez, C.; Caceres, M.; Martinez, J., Research on growth factors in periodontology. *Periodontology 2000* **2015,** *67* (1), 234-50.

6. Mitchell, A. C.; Briquez, P. S.; Hubbell, J. A.; Cochran, J. R., Engineering growth factors for regenerative medicine applications. *Acta Biomaterialia* **2016,** *30*, 1-12.

7. Rose, F. R.; Hou, Q.; Oreffo, R. O., Delivery systems for bone growth factors - the new players in skeletal regeneration. *The Journal of pharmacy and pharmacology* **2004,** *56* (4), 415-27.

8. Lee, J.; Blaber, M., Increased functional half-life of fibroblast growth factor-1 by recovering a vestigial disulfide bond. *Journal of Proteins & Proteomics; Vol 1, No 2* **2013**.

9. Lee, K.; Silva, E. A.; Mooney, D. J., Growth factor delivery-based tissue engineering: general approaches and a review of recent developments. *Journal of The Royal Society Interface* **2010,** *8* (55), 153.

10. Atanasova, M.; Whitty, A., Understanding Cytokine and Growth Factor Receptor Activation Mechanisms. *Critical reviews in biochemistry and molecular biology* **2012,** *47* (6), 502-530.

11. Rengachary, S. S., Bone morphogenetic proteins: basic concepts. *Neurosurgical Focus* **2002,** *13* (6), 1-6.

12. Mohan, S.; Baylink, D. J., Bone growth factors. *Clinical orthopaedics and related research* **1991,** (263), 30-48.

13. Carreira, A. C.; Alves, G. G.; Zambuzzi, W. F.; Sogayar, M. C.; Granjeiro, J. M., Bone Morphogenetic Proteins: Structure, biological function and therapeutic applications. *Archives of Biochemistry and Biophysics* **2014,** *561*, 64-73.

14. Urist, M. R., Bone: formation by autoinduction. *Science (New York, N.Y.)* **1965,** *150* (3698), 893-9.

15. Urist, M. R.; Strates, B. S., Bone Morphogenetic Protein. *Journal of Dental Research* **1971,** *50* (6), 1392-1406.

16. Reddi, A. H.; Huggins, C., Biochemical Sequences in the Transformation of Normal Fibroblasts in Adolescent Rats. *Proceedings of the National Academy of Sciences of the United States of America* **1972,** *69* (6), 1601-1605.

17. Wang, E. A.; Rosen, V.; Cordes, P.; Hewick, R. M.; Kriz, M. J.; Luxenberg, D. P.; Sibley, B. S.; Wozney, J. M., Purification and characterization of other distinct bone-inducing factors. *Proc Natl Acad Sci U S A* **1988,** *85* (24), 9484-8.

18. Ali, I. H.; Brazil, D. P., Bone morphogenetic proteins and their antagonists: current and emerging clinical uses. *British journal of pharmacology* **2014,** *171* (15), 3620-32.

19. Lieberman, J. R.; Daluiski, A.; Einhorn, T. A., The role of growth factors in the repair of bone. Biology and clinical applications. *The Journal of bone and joint surgery. American volume* **2002,** *84-a* (6), 1032-44.

20. Butler, S. J.; Dodd, J., A role for BMP heterodimers in roof plate-mediated repulsion of commissural axons. *Neuron* **2003,** *38* (3), 389-401.

21. Griffith, D. L.; Keck, P. C.; Sampath, T. K.; Rueger, D. C.; Carlson, W. D., Three-dimensional structure of recombinant human osteogenic protein 1: structural paradigm for the transforming growth factor beta superfamily. *Proc Natl Acad Sci U S A* **1996,** *93* (2), 878-83.

22. Daluiski, A.; Engstrand, T.; Bahamonde, M. E.; Gamer, L. W.; Agius, E.; Stevenson, S. L.; Cox, K.; Rosen, V.; Lyons, K. M., Bone morphogenetic protein-3 is a negative regulator of bone density. *Nature genetics* **2001,** *27* (1), 84-8.

23. Xiao, Y.-T.; Xiang, L.-X.; Shao, J.-Z., Bone morphogenetic protein. *Biochemical and Biophysical Research Communications* **2007,** *362* (3), 550-553.

24. Kessler, E.; Takahara, K.; Biniaminov, L.; Brusel, M.; Greenspan, D. S., Bone morphogenetic protein-1: The type I procollagen C-proteinase. *Science (New York, N.Y.)* **1996,** *271* (5247), 360-362.

25. Reddi, A. H., BMPs: From bone morphogenetic proteins to body morphogenetic proteins. *Cytokine & Growth Factor Reviews* **2005,** *16* (3), 249-250.

26. Lyons, K. M.; Pelton, R. W.; Hogan, B. L., Patterns of expression of murine Vgr-1 and BMP-2a RNA suggest that transforming growth factor-beta-like genes coordinately regulate aspects of embryonic development. *Genes & development* **1989,** *3* (11), 1657-68.

27. Celeste, A. J.; Iannazzi, J. A.; Taylor, R. C.; Hewick, R. M.; Rosen, V.; Wang, E. A.; Wozney, J. M., Identification of transforming growth factor beta family members present in

bone-inductive protein purified from bovine bone. *Proc Natl Acad Sci U S A* **1990,** *87* (24), 9843-7.

28. Vukicevic, S.; Grgurevic, L., BMP-6 and mesenchymal stem cell differentiation. *Cytokine Growth Factor Rev* **2009,** *20* (5-6), 441-8.

29. Valera, E.; Isaacs, M. J.; Kawakami, Y.; Izpisua Belmonte, J. C.; Choe, S., BMP-2/6 heterodimer is more effective than BMP-2 or BMP-6 homodimers as inductor of differentiation of human embryonic stem cells. *PloS one* **2010,** *5* (6), e11167.

30. Saremba, S.; Nickel, J.; Seher, A.; Kotzsch, A.; Sebald, W.; Mueller, T. D., Type I receptor binding of bone morphogenetic protein 6 is dependent on N-glycosylation of the ligand. *The FEBS journal* **2008,** *275* (1), 172-83.

31. Urrutia, H.; Aleman, A.; Eivers, E., Drosophila Dullard functions as a Mad phosphatase to terminate BMP signaling. *Sci Rep* **2016,** *6*, 32269.

32. Ebisawa, T.; Tada, K.; Kitajima, I.; Tojo, K.; Sampath, T. K.; Kawabata, M.; Miyazono, K.; Imamura, T., Characterization of bone morphogenetic protein-6 signaling pathways in osteoblast differentiation. *Journal of Cell Science* **1999,** *112* (20), 3519.

33. Sieber, C.; Kopf, J.; Hiepen, C.; Knaus, P., Recent advances in BMP receptor signaling. *Cytokine & Growth Factor Reviews* **2009,** *20* (5–6), 343-355.

34. Zhang, Y. E., Non-Smad pathways in TGF-beta signaling. *Cell research* **2009,** *19* (1), 128-39.

35. Herpin, A.; Cunningham, C., Cross-talk between the bone morphogenetic protein pathway and other major signaling pathways results in tightly regulated cell-specific outcomes. *FEBS Journal* **2007,** *274* (12), 2977-2985.

36. Sumi, T.; Tsuneyoshi, N.; Nakatsuji, N.; Suemori, H., Defining early lineage specification of human embryonic stem cells by the orchestrated balance of canonical

Wnt/beta-catenin, Activin/Nodal and BMP signaling. *Development (Cambridge, England)* **2008,** *135* (17), 2969-79.

37. Shukunami, C.; Shigeno, C.; Atsumi, T.; Ishizeki, K.; Suzuki, F.; Hiraki, Y., Chondrogenic differentiation of clonal mouse embryonic cell line ATDC5 in vitro: differentiation-dependent gene expression of parathyroid hormone (PTH)/PTH-related peptide receptor. *The Journal of cell biology* **1996,** *133* (2), 457-68.

38. Paralkar, V. M.; Weeks, B. S.; Yu, Y. M.; Kleinman, H. K.; Reddi, A. H., Recombinant human bone morphogenetic protein 2B stimulates PC12 cell differentiation: potentiation and binding to type IV collagen. *The Journal of cell biology* **1992,** *119* (6), 1721-8.

39. Katagiri, T.; Yamaguchi, A.; Komaki, M.; Abe, E.; Takahashi, N.; Ikeda, T.; Rosen, V.; Wozney, J. M.; Fujisawa-Sehara, A.; Suda, T., Bone morphogenetic protein-2 converts the differentiation pathway of C2C12 myoblasts into the osteoblast lineage. *The Journal of cell biology* **1994,** *127* (6 Pt 1), 1755-66.

40. Takeda, K.; Ichijo, H.; Fujii, M.; Mochida, Y.; Saitoh, M.; Nishitoh, H.; Sampath, T. K.; Miyazono, K., Identification of a novel bone morphogenetic protein-responsive gene that may function as a noncoding RNA. *The Journal of biological chemistry* **1998,** *273* (27), 17079-85.

41. Luu, H. H.; Song, W. X.; Luo, X.; Manning, D.; Luo, J.; Deng, Z. L.; Sharff, K. A.; Montag, A. G.; Haydon, R. C.; He, T. C., Distinct roles of bone morphogenetic proteins in osteogenic differentiation of mesenchymal stem cells. *Journal of orthopaedic research : official publication of the Orthopaedic Research Society* **2007,** *25* (5), 665-77.

42. Cheng, H.; Jiang, W.; Phillips, F. M.; Haydon, R. C.; Peng, Y.; Zhou, L.; Luu, H. H.; An, N.; Breyer, B.; Vanichakarn, P.; Szatkowski, J. P.; Park, J. Y.; He, T. C., Osteogenic

activity of the fourteen types of human bone morphogenetic proteins (BMPs). *The Journal of bone and joint surgery. American volume* **2003,** *85-a* (8), 1544-52.

43. Friedman, M. S.; Long, M. W.; Hankenson, K. D., Osteogenic differentiation of human mesenchymal stem cells is regulated by bone morphogenetic protein-6. *Journal of cellular biochemistry* **2006,** *98* (3), 538-54.

44. Mizrahi, O.; Sheyn, D.; Tawackoli, W.; Kallai, I.; Oh, A.; Su, S.; Da, X.; Zarrini, P.; Cook-Wiens, G.; Gazit, D.; Gazit, Z., BMP-6 is more efficient in bone formation than BMP-2 when overexpressed in mesenchymal stem cells. *Gene therapy* **2013,** *20* (4), 370-7.

45. Goldschmidt, H., Das multiple Myelom (Plasmozytom) : Diagnose und Therapie. 2. Aufl. ed.; *UNI-MED-Verl.*: Bremen [u.a.], **2011**; p 133 S.

46. Kortüm, M.; Driessen, C.; Einsele, H.; Goldschmidt, H.; Gunsilius, H.; Kropff, M.; Kröger, N.; Liebisch, P.; Ludwig, H.; Naumann, R.; Peest, D.; Taverna, C.; Wörmann, B.; Multiples Myelom. *onkopedia* **2013,** https://www.onkopedia.com/de/onkopedia/guidelines/multiples-myelom/@@view/html/index.html (accessed 17.05.2017).

47. Kumar, S. K.; Rajkumar, S. V.; Dispenzieri, A.; Lacy, M. Q.; Hayman, S. R.; Buadi, F. K.; Zeldenrust, S. R.; Dingli, D.; Russell, S. J.; Lust, J. A.; Greipp, P. R.; Kyle, R. A.; Gertz, M. A., Improved survival in multiple myeloma and the impact of novel therapies. *Blood* **2008,** *111* (5), 2516.

48. Moreau, P., The Future of Therapy for Relapsed/Refractory Multiple Myeloma: Emerging Agents and Novel Treatment Strategies. *Seminars in Hematology* **2012,** *49, Supplement 1*, S33-S46.

49. Gentile, M.; Recchia, A. G.; Mazzone, C.; Morabito, F., Emerging biological insights and novel treatment strategies in multiple myeloma. *Expert Opinion on Emerging Drugs* **2012,** *17* (3), 407-438.

50. Klein, B.; Seckinger, A.; Moehler, T.; Hose, D., Molecular pathogenesis of multiple myeloma: chromosomal aberrations, changes in gene expression, cytokine networks, and the bone marrow microenvironment. *Recent results in cancer research. Fortschritte der Krebsforschung. Progres dans les recherches sur le cancer* **2011,** *183*, 39-86.

51. Andersen, T. L.; Sondergaard, T. E.; Skorzynska, K. E.; Dagnaes-Hansen, F.; Plesner, T. L.; Hauge, E. M.; Plesner, T.; Delaisse, J. M., A physical mechanism for coupling bone resorption and formation in adult human bone. *The American journal of pathology* **2009,** *174* (1), 239-47.

52. Seckinger, A.; Hose, D., Interaktion zwischen Myelomzellen und Knochengewebe. *Der Radiologe* **2014,** *54* (6), 545-550.

53. Seckinger, A.; Meissner, T.; Moreaux, J.; Goldschmidt, H.; Fuhler, G. M.; Benner, A.; Hundemer, M.; Reme, T.; Shaughnessy, J. D., Jr.; Barlogie, B.; Bertsch, U.; Hillengass, J.; Ho, A. D.; Pantesco, V.; Jauch, A.; De Vos, J.; Rossi, J. F.; Mohler, T.; Klein, B.; Hose, D., Bone morphogenic protein 6: a member of a novel class of prognostic factors expressed by normal and malignant plasma cells inhibiting proliferation and angiogenesis. *Oncogene* **2009,** *28* (44), 3866-79.

54. Mason, C.; Dunnill, P., A brief definition of regenerative medicine. *Regenerative medicine* **2008,** *3* (1), 1-5.

55. Ige, O. O.; Umoru, L. E.; Aribo, S., Natural Products: A Minefield of Biomaterials. *ISRN Materials Science* **2012,** *2012*, 20.

56. Sahni, A.; Altland, O. D.; Francis, C. W., FGF-2 but not FGF-1 binds fibrin and supports prolonged endothelial cell growth. *Journal of thrombosis and haemostasis : JTH* **2003,** *1* (6), 1304-10.

57. Sahni, A.; Francis, C. W., Vascular endothelial growth factor binds to fibrinogen and fibrin and stimulates endothelial cell proliferation. *Blood* **2000,** *96* (12), 3772-8.

58. Zisch, A. H.; Lutolf, M. P.; Hubbell, J. A., Biopolymeric delivery matrices for angiogenic growth factors. *Cardiovascular Pathology* **2003,** *12* (6), 295-310.

59. Igai, H.; Chang, S. S.; Gotoh, M.; Yamamoto, Y.; Misaki, N.; Okamoto, T.; Yamamoto, M.; Tabata, Y.; Yokomise, H., Regeneration of canine tracheal cartilage by slow release of basic fibroblast growth factor from gelatin sponge. *ASAIO journal (American Society for Artificial Internal Organs : 1992)* **2006,** *52* (1), 86-91.

60. Yamamoto, M.; Takahashi, Y.; Tabata, Y., Enhanced bone regeneration at a segmental bone defect by controlled release of bone morphogenetic protein-2 from a biodegradable hydrogel. *Tissue engineering* **2006,** *12* (5), 1305-11.

61. Sakiyama-Elbert, S. E.; Hubbell, J. A., Controlled release of nerve growth factor from a heparin-containing fibrin-based cell ingrowth matrix. *Journal of Controlled Release* **2000,** *69* (1), 149-158.

62. Migliorini, E.; Horn, P.; Haraszti, T.; Wegner, S. V.; Hiepen, C.; Knaus, P.; Richter, R. P.; Cavalcanti-Adam, E. A., Enhanced Biological Activity of BMP-2 Bound to Surface-Grafted Heparan Sulfate. *Advanced Biosystems* **2017,** *1* (4).

63. Sun, W.; Lin, H.; Chen, B.; Zhao, W.; Zhao, Y.; Xiao, Z.; Dai, J., Collagen scaffolds loaded with collagen-binding NGF-beta accelerate ulcer healing. *Journal of biomedical materials research. Part A* **2010,** *92* (3), 887-95.

64. Han, Q.; Sun, W.; Lin, H.; Zhao, W.; Gao, Y.; Zhao, Y.; Chen, B.; Xiao, Z.; Hu, W.; Li, Y.; Yang, B.; Dai, J., Linear ordered collagen scaffolds loaded with collagen-binding brain-derived neurotrophic factor improve the recovery of spinal cord injury in rats. *Tissue engineering. Part A* **2009,** *15* (10), 2927-35.

65. Hauff, K.; Zambarda, C.; Dietrich, M.; Halbig, M.; Grab, A. L.; Medda, R.; Cavalcanti-Adam, E. A., Matrix-Immobilized BMP-2 on Microcontact Printed Fibronectin as an in vitro Tool to Study BMP-Mediated Signaling and Cell Migration. *Frontiers in bioengineering and biotechnology* **2015,** *3*, 62.

66. Ehrbar, M.; Djonov, V. G.; Schnell, C.; Tschanz, S. A.; Martiny-Baron, G.; Schenk, U.; Wood, J.; Burri, P. H.; Hubbell, J. A.; Zisch, A. H., Cell-demanded liberation of VEGF121 from fibrin implants induces local and controlled blood vessel growth. *Circulation research* **2004,** *94* (8), 1124-32.

67. Ehrbar, M.; Rizzi, S. C.; Hlushchuk, R.; Djonov, V.; Zisch, A. H.; Hubbell, J. A.; Weber, F. E.; Lutolf, M. P., Enzymatic formation of modular cell-instructive fibrin analogs for tissue engineering. *Biomaterials* **2007,** *28* (26), 3856-66.

68. Hajimiri, M.; Shahverdi, S.; Kamalinia, G.; Dinarvand, R., Growth factor conjugation: strategies and applications. *Journal of biomedical materials research. Part A* **2015,** *103* (2), 819-38.

69. Chiu, L. L. Y.; Radisic, M., Scaffolds with covalently immobilized VEGF and Angiopoietin-1 for vascularization of engineered tissues. *Biomaterials* **2010,** *31* (2), 226-241.

70. Pohl, T. L. M.; Boergermann, J. H.; Schwaerzer, G. K.; Knaus, P.; Cavalcanti-Adam, E. A., Surface immobilization of bone morphogenetic protein 2 via a self-assembled monolayer formation induces cell differentiation. *Acta Biomaterialia* **2012,** *8* (2), 772-780.

71. Pohl, T. L. M.; Schwab, E. H.; Cavalcanti-Adam, E. A., Covalent Binding of BMP-2 on Surfaces Using a Self-assembled Monolayer Approach. **2013,** (78), e50842.

72. Schwab, E. H.; Pohl, T. L. M.; Haraszti, T.; Schwaerzer, G. K.; Hiepen, C.; Spatz, J. P.; Knaus, P.; Cavalcanti-Adam, E. A., Nanoscale Control of Surface Immobilized BMP-2: Toward a Quantitative Assessment of BMP-Mediated Signaling Events. *Nano Letters* **2015,** *15* (3), 1526-1534.

73. Hynes, R. O., Integrins: Bidirectional, Allosteric Signaling Machines. *Cell* **2002,** *110* (6), 673-687.

74. Hynes, R. O., Integrins: A family of cell surface receptors. *Cell* **1987,** *48* (4), 549-554.

75. Mas-Moruno, C.; Fraioli, R.; Rechenmacher, F.; Neubauer, S.; Kapp, T. G.; Kessler, H., alphavbeta3- or alpha5beta1-Integrin-Selective Peptidomimetics for Surface Coating. *Angewandte Chemie (International ed. in English)* **2016,** *55* (25), 7048-67.

76. Geiger, B.; Spatz, J. P.; Bershadsky, A. D., Environmental sensing through focal adhesions. *Nat Rev Mol Cell Biol* **2009,** *10* (1), 21-33.

77. Pytela, R.; Pierschbacher, M. D.; Ruoslahti, E., Identification and isolation of a 140 kd cell surface glycoprotein with properties expected of a fibronectin receptor. *Cell* **1985,** *40* (1), 191-198.

78. Pierschbacher, M. D.; Ruoslahti, E., Cell attachment activity of fibronectin can be duplicated by small synthetic fragments of the molecule. *Nature* **1984,** *309* (5963), 30-33.

79. Aumailley, M.; Gurrath, M.; Muller, G.; Calvete, J.; Timpl, R.; Kessler, H., Arg-Gly-Asp constrained within cyclic pentapeptides. Strong and selective inhibitors of cell adhesion to vitronectin and laminin fragment P1. *FEBS letters* **1991,** *291* (1), 50-4.

80. Gurrath, M.; Muller, G.; Kessler, H.; Aumailley, M.; Timpl, R., Conformation/activity studies of rationally designed potent anti-adhesive RGD peptides. *European journal of biochemistry* **1992,** *210* (3), 911-21.

81. Haubner, R.; Kessler, I. H., Stereoisomere Peptid-Bibliotheken und Peptidmimetika zum Design von selektiven Inhibitoren des αv β3-Integrins für eine neuartige Krebstherapie. *Angewandte Chemie* **1997,** *109* (13-14), 1440-1456.

82. Rechenmacher, F.; Neubauer, S.; Polleux, J.; Mas-Moruno, C.; De Simone, M.; Cavalcanti-Adam, E. A.; Spatz, J. P.; Fässler, R.; Kessler, H., Functionalizing αvβ3- or α5β1-Selective Integrin Antagonists for Surface Coating: A Method To Discriminate Integrin Subtypes In Vitro. *Angewandte Chemie International Edition* **2013,** *52* (5), 1572-1575.

83. Schenk, F. C.; Boehm, H.; Spatz, J. P.; Wegner, S. V., Dual-Functionalized Nanostructured Biointerfaces by Click Chemistry. *Langmuir* **2014,** *30* (23), 6897-6905.

84. Masters, K. S., Covalent growth factor immobilization strategies for tissue repair and regeneration. *Macromolecular bioscience* **2011,** *11* (9), 1149-63.

85. Spatz, J. P.; Mössmer, S.; Hartmann, C.; Möller, M.; Herzog, T.; Krieger, M.; Boyen, H.-G.; Ziemann, P.; Kabius, B., Ordered Deposition of Inorganic Clusters from Micellar Block Copolymer Films. *Langmuir* **2000,** *16* (2), 407-415.

86. Lohmüller, T.; Aydin, D.; Schwieder, M.; Morhard, C.; Louban, I.; Pacholski, C.; Spatz, J. P., Nanopatterning by block copolymer micelle nanolithography and bioinspired applications. *Biointerphases* **2011,** *6* (1), MR1-MR12.

87. Bansmann, J.; Kielbassa, S.; Hoster, H.; Weigl, F.; Boyen, H. G.; Wiedwald, U.; Ziemann, P.; Behm, R. J., Controlling the Interparticle Spacing of Au−Salt Loaded Micelles and Au Nanoparticles on Flat Surfaces. *Langmuir* **2007,** *23* (20), 10150-10155.

88. Baha-Schwab, E. H. Directing osteogenic signaling and differentiation by surfaces modified with adhesive proteins and immobilized bone morphogenetic protein 2. Heidelberg, Univ., Diss., **2015**.

89. Glass, R.; Möller, M.; Spatz, J. P., Block Copolymer Micelle Nanolithography. *Nanotechnology* **2003,** *14*, 1153 - 1160.

90. Meiners, J. C.; Elbs, H.; Ritzi, A.; Mlynek, J.; Krausch, G., Chemically functionalized surfaces from ultrathin block-copolymer films. *Journal of Applied Physics* **1996,** *80* (4), 2224-2227.

91. Arnold, M.; Hirschfeld-Warneken, V. C.; Lohmuller, T.; Heil, P.; Blummel, J.; Cavalcanti-Adam, E. A.; Lopez-Garcia, M.; Walther, P.; Kessler, H.; Geiger, B.; Spatz, J. P., Induction of cell polarization and migration by a gradient of nanoscale variations in adhesive ligand spacing. *Nano Lett* **2008,** *8* (7), 2063-9.

92. Hirschfeld-Warneken, V. C.; Arnold, M.; Cavalcanti-Adam, A.; Lopez-Garcia, M.; Kessler, H.; Spatz, J. P., Cell adhesion and polarisation on molecularly defined spacing gradient surfaces of cyclic RGDfK peptide patches. *European journal of cell biology* **2008,** *87* (8-9), 743-50.

93. Kästle, G.; Boyen, H. G.; Weigl, F.; Lengl, G.; Herzog, T.; Ziemann, P.; Riethmüller, S.; Mayer, O.; Hartmann, C.; Spatz, J. P.; Möller, M.; Ozawa, M.; Banhart, F.; Garnier, M. G.; Oelhafen, P., Micellar Nanoreactors—Preparation and Characterization of Hexagonally Ordered Arrays of Metallic Nanodots. *Advanced functional materials* **2003,** *13* (11), 853-861.

94. Groll, J.; Albrecht, K.; Gasteier, P.; Riethmueller, S.; Ziener, U.; Moeller, M., Nanostructured ordering of fluorescent markers and single proteins on substrates. *Chembiochem : a European journal of chemical biology* **2005,** *6* (10), 1782-7.

95. Wolfram, T.; Belz, F.; Schoen, T.; Spatz, J. P., Site-specific presentation of single recombinant proteins in defined nanoarrays. *Biointerphases* **2007,** *2* (1), 44-8.

96. Pohl, T. L. M. Covalently immobilized bone morphogenetic protein 2 induces signaling responses for osteoblast differentiation. Heidelberg, Univ., Diss., **2012**.

97. Kolb, H. C.; Finn, M. G.; Sharpless, K. B., Click Chemistry: Diverse Chemical Function from a Few Good Reactions. *Angewandte Chemie International Edition* **2001,** *40* (11), 2004-2021.

98. Martin, V.; Zambarda, C.; Francesca, P.; Giorgio, M.; Seckinger, A.; Grgurevic, L.; Vukicevic, S.; Cavalcanti-Adam, E. A., Surface immobilization of BMP-6 and RGD ligands at the nanoscale promotes myoblast adhesion and SMAD signaling. *Scientific Reports* **2017 (submitted)**.

99. Hersel, U.; Dahmen, C.; Kessler, H., RGD modified polymers: biomaterials for stimulated cell adhesion and beyond. *Biomaterials* **2003,** *24* (24), 4385-4415.

100. Lagunas, A.; Comelles, J.; Martínez, E.; Prats-Alfonso, E.; Acosta, G. A.; Albericio, F.; Samitier, J., Cell adhesion and focal contact formation on linear RGD molecular gradients: study of non-linear concentration dependence effects. *Nanomedicine: Nanotechnology, Biology and Medicine* **2012,** *8* (4), 432-439.

101. Orgovan, N.; Peter, B.; Bősze, S.; Ramsden, J. J.; Szabó, B.; Horvath, R., Dependence of cancer cell adhesion kinetics on integrin ligand surface density measured by a high-throughput label-free resonant waveguide grating biosensor. *Scientific Reports* **2014,** *4*, 4034.

102. VandeVondele, S.; Vörös, J.; Hubbell, J. A., RGD-grafted poly-l-lysine-graft-(polyethylene glycol) copolymers block non-specific protein adsorption while promoting cell adhesion. *Biotechnology and Bioengineering* **2003,** *82* (7), 784-790.

103. Elbert, D. L.; Pratt, A. B.; Lutolf, M. P.; Halstenberg, S.; Hubbell, J. A., Protein delivery from materials formed by self-selective conjugate addition reactions. *Journal of Controlled Release* **2001,** *76* (1–2), 11-25.

104. Sauerbrey, G., Verwendung von Schwingquarzen zur Wägung dünner Schichten und zur Mikrowägung. *Zeitschrift für Physik* **1959,** *155* (2), 206-222.

105. Homola, J.; Yee, S. S.; Gauglitz, G., Surface plasmon resonance sensors: review. *Sensors and Actuators B: Chemical* **1999,** *54* (1–2), 3-15.

106. Ladam, G.; Schaaf, P.; Decher, G.; Voegel, J.-C.; Cuisinier, F. J. G., Protein adsorption onto auto-assembled polyelectrolyte films. *Biomolecular Engineering* **2002,** *19* (2–6), 273-280.

107. Elwing, H., Protein absorption and ellipsometry in biomaterial research. *Biomaterials* **1998,** *19* (4), 397-406.

108. Attard, G.; Barnes, C., Surfaces. *Oxford University Press*: Oxford [u.a.], **1998**.

109. Stamm, M., Polymer Surfaces and Interfaces : Characterization, Modification and Applications. *Springer Berlin Heidelberg*: Berlin, Heidelberg, **2008**; p Online-Ressource (digital).

110. Smith, G. C., Surface analysis by electron spectroscopy : measurement and interpretation. *Plenum Press*: New York [u.a.], **1994**.

111. Bomben, K. D.; Moulder, J. F.; Sobol, P. E.; Stickle, W. F., Handbook of x-ray photoelectron spectroscopy. A reference book of standard spectra for identification and interpretation of xps data. *Physical Electronics*: Eden Prairie, MN, **1995**.

112. Raymund, W. M., Kwok. XPS Peak 4.1.

113. Reimer, L., Scanning electron microscopy : physics of image formation and microanalysis. 2., completely rev. and updated ed. ed.; *Springer*: Berlin ; Heidelberg [u.a.], **1998**.

114. Kuo, W. C. H.; Briceno, M.; Ozkaya, D., FINAL ANALYSIS: Characterisation of Catalysts Using Secondary and Backscattered Electron In-lens Detectors. *Platinum Metals Review* **2014,** *58* (2), 106-110.

115. Hermanowicz, P.; Sarna, M.; Burda, K.; Gabryś, H., AtomicJ: An open source software for analysis of force curves. *Review of Scientific Instruments* **2014,** *85* (6), 063703.

116. McColl, R.; Nkosi, M.; Snyman, C.; Niesler, C., Analysis and quantification of in vitro myoblast fusion using the LADD Multiple Stain. *BioTechniques* **2016,** *61* (6), 323-326.

117. Anderson, G. W.; Zimmerman, J. E.; Callahan, F. M., N-Hydroxysuccinimide Esters in Peptide Synthesis. *Journal of the American Chemical Society* **1963,** *85* (19), 3039-3039.

118. Anderson, G. W.; Zimmerman, J. E.; Callahan, F. M., The Use of Esters of N-Hydroxysuccinimide in Peptide Synthesis. *Journal of the American Chemical Society* **1964,** *86* (9), 1839-1842.

119. Anderson, G. W., The use of activated esters in peptide synthesis. *Metabolism* **1964,** *13* (10), 1026-1031.

120. Klykov, O.; Weller, M. G., Quantification of N-hydroxysuccinimide and N-hydroxysulfosuccinimide by hydrophilic interaction chromatography (HILIC). *Analytical Methods* **2015,** *7* (15), 6443-6448.

121. Hesse, M.; Meier, H.; Zeeh, B.; Bienz, S.; Bigler, L.; Fox, T., Spektroskopische Methoden in der organischen Chemie. 9., überarbeitete und erweiterte Auflage / Stefan Bienz, Laurent Bigler, Thomas Fox, Herbert Meier ed.; *Georg Thieme Verlag*: Stuttgart ; New York, **2016**.

122. Stuart, B., Modern infrared spectroscopy. Published on behalf of *ACOL (University of Greenwich) by Wiley*: Chichester [u.a.], **1996**.

123. Yang, W.-C.; Mirzaei, H.; Liu, X.; Regnier, F. E., Enhancement of Amino Acid Detection and Quantification by Electrospray Ionization Mass Spectrometry. *Analytical Chemistry* **2006,** *78* (13), 4702-4708.

124. Madler, S.; Bich, C.; Touboul, D.; Zenobi, R., Chemical cross-linking with NHS esters: a systematic study on amino acid reactivities. *Journal of mass spectrometry : JMS* **2009,** *44* (5), 694-706.

125. Vericat, C.; Vela, M. E.; Benitez, G.; Carro, P.; Salvarezza, R. C., Self-assembled monolayers of thiols and dithiols on gold: new challenges for a well-known system. *Chemical Society Reviews* **2010,** *39* (5), 1805-1834.

126. Fourel, L.; Valat, A.; Faurobert, E.; Guillot, R.; Bourrin-Reynard, I.; Ren, K.; Lafanechere, L.; Planus, E.; Picart, C.; Albiges-Rizo, C., beta3 integrin-mediated spreading induced by matrix-bound BMP-2 controls Smad signaling in a stiffness-independent manner. *The Journal of cell biology* **2016,** *212* (6), 693-706.

127. Oberhansl, S.; Castano, A. G.; Lagunas, A.; Prats-Alfonso, E.; Hirtz, M.; Albericio, F.; Fuchs, H.; Samitier, J.; Martinez, E., Mesopattern of immobilised bone morphogenetic protein-2 created by microcontact printing and dip-pen nanolithography influence C2C12 cell fate. *RSC Advances* **2014,** *4* (100), 56809-56815.

128. Heckmann, D.; Meyer, A.; Laufer, B.; Zahn, G.; Stragies, R.; Kessler, H., Rational design of highly active and selective ligands for the alpha5beta1 integrin receptor. *Chembiochem : a European journal of chemical biology* **2008,** *9* (9), 1397-407.

129. Bochen, A.; Marelli, U. K.; Otto, E.; Pallarola, D.; Mas-Moruno, C.; Di Leva, F. S.; Boehm, H.; Spatz, J. P.; Novellino, E.; Kessler, H.; Marinelli, L., Biselectivity of isoDGR

Peptides for Fibronectin Binding Integrin Subtypes α5β1 and αvβ6: Conformational Control through Flanking Amino Acids. *Journal of Medicinal Chemistry* **2013,** *56* (4), 1509-1519.

130. Kibler, C.; Schermutzki, F.; Waller, H. D.; Timpl, R.; Muller, C. A.; Klein, G., Adhesive interactions of human multiple myeloma cell lines with different extracellular matrix molecules. *Cell Adhes Commun* **1998,** *5* (4), 307-23.

131. Dickinson, M. H.; Farley, C. T.; Full, R. J.; Koehl, M. A.; Kram, R.; Lehman, S., How animals move: an integrative view. *Science (New York, N.Y.)* **2000,** *288* (5463), 100-6.

132. Holle, A. W.; Engler, A. J., More than a feeling: discovering, understanding, and influencing mechanosensing pathways. *Current opinion in biotechnology* **2011,** *22* (5), 648-54.

133. Paxton, J. Z.; Donnelly, K.; Keatch, R. P.; Baar, K., Engineering the bone-ligament interface using polyethylene glycol diacrylate incorporated with hydroxyapatite. *Tissue engineering. Part A* **2009,** *15* (6), 1201-9.

134. Mammoto, A.; Ingber, D. E., Cytoskeletal control of growth and cell fate switching. *Current Opinion in Cell Biology* **2009,** *21* (6), 864-870.

135. Discher, D. E.; Janmey, P.; Wang, Y.-l., Tissue Cells Feel and Respond to the Stiffness of Their Substrate. *Science (New York, N.Y.)* **2005,** *310* (5751), 1139.

136. Engler, A. J.; Griffin, M. A.; Sen, S.; Bonnemann, C. G.; Sweeney, H. L.; Discher, D. E., Myotubes differentiate optimally on substrates with tissue-like stiffness: pathological implications for soft or stiff microenvironments. *The Journal of cell biology* **2004,** *166* (6), 877-87.

137. Ren, K.; Crouzier, T.; Roy, C.; Picart, C., Polyelectrolyte multilayer films of controlled stiffness modulate myoblast cells differentiation. *Advanced functional materials* **2008,** *18* (9), 1378-1389.

138. Gilde, F.; Fourel, L.; Guillot, R.; Pignot-Paintrand, I.; Okada, T.; Fitzpatrick, V.; Boudou, T.; Albiges-Rizo, C.; Picart, C., Stiffness-dependent cellular internalization of matrix-bound BMP-2 and its relation to Smad and non-Smad signaling. *Acta Biomater* **2016,** *46*, 55-67.

139. Tabisz, B.; Schmitz, W.; Schmitz, M.; Luehmann, T.; Heusler, E.; Rybak, J. C.; Meinel, L.; Fiebig, J. E.; Mueller, T. D.; Nickel, J., Site-Directed Immobilization of BMP-2: Two Approaches for the Production of Innovative Osteoinductive Scaffolds. *Biomacromolecules* **2017,** *18* (3), 695-708.

140. Oryan, A.; Alidadi, S.; Moshiri, A.; Bigham-Sadegh, A., Bone morphogenetic proteins: a powerful osteoinductive compound with non-negligible side effects and limitations. *BioFactors (Oxford, England)* **2014,** *40* (5), 459-81.

141. Utturkar, A.; Paul, B.; Akkiraju, H.; Bonor, J.; Dhurjati, P.; Nohe, A., Development of Physiologically Based Pharmacokinetic Model (PBPK) of BMP2 in Mice. *Biological systems, open access* **2013,** *2*, 1000123.

142. Luginbuehl, V.; Meinel, L.; Merkle, H. P.; Gander, B., Localized delivery of growth factors for bone repair. *European journal of pharmaceutics and biopharmaceutics : official journal of Arbeitsgemeinschaft fur Pharmazeutische Verfahrenstechnik e.V* **2004,** *58* (2), 197-208.

143. Haidar, Z. S.; Hamdy, R. C.; Tabrizian, M., Delivery of recombinant bone morphogenetic proteins for bone regeneration and repair. Part A: Current challenges in BMP delivery. *Biotechnology letters* **2009,** *31* (12), 1817-24.

144. Meinel, L.; Kaplan, D. L., Silk constructs for delivery of musculoskeletal therapeutics. *Advanced Drug Delivery Reviews* **2012,** *64* (12), 1111-1122.

145. Kim, I. Y.; Lee, D. H.; Lee, D. K.; Kim, B. C.; Kim, H. T.; Leach, F. S.; Linehan, W. M.; Morton, R. A.; Kim, S. J., Decreased expression of bone morphogenetic protein (BMP) receptor type II correlates with insensitivity to BMP-6 in human renal cell carcinoma cells. *Clinical cancer research : an official journal of the American Association for Cancer Research* **2003,** *9* (16 Pt 1), 6046-51.

146. Hamdy, F. C.; Autzen, P.; Robinson, M. C.; Horne, C. H. W.; Neal, D. E.; Robson, C. N., Immunolocalization and Messenger RNA Expression of Bone Morphogenetic Protein-6 in Human Benign and Malignant Prostatic Tissue. *Cancer research* **1997,** *57* (19), 4427.

147. Dai, J.; Keller, J.; Zhang, J.; Lu, Y.; Yao, Z.; Keller, E. T., Bone morphogenetic protein-6 promotes osteoblastic prostate cancer bone metastases through a dual mechanism. *Cancer research* **2005,** *65* (18), 8274-85.

148. Tateyama, S.; Uchida, K.; Hidaka, T.; Hirao, M.; Yamaguchi, R., Expression of Bone Morphogenetic Protein-6 (BMP-6) in Myoepithelial Cells in Canine Mammary Gland Tumors. *Veterinary Pathology* **2001,** *38* (6), 703-709.

149. Damiano, J. S.; Cress, A. E.; Hazlehurst, L. A.; Shtil, A. A.; Dalton, W. S., Cell adhesion mediated drug resistance (CAM-DR): role of integrins and resistance to apoptosis in human myeloma cell lines. *Blood* **1999,** *93* (5), 1658-67.

150. Neri, P.; Ren, L.; Azab, A. K.; Brentnall, M.; Gratton, K.; Klimowicz, A. C.; Lin, C.; Duggan, P.; Tassone, P.; Mansoor, A.; Stewart, D. A.; Boise, L. H.; Ghobrial, I. M.; Bahlis, N. J., Integrin β7-mediated regulation of multiple myeloma cell adhesion, migration, and invasion. *Blood* **2011,** *117* (23), 6202-6213.

151. Vacca, A.; Ria, R.; Presta, M.; Ribatti, D.; Iurlaro, M.; Merchionne, F.; Tanghetti, E.; Dammacco, F., alpha(v)beta(3) integrin engagement modulates cell adhesion,

proliferation, and protease secretion in human lymphoid tumor cells. *Experimental hematology* **2001,** *29* (8), 993-1003.

11 List of Figures

12 List of Tables

13 Abbreviations

°C	degree Celsius
A	amplitude
Ac-BMP-6	acetylated BMP-6
ActR	activin receptor
AFM	atomic force microscopy
ALK	activin receptor-like kinase
ALP	alkaline phosphatase
APS	ammonium persulfate
APTES	(3-aminopropyl)triethoxysilane
BCA	bicinchominic acid
BCMN	block-copolymer micellar nanolithography
BDNF	brain-derived neurotrophic factor
BISC	BMP-induced sgnaling complex
BMP	bone/body morphogenetic protein
BMPR	BMP receptor
BMSC	bone mesenchymal stem cell
BRC	bone remodeling compartments
BRI	BMP receptor I
BRII	BMP receptor II
BSA	bovine serum albumin
BSE	backscattered electrons
c	concentration
CBD	collagen-binding domains
cDNA	complementary DNA
cFN	cellular fibronectin
CL	chemical luminescence
cm	centimeter
CMC	critical micelle concentration
co-SMAD	common mediator SMAD
cRGD	cyclic RGD
Ctrl	control
CuAAC	copper(I)-catalyzed azide alkyne cycloaddition
DABCO	1,4-diazabicyclo-[2,2,2]-octane
DNA	deoxyribonucleic acid
DAPI	4',6-diamidino-2-phenylindole
DMEM	Dulbecco’s modified Eagle's minimal essential medium
DMF	dimethyl formamide

DMSO	dimethyl sulfoxide
Dvr-6	decapentaplegic vegetal related
ECM	extracellular matrix
EDTA	ethylenediaminetetraacetic acid
eV	electron volt
f	frequency
FACS	fluorescence-activated cell sorting
FBS	fetal bovine serum
FGF-1	fibroblast growth factor 1
g	gram
GAGs	glycosaminoglycans
GDF	growth differentiation factor
GF	growth factor
GFP	green fluorescent protein
h	hour
HRP	horseradish peroxidase
HS	heparan sulfate
Hz	Hertz
iBMP-6	immobilized BMP-6
IF	immunofluorescence
IgG	immunoglobulin G
IR	infrared
IRRAS	infrared reflection absorption spectroscopy
kPa	kilopascal
l	liter
L	loading rate
M	molecular concentration
m	meter
MAD	mother against decapentaplegic
mbar	millibar
MeOH	methanol
MHC	myosin heavy chain
min	minute
MOPS	3-(*N*-morpholino)propanesulfonic acid
mRNA	messenger RNA
MSC	mesenchymal stem cell
MU-NHS	11-mercaptoundecanoyl-*N*-hydroxysuccinimide
MΩ	megaohm
n	number
N	Newton
NCT	National Centre of Tumor Diseases

NGFβ	nerve growth factor β
NHS	*N*-hydroxysuccinimide
nm	nanometer
nM	nanomolar
OP	osteogenic protein
p	pressure
p. a.	pro analysi / analytical grade
P2VP	poly(2-vinylpyridine)
PAGE	polyacrylamide gel electrophoresis
PBS	phosphate buffered saline
PDMS	poly(dimethyl siloxane)
PE	primary electron
PEG	polyethylene glycol
PEG-DA	PEG diacrylate
PES	photoemission spectroscopy
PFA	*para*formaldehyde
PFC	preformed complex
pNPP	p-nitrophenyl phosphate
PS	polystyrene
PS-*b*-P2VP	poly(styrene-b-2-vinylpyridine)
pSMAD	phosphorylated SMAD
PTFE	polytetrafluoroethylene
QCM-D	quartz crystal microbalance with dissipation
R-SMAD	receptor-redulated SMAD
RGD	arginine, glyacine, aspartic acid
RIPA buffer	radioimmunoprecipitation assay buffer
RNA	ribonucleic acid
rpm	rounds per minute
RPMI	Roswell Park Memorial Institute medium
RT	room temperature
s	second
SAM	self-assembled monolayer
sBMP-6	soluble BMP-6
SDS	sodium dodecyl sulfate
SE	secondary electron
SEM	scanning electron microscope/microscopy
Sma	small body size
SPR	surface plasmon resonance
TBS-T	tris-buffered saline with Tween 20
TEMED	tetramethylethylenediamine
TGF-β	transforming growth factor β
Tris	tris(hydroxymethyl)aminomethane

V	volume
VEGF-A	vascular endothelial growth factor A
Vgr-1	vegetal related 1
W	watt
w	weight
WB	western blot
WST-1	water soluble tetrazolium-1
XPS	X-ray photoelectron spectroscopy
θ	phase angle

14 Acknowledgements

Ich möchte mich besonders bei Prof. Dr. Joachim P. Spatz bedanken, der die Möglichkeit gab, dieses interessante, spannende und interdisziplinäre Projekt zu bearbeiten und mir alle Freiheiten zur Bearbeitung dieses Themas gewährt hat. Bei Prof. Dr. Reiner Dahint bedanke ich mich recht herzlich für die Übernahme des Zweitgutachtens. Außerdem danke ich allen beteiligten Prüfern für die Mühe, sich mit der Thematik meiner Arbeit vertraut gemacht zu haben.

Insbesondere bedanke ich mich bei PD Dr. Elisabetta Ada Cavalcanti-Adam für die Aufnahme in die *cell adhesion group* und die tolle Betreuung während der gesamten Zeit. Die vielen konstruktiven Diskussionen sowie die Unterstützung und Motivation waren besonders wertvoll, vor allem aber das mir entgegengebrachte Vertrauen.

Mein Dank gilt auch Dr. Anja Seckinger und Dr. Dirk Hose vom Myelomzentrum Heidelberg sowie allen andern Kooperations- und Projektpartnern für die gute Zusammenarbeit im Sonderforschungsbereich Transregio 79 und die konstruktiven Gespräche. Außerdem möchte ich an dieser Stelle Maria Dörner, Ewelina Nickel, Hendrike Seidt und Marie-Louise Brygider für ihre Unterweisung und Unterstützung bei den Zellexperimenten mit dem Multiplen Myelom bedanken.

Ein herzliches Dankeschön geht an Dr. Elisabeth Baha-Schwab für wertvolle Unterstützung und Einarbeitung in die Welt der Proteinimmobilisierung. Bei Dr. Rebecca Medda bedanke ich mich für Hilfe und Unterstützung bei biologischen Fragen und Problemen, insbesondere aber bei Fragen rund um die Mikroskopie. Chiara Zambarda danke ich für die wertvollen Diskussionen und Gespräche, sowie für die lustige Zeit im Büro. Bei Dr. Tamás Haraszti bedanke ich mich für die Hilfe bei technischen Problemen und Fragen bei Laptop, Drucker, REM oder AFM. Für die Unterstützung bei XPS Experimenten danke ich Dr. Franziska Schenk und für die Hilfe bei der Auswertung bin ich Eric Sauter sehr dankbar. Bei Janis Grigordis bedanke ich mich für die Unterstützung bei Analysen mit dem Cryo-REM. Für gute und kompetente Unterstützung bei administrativen Fragen danke ich Swetlana Duchnay, Karin Jordan, Angelika Neuner, Benjamin Scherke, Carola Fanther und Elisabeth Pfeilmeier. Ein reibungsloser Laboralltag wäre ohne die gute Organisation von Sigrid Riese, Helmi Czichos-Medda und Sabine Grünewald nicht möglich gewesen. Ich danke allen die

diese Arbeit Korrektur gelesen haben, insbesonders Dr. Rebecca Medda, Dr. Jan Janiesch und Dr. Franziska Schenk.

Dem gesamten AK Spatz danke ich für die tolle Zeit, die gute Zusammenarbeit, für Grill-, Glühwein- und Filmabende, für die verrückte und angenehme Zooatmosphäre und für die vielen lustigen und unvergesslichen Momente.

Ein ganz besonderer Dank für den Rückhalt, die Geduld, die Unterstützung und das entgegengebrachte Verständnis während all den Jahren gilt meinen Eltern. Meinen Brüder Carsten und Matthias danke für die all die Ratschläge und wertvollen Gespräche während des gesamten Studiums. Schließlich noch ein besonderes Dankeschön an meine Freundin Rike, die mir eine große Stütze ist und in schwierigen Situationen immer eine Möglichkeit fand, mich wieder aufzumuntern, insbesondere in den letzten Wochen und Monaten.